SUPPRESSION AND REVIVAL OF OSCILLATIONS AND CONTROL OF CHAOS IN NONLINEAR SYSTEMS

SUDHANSHU SHEKHAR CHAURASIA

(PH14015)

A thesis submitted for the partial fulfillment of
the degree of Doctor of Philosophy

Department of Physical Sciences

Indian Institute of Science Education and Research Mohali
Knowledge city, Sector 81, SAS Nagar, Manauli PO, Mohali 140306,
Punjab, India.

August 2019

Certificate of Examination

This is to certify that the dissertation titled *"Suppression and Revival of Oscillations and Control of Chaos in Nonlinear Systems"* submitted by **Mr. Sudhanshu Shekhar Chaurasia** (Reg. No. PH14015) for the partial fulfillment of Doctor of Philosophy programme of the Institute, has been examined by the thesis committee duly appointed by the Institute. The committee finds the work done by the candidate satisfactory and recommends that the report be accepted.

Dr. Rajeev Kapri Dr. Sanjeev Kumar Prof. Sudeshna Sinha

(Supervisor)

Declaration

The work presented in this thesis has been carried out by me under the guidance of Prof. Sudeshna Sinha at the Indian Institute of Science Education and Research Mohali. This work has not been submitted in part or in full for a degree, a diploma, or a fellowship to any other university or institute. Whenever contributions of others are involved, every effort is made to indicate this clearly, with due acknowledgment of collaborative research and discussions. This thesis is a bonafide record of original work done by me and all sources listed within have been detailed in the bibliography.

Sudhanshu Shekhar Chaurasia

(Candidate)

In my capacity as the supervisor of the candidate's thesis work, I certify that the above statements by the candidate are true to the best of my knowledge.

Prof. Sudeshna Sinha

(Supervisor)

Acknowledgements

I would like to thank and express my deep gratitude to my thesis supervisor, Prof. Sudeshna Sinha. She has helped me from the first day in the institute and still continues to encourage me. It is because of her guidance, my PhD went so smoothly, without any trouble. Her way of dealing with students is amazing, and it never felt to me that I was new to the field of Nonlinear Dynamics. She has always encouraged to look for the new problems and not only solving them. I shall always be grateful to her for all these. Apart from the supervisor, she is also a great mentor.

I would also like to thank my doctoral committee, Dr Rajeev Kapri and Dr Ananth Venkatesan, for supporting me entire time in IISER Mohali. I want to thank Dr Rajeev Kapri especially for helping me to learn topics like fractal concepts in surface growth, finite-size scaling and DNA unzipping. I also thank Prof. Jasjeet Singh Bagla, whose course work and project have polished my computational techniques and skills. I am grateful to all faculty members and staffs of IISER Mohali for their direct or indirect support. Of course, I can not forget to mention Dr Manish Dev Shrimali for continuous discussion through my PhD time, and he is also my collaborator. My sincere thanks go to Prof. Tomasz Kapitaniak for offering me the opportunity to visit his group at Lodz and supporting my stay.

I am also thankful to CSIR and IISER Mohali for funding my PhD, CCSTDS for partial travel fellowship to attend a conference in Rome, DST-SERC and ICTP for selecting me in the school and supporting my stay. The work I have done in this period is computationally intensive, and this acknowledgement cannot be complete without mentioning the computational facility at IISER Mohali.

When it comes to research, there is also a research group. Here are the people in my group, I would like to thank, who have helped me in every discussions and presentation. The first name comes in my mind is Dr Neeraj Kamal, always motivates me and taught the correct way of writing the codes. Dr. Vivek Kohar for suggesting the future options after PhD, Dr. Anshul Choudhary, small guy but full of energy and also my collaborator, Dr. Chandrakala Meena for discussions regarding research problems, Dr. Pranay Deep Rungta for always motivating to learn new computational skills, Manaoj Arvind and Promit Moitra for helping me to prepare talks, Dr. Umesh Verma for helping me to write thesis and also my collaborator, Dr. Ajay Deep for helping me to solve delay differential equations and Manish Yadav for discussion and collaboration.

Also, there is one component of life, without which it can not be cheerful and imagined, and it is friends. I have enjoyed my time here to the fullest because of their presence. First I would like to thanks the man of patience, Satyam Srivastava, his room has been our daily adda. In the name of patience, one can not forget Deepak Singh Kathyat. Then comes Swagatam Nayak, our baba, slow in nature, but does work with perfection. Arnob Mukherjee, our chacha jaan, my dear friend and in love with games. Avinash Singh, the movie man. Ankit Singh, the simulation guy. Priyanka Madhu, our chulbuli, always makes the surrounding cheerful. Ayushi Singhania, very emotional but chhota packet bada dhamaka. Geeta Sharma, my moti and a close friend. Here are some more quick names : Sandeep Rana, Mayank Srivastava, Shubhendu Shekhar Khali, Anirban Ghosh, Ramu Kumar Yadav, Shekhar Das, Garima Choudhary, Nijil Lal CK, Aman Bajaj, Pawan Dahiya, Priyanka Mondal, Jyotsana Ojha, Anshu Sirohi, Akhilesh Patel, Harishchandra Singh, Aman Suhag, Rajneesh Parhate, Deepraj Meena, Shailesh Dhasmana, Ankur Sharma, Sanjay Singh, Arka Mitra, Soumen Ash, Swati Tanvar, Kavita Choudhary, Ashwini Balodhi, Karishma Bhasne, Hema Swasthi, Kanika Pasrija, Mayank Saraswat, Vaibhav Varshney, Vikash and Yogesh Tak.

Finally comes the family time. I would like to thanks my parents for believing in me and providing the environment so that I can achieve my goal. My father has always been career-oriented, and my mother always tried to make me a good human being. I also thank my brother, Himanshu and my cousin Poonam, for their love and support. These people have always supported me mentally and boosted my morale so that I can work efficiently without any worries; for this, I shall always be grateful to them in my life.

List of Publications

Chaurasia, S. S., Sinha, S., "Suppression of chaos through coupling to an external chaotic system", ***Nonlinear Dynamics*** 87., (2016) 159–167

Chaurasia, S. S., Yadav, M., Sinha, S., "Environment-induced symmetry breaking of the oscillation-death state". ***Phys. Rev. E*** 98., (2018) 032223

Chaurasia, S. S., Choudhary, A., Shrimali, M. D., Sinha, S., "Suppression and Revival of Oscillations through Time-varying Interaction". ***Chaos, Solitons & Fractals*** 118., (2019) 249-254

Chaurasia, S. S., Sinha, S., "Control of hierarchical networks by coupling to an external chaotic system". ***Europhysics Letters*** 125., (2019) 50006

Yadav, M., **Chaurasia, S. S.**, Sinha, S., "Asymmetry in the basin stability of oscillation death states under variation of environment-oscillator links". (To appear in ***NODYCON 2019 Springer Proceedings***).

Verma, U. K., **Chaurasia, S. S.**, Sinha, S., "Explosive death in nonlinear oscillators coupled by quorum sensing". ***arXiv*** 1904.11389, (2019) [Accepted for publication in ***Phys. Rev. E***]

Contents

Chapter 1

Introduction

Differential equations describing nonlinear dynamics are often not complicated in form, and just involve some additional nonlinear terms. However their analysis is not easy, starting from the example of a simple pendulum, where one needs the help of elliptic function to solve the system analytically without small angle approximation. The simple pendulum is a two-dimensional oscillator in phase space. Since trajectories cannot intersect in the phase plane, for two-dimensional systems the Poincaré-Bendixson theorem implies that the dynamics is quite simple. But it becomes complicated when we add one more dimension to phase space and the newly born interesting dynamics that may arise in systems of 3 or more dimensions is known as **chaos**. The word *chaos* itself suggests the unpredictability and great sensitivity to initial conditions. So in such dynamical systems, two different but very close initial conditions can show completely uncorrelated dynamics after some time, i.e. with time, the information of the previous states decay. Here is a quote relevant to this behaviour:

Physicists like to think that all you have to do is say, these are the conditions, now what happens next?

—RICHARD P. FEYNMAN

The effective unpredictability of deterministic dynamical systems is popularly known as the ***The Butterfly Effect***, and more technically this captures the *extreme sensitive dependence on initial conditions*. First observed in the Lorenz attractor, many chaotic oscillators have been found since now in chemical, biological and mechanical systems. Since the start of the study of complex systems, chaotic behaviour is quite often seen in

such systems due to the high dimensionality of these systems.

1.1 Dynamical systems

In nature, every system that evolves in time is a dynamical system. Dynamical systems can be represented by ordinary differential equations, partial differential equations or difference equations. The dynamical equations may be autonomous (explicit time independence) or non-autonomous (explicit time dependence), discrete (iterated maps) or continuous in time. In particular, continuous time systems are widely used to model a large class of natural phenomena, and have a lot of applications in wide-ranging engineered systems. In this thesis, we have only considered continuous-time systems, more specifically nonlinear ordinary differential equations with limit cycle and chaotic dynamics. We give below all the oscillators considered in this thesis.

1.1.1 Stuart-Landau oscillator

Stuart-Landau oscillator is a phase oscillator in two-dimensional phase space. Any oscillator near the Hopf-bifurcation point can be described by Stuart-Landau oscillators [1] given by equations:

$$\dot{z}(t) = [(\rho + i\omega) - |z(t)|^2]z(t) \tag{1.1}$$

where $\sqrt{\rho}$ is the amplitude and ω is the frequency of the oscillator. Fig 1.1(a) shows the time-series of the x and y variable after the transient behaviour and Fig. 1.1(b) shows the phase-portrait in the x-y phase plane with angular frequency $\omega = 2.0$ and amplitude 1.0.

Substitution of $z(t) = re^{i\theta}$ into the Eqn. 1.1, reduces the system to the following set of equations:

$$\begin{aligned} \dot{r} &= r(\rho - r^2) \\ \dot{\theta} &= \omega \end{aligned} \tag{1.2}$$

which clearly shows that the system is a phase oscillator with a limit cycle.

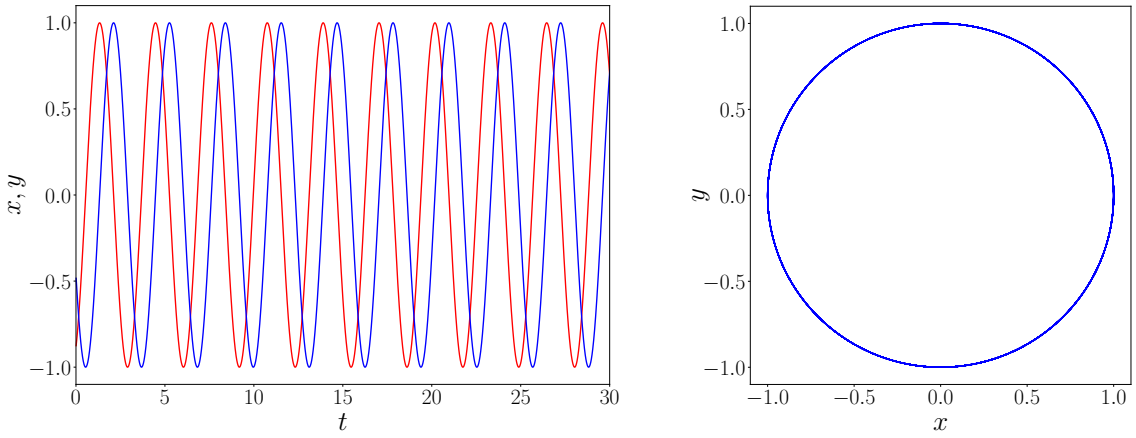

(a) (b)

Figure 1.1: (a) Time-series and (b) Phase-portrait of the Stuart-Landau oscillator with $\omega = 2.0$ and $\rho = 1.0$.

1.1.2 Lorenz Attractor

This is a system of three coupled first order ordinary differential equations, developed by Edward Lorenz as a simplified model of atmospheric convection. The three state variables make it possible to show chaotic behaviour, as allowed by the Poincaré-Bendixson theorem. The equations of the system are:

$$\begin{aligned} \dot{x} &= \sigma(y - x) \\ \dot{y} &= (r - z)x - y \\ \dot{z} &= xy - \beta z \end{aligned} \tag{1.3}$$

Setting time derivative terms on the LHS to zero gives three fixed points: $(0, 0, 0)$, $(\sqrt{\beta(r-1)}, \sqrt{\beta(r-1)}, r-1)$ and $(-\sqrt{\beta(r-1)}, -\sqrt{\beta(r-1)}, r-1)$. Estimation of linear stability analysis around these fixed points suggest that the stability of the fixed point changes for different parameter values. In this thesis, we have fixed the value of $\sigma = 10.0$, $\beta = 8.0/3.0$ and varied the parameter r. For $r > 24.74$, all the fixed points are unstable and the Lorenz system yields a chaotic attractor. Fig. 1.2 shows the time-series and phase-portraits of the Lorenz system described by Eqn 1.3.

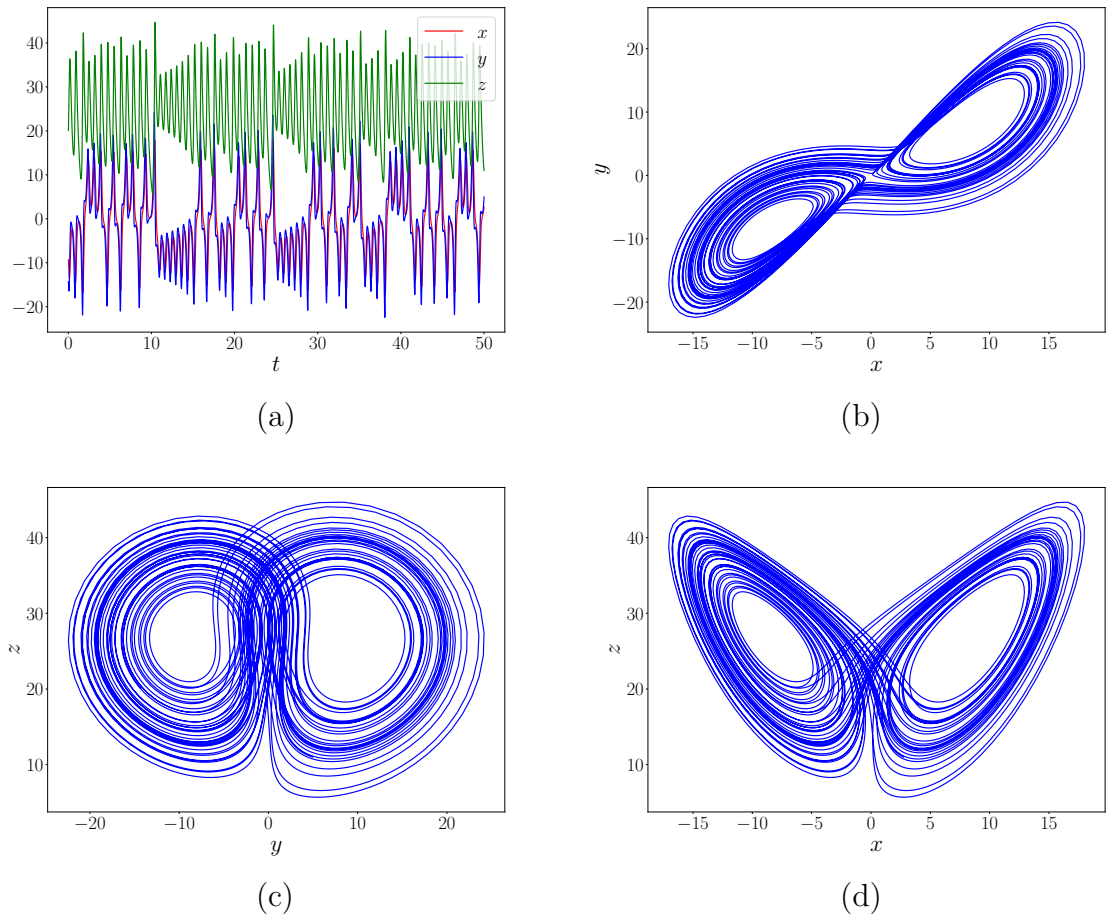

Figure 1.2: (a) Time-series and Phase-portraits of Lorenz system in the (b) $x - y$, (c) $y - z$ and (d) $x - z$ plane, with parameter values $\sigma = 10.0$, $\beta = 8.0/3.0$ and $r = 28.0$.

1.1.3 Rössler Oscillator

First studied by Otto Rössler, the dynamics of the Rössler oscillator is given by the following coupled non-linear first order ordinary differential equations:

$$\begin{aligned} \dot{x} &= -y - z \\ \dot{y} &= x + ay \\ \dot{z} &= b + z(x - c) \end{aligned} \tag{1.4}$$

It is a simple model of the dynamics of chemical reaction observed in a stirred tank

of reactants [2]. Setting time derivative terms on the LHS to zero gives two fixed points: $(\frac{c+\sqrt{c^2-4ab}}{2}, \frac{-c-\sqrt{c^2-4ab}}{2a}, \frac{c+\sqrt{c^2-4ab}}{2a})$ and $(\frac{c-\sqrt{c^2-4ab}}{2}, \frac{-c+\sqrt{c^2-4ab}}{2a}, \frac{c-\sqrt{c^2-4ab}}{2a})$. Out of these two fixed points, one fixed point lies in the centre of the attractor and other lies far away. Depending upon the parameter values, this system can show period one, period two, period four oscillations, all the way to chaos. Fig. 1.3 shows the time-series and phase-portraits of representative Rössler systems described by Eqns. 1.4.

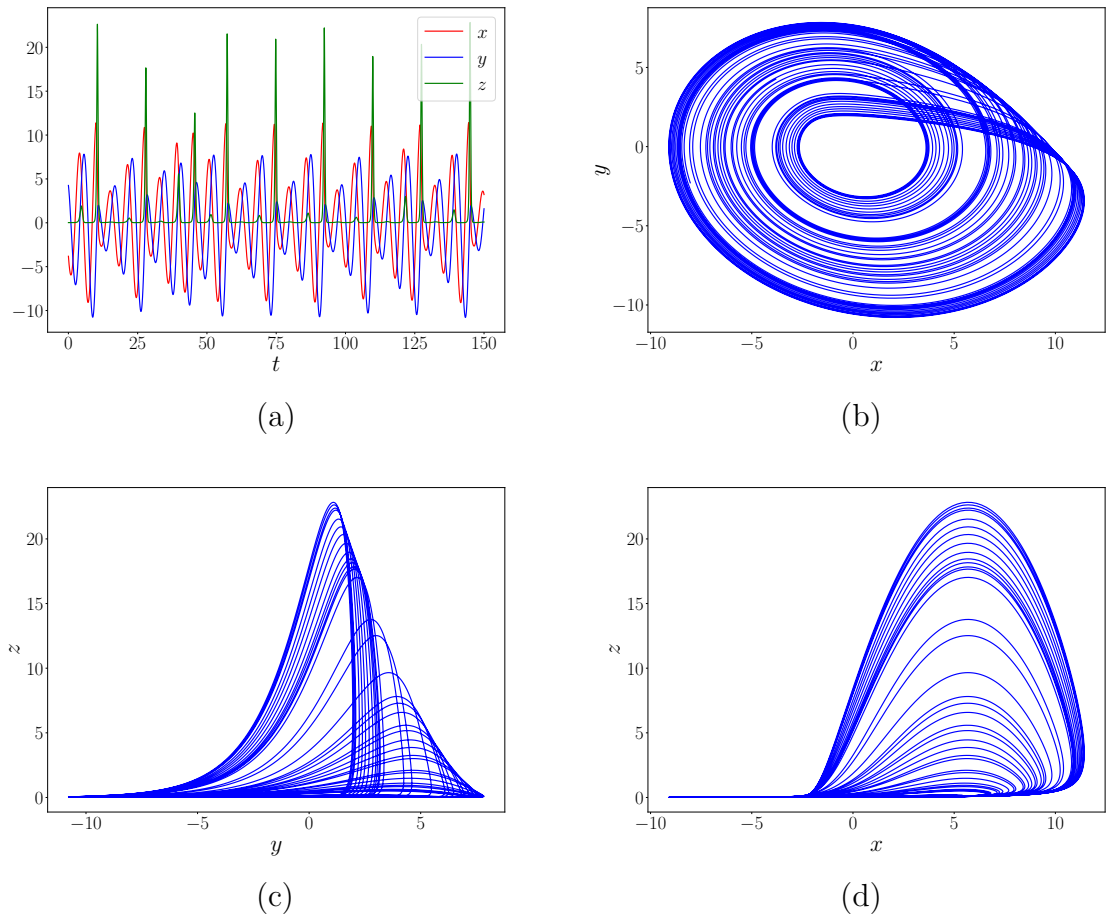

Figure 1.3: (a) Time-series and Phase-portraits of Rössler oscillator in the (b) $x-y$, (c) $y-z$ and (d) $x-z$ plane, with parameter values $a = 0.2$, $b = 0.2$ and $c = 5.7$.

1.2 Analysis of the dynamics of the oscillators

In this section, we present an outline of the various analyses undertaken in the thesis to characterize the dynamics of the oscillators.

1.2.1 Linear Stability Analysis

The qualitative behaviour of an oscillator can be obtained by the linear stability analysis around the fixed point. The analysis is the approximation of nonlinearity in the small neighbourhood of fixed point but is sufficient to describe the flow of the system in the phase plane. To begin with, let's take a set of functions describing the dynamics in two-dimensional phase plane:

$$\begin{aligned} \dot{x} &= f(x, y) \\ \dot{y} &= g(x, y) \end{aligned}$$

Expansion of these functions in the neighbourhood of the fixed points (x_0, y_0) produce a set of linear equations:

$$\begin{aligned} \dot{\zeta} &= \left.\frac{\partial f}{\partial x}\right|_{x_0} \zeta + \left.\frac{\partial f}{\partial y}\right|_{y_0} \eta \\ \dot{\eta} &= \left.\frac{\partial g}{\partial x}\right|_{x_0} \zeta + \left.\frac{\partial g}{\partial y}\right|_{y_0} \eta \end{aligned}$$

and the eigen values of this matrix determine the nature of the flow in the phase-plane in the neighbourhood of the fixed point. We give below a table describing the dynamical behaviour depending upon the eigen values of the Jacobian:

λ_1	λ_2	Dynamics
-Real	-Real	Stable node
+Real	+Real	Unstable node
-Real	+Real	Saddle node
Imaginary	Imaginary	Center
-Real and Imaginary	-Real and Imaginary	Stable focus
+Real and Imaginary	+Real and Imaginary	Unstable focus

1.2.2 Basin Stability

Linear stability analysis provides qualitative behaviour around the fixed points. If there are more than one fixed points, we have to check the stability of each of them to understand the system. But this analysis is very local and does not account for dynamics outside of the neighbourhood of the fixed points, i.e. nonlinearity of the system is completely ignored. It becomes more complicated when there is more than one attractor.

So to obtain some idea of the global stability of complex systems, it is more useful to implement the concept of basin stability [3] given as follows: We take initial conditions with a uniform random distribution in a designated volume of phase space, and evolve the system. Then we determine how many initial conditions go to a specific attractor. The fraction of initial conditions going to a particular attractor, is used to define the global stability of the attractor and reflects the probability of a random initial condition going to the attractor. In a sense, this idea is more general, because typically the dynamics can be very different in regions of phase space far from the neighbourhood of an attractor, and so linear stability cannot account for the global stability of an attractor.

1.2.3 Lyapunov Exponents

With the linear stability analysis, one can calculate the eigen values of the Jacobian and find out whether the system is oscillatory or not. But if the system is oscillatory, it cannot further classify the type of oscillations, namely whether periodic or chaotic. For identification of chaotic oscillators, we use the definition of chaos. Lyapunov exponent of dynamical systems quantifies the rate of separation of two trajectories starting from very close initial conditions. If the separation of the trajectories after some time t is $\delta(t)$ then the definition of Lyapunov exponent is:

$$||\delta(t)|| \quad = \quad ||\delta(0)||e^{\lambda t}$$

where λ is the Lyapunov exponent. The maximum value of the Lyapunov exponent quantifies the characteristics of the dynamics, as follows:

- $\lambda > 0$: chaos
- $\lambda = 0$: periodic or quasi-periodic
- $\lambda < 0$: stable equilibrium

1.3 Coupled Oscillators

Coupled oscillators are quite often found in nature, and the interaction of the system leads to the various complex phenomenon like multistable systems, chimera states, synchronization, oscillation suppression. The type of interaction may be broadly classified

into two classes: directional (or unidirectional) and un-directional (or bidirectional). A general form of coupling can be formally written as

$$\begin{aligned} \dot{X}_1 &= F(X_1) + \varepsilon G_1(X_2, X_1) \\ \dot{X}_2 &= F(X_2) + \varepsilon G_2(X_1, X_2) \end{aligned}$$

where $F(X)$ is the function determining the time evolution of uncoupled oscillator, $G(X_1, X_2)$ is the functional form of coupling and ε is the strength of coupling of both the oscillators. All these three factors play a crucial role to determine the dynamics of the system. For $\varepsilon = 0$, there is no coupling between the oscillators and they sustain their dynamics as defined by the function $F(X)$, which might be limit cycle, quasi-periodic or chaotic attractor. The coupling form $G(X_1, X_2)$ starts playing a role in determining the dynamics when we turn on the coupling strength. Depending upon the system, there are different types of interaction or coupling functions used:

Type of coupling	**Functional form**
Diffusive	$(x_j - x_i)$
Conjugate	$(y_j - x_i)$
Mean field	$(\bar{x} - x_i)$
Lotka-Volterra	$(y_j \times x_i)$

Additionally, there may be coupling to an external environment, through feedback from an external variable (often denoted as u).

In the real-world, typically not just two oscillators, but a lot of oscillators interact with each other to form a complex network. The connectivity of a complex network may a have a wide range of topologies, such as: a star network, ring network, small-world network, scale-free network, random scale-free network, random network, globally connected network. The implementation of these topologies requires an appropriate adjacency matrix (A) in the dynamical equations:

$$\dot{X}_i = F(X_i) + \frac{\varepsilon}{k} \sum_{i=1}^{N} A_{ij} G(X_j)$$

where $X_i = [x_i^1, x_i^2, ..., x_i^m]^T$ denotes states of m-dimensional nonlinear oscillators and A represents $N \times N$ matrix with entries 0 (not connected) and 1 (connected). These complex systems exhibit wide-ranging phenomena, and we outline some of the important and interesting ones below.

1.3.1 Synchronization

Synchronization is a phenomenon in nature where dynamical systems acquire the same synchronized rhythm if there is a transfer of some information. When a system does not feel the presence of another system, its dynamics is independent of the other system, and hence uncorrelated. However when coupled, a collection of systems may adjust their dynamics, and start evolving in a correlated manner, i.e. their collective dynamics changes from incoherent to coherent. Fire-flies, swimming fishes, bird flocks, pacemaker are some of the classic examples of synchronization. Depending upon the nature of interaction and type of system, different types of synchronization have been observed, such as complete synchronization, phase synchronization, anti-phase synchronization, delayed or lag synchronization.

In order to quantify complete synchronization, in this thesis, we have calculated the synchronization error:

$$Z = \frac{1}{T}\sum_{t}\sqrt{\frac{\sum_{i=1}^{N}(x_i - \bar{x})^2}{N}} \tag{1.5}$$

where Z represents the time averaged standard deviation of the state variables and $\bar{x} = \frac{1}{N}\sum_{i=1}^{N} x_i$. Further we average Z over different initial states to obtain an ensemble averaged synchronization error $\langle Z \rangle$.

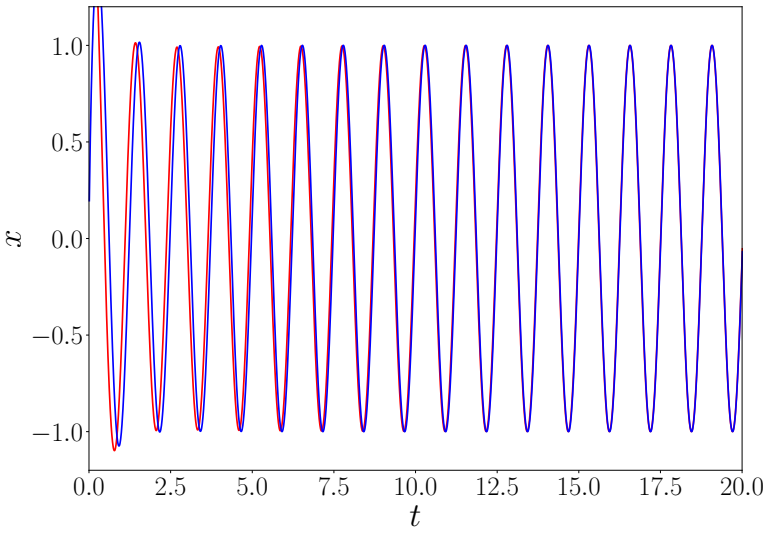

Figure 1.4: Time-series of x-variable of two Stuart-Landau oscillators coupled via diffusive coupling, with $\omega = 5.0$ and $\varepsilon = 0.2$.

Now we show an illustrative example of synchronization of two Stuart-Landau oscillators, when coupled diffusively via state variable x.

$$\begin{aligned} \dot{z_1}(t) &= [(1+i\omega) - |z_1(t)|^2]z_1(t) + \varepsilon(Re(z_2) - Re(z_1)) \\ \dot{z_2}(t) &= [(1+i\omega) - |z_2(t)|^2]z_2(t) + \varepsilon(Re(z_1) - Re(z_2)) \end{aligned} \tag{1.6}$$

Fig 1.4 shows the time-series of two coupled Stuart-Landau oscillators. It is evident from the figure that starting from the different initial condition, both the oscillators become synchronized when we turn on the coupling.

1.3.2 Suppression of Oscillations

Suppression of oscillation is yet another interesting phenomenon of coupled oscillators. When two or more systems are coupled to each other, depending upon the oscillator and the form and strength of coupling, oscillations may be quenched. Oscillation suppression can be characterized into two broad categories: amplitude death and oscillation death.

Amplitude death	**Oscillation death**
Also referred as Homogeneous Steady State (HSS)	Also referred as In-homogeneous Steady State (IHSS)
System of oscillators stabilizes to one fixed point	System of oscillators stabilizes to different fixed points
Usually obtained from limit cycle via Hopf bifurcation	Usually obtained from amplitude death via pitchfork bifurcation
Relevant in laser systems and others, where it is important to stabilize the system to a particular fixed point	Relevant in systems, where homogeneous systems evolve to heterogeneous solutions, like cellular differentiation

Now we present an illustrative demonstration of amplitude death and oscillation death in two conjugately coupled Stuart-Landau oscillators, with equations:

$$\begin{aligned} \dot{z_1}(t) &= [(1+i\omega) - |z_1(t)|^2]z_1(t) + \varepsilon(Img(z_2) - Re(z_1)) \\ \dot{z_2}(t) &= [(1+i\omega) - |z_2(t)|^2]z_2(t) + \varepsilon(Img(z_1) - Re(z_2)) \end{aligned} \tag{1.7}$$

where $z_j = x_j + iy_j$ is a complex number and the coupling is only in real part, i.e. in x-variable.

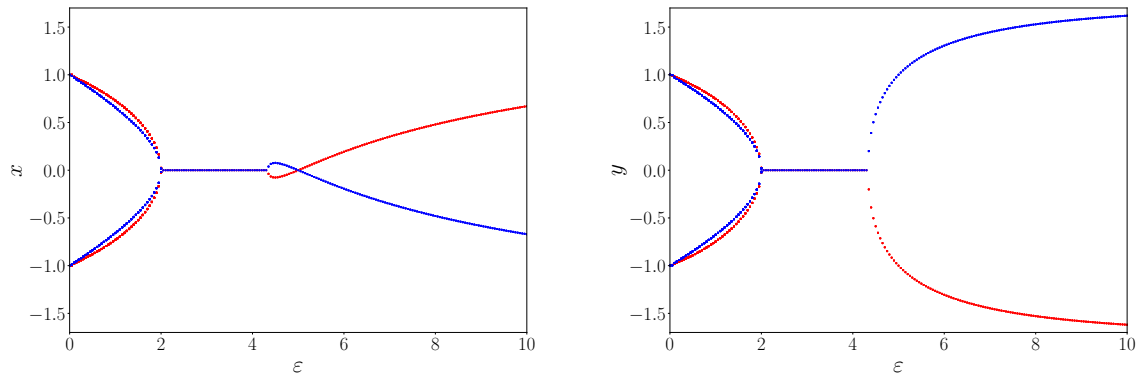

Figure 1.5: Bifurcation diagram of (a) x-variable and (b) y-variable of two conjugately coupled Stuart-Landau oscillators, with $\omega = 2.0$.

Fig 1.5 shows the bifurcation diagram of x and y variable of both the oscillators. It is evident that at low coupling strength, both the oscillators are limit cycles, with decreasing amplitude as coupling strength increases. When the coupling strength increases beyond a critical value, the fixed points become stable via Hopf bifurcation. On further increasing the coupling strength, these fixed points are de-stabilized again, and new sets of stable fixed points are created via pitchfork bifurcation. Though this route to Amplitude Death and Oscillation Death is common, other mechanisms of obtaining Amplitude Death and Oscillation Death also exist.

1.4 Outline of the Thesis

Now we present an outline of the work done in this thesis. In this thesis we have considered four broad problems and I give the central ideas of these problems below.

In chapter 2 we present the collective behaviour of an ensemble of chaotic oscillators diffusively coupled only to an external chaotic system, whose intrinsic dynamics may be similar or dissimilar to the group. Counter-intuitively, we find that a dissimilar external system manages to suppress the intrinsic chaos of the oscillators to fixed point dynamics, at sufficiently high coupling strengths. So, while synchronization is induced readily by coupling to an identical external system, control to fixed states is achieved only if the

external system is dissimilar. We quantify the efficacy of control by estimating the fraction of random initial states that go to fixed points, a measure analogous to basin stability. Lastly, we indicate the generality of this phenomenon by demonstrating suppression of chaotic oscillations by coupling to a common hyper-chaotic system.

In chapter 3 we present the behaviour of chaotic oscillators in hierarchical networks coupled to an external chaotic system whose intrinsic dynamics is dissimilar to all the oscillators in the network. We find that coupling to one such dissimilar external system manages to suppress the chaotic dynamics of all the oscillators at all levels of the network, at sufficiently high coupling strength. The chaos suppression is independent of system size and occurs irrespective of whether the connection to the external system is direct, or indirect through oscillators at another level in the hierarchy. Though the steady states vary across different tiers, the oscillators are synchronized to the same steady state at a particular level of hierarchy. For this problem also, we quantify the efficacy of control by estimating a global stability measure analogous to the basin stability of the emergent steady state.

In chapter 4 we present the impact of a common external system, which we call a common environment, on the Oscillator Death (OD) states of a group of Stuart-Landau oscillators. The group of oscillators yield a completely symmetric OD state when uncoupled to the external system, i.e., the two OD states occur with equal probability. However, remarkably, when coupled to a common external system this symmetry is significantly broken. For exponentially decaying external systems, the symmetry breaking is very pronounced for low environmental damping and strong oscillator-environment coupling. Further, we consider time-varying connections to the common external environment, with a fraction of oscillator-environment links switching on and off. Interestingly, we find that the asymmetry induced by environmental coupling decreases as a power law with increase in fraction of such on-off connections. This suggests that blinking oscillator-environment links can restore the symmetry of the OD state. We also considered the effect of disconnections of the oscillator-environment links on this asymmetry in the basin stability of the OD states. Interestingly, we find that the asymmetry induced by environmental coupling decreases with increase in fraction of such disconnections, and at some intermediate fraction close to half the symmetry is restored. However, further increase in disconnections induce asymmetry in the OD state again, until all oscillator-environment links are switched off. Lastly, we demonstrate the generality of our results for a constant external drive and find marked breaking of symmetry in the OD states there as well. When the constant environmental drive is large, the asymmetry in the OD states is very large, and the transition between the symmetric and asymmetric state with increasing

oscillator-environment coupling is very sharp.

In chapter 5 we present the emergent dynamical patterns in a system of coupled Stuart-Landau oscillators whose coupling form varies periodically and probabilistically in time. We find, through bifurcation diagrams and Basin Stability analysis, that there exists a window in coupling strength where the oscillations get suppressed. Beyond this window, the oscillations are revived again. A similar trend emerges with respect to the relative predominance of the coupling forms, with the largest window of fixed point dynamics arising where there is balance in the occurrence of the coupling forms. Further, significantly, more rapid switching of coupling forms yields large regions of oscillation suppression. Lastly, we propose an effective model for the dynamics arising from switched coupling forms and demonstrate how the bifurcations in this model capture the basic features observed in numerical simulations and also offers an accurate estimate of the fixed point region through linear stability analysis.

In summary, we have explored a broad range of problems concerning the control of networks of chaotic oscillators, including hierarchical networks. Further we have explored the suppression and revival of oscillations, as well as the phenomena of symmetry breaking in the basin stability of Oscillation Death states in coupled nonlinear oscillators. So our results shed light on the emergent collective dynamics of interactive nonlinear systems, thus serving to enhance the general understanding of such complex systems.

Chapter 2

Suppression of chaos through coupling to an external chaotic system

Adapted from the work published in :

Chaurasia, S. S., Sinha, S., "Suppression of chaos through coupling to an external chaotic system", ***Nonlinear Dynamics*** 87., (2016) 159–167

2.1 Introduction

The rapidly growing science of complex systems has helped in understanding spatiotemporal pattern formation in wide-ranging systems, from natural systems such as climate and biological systems on one hand, to man-made systems such as lasers and electronic circuits on the other hand. From the broad perspective of dynamical systems, the emergent behaviour of networks with different dynamical constituents is important. The basic ingredient of network models consists of local dynamical units, which may range from simple linear systems to chaotic systems. For instance, the electrical activities of neurons can be very complex, and experiments show quiescent, spiking, or bursting behaviour under varying excitability or external forcing current [4, 5]. The second important aspect of such models is the nature of the coupling interaction, for instance it may be diffusive or pulsatile, with or without delay. The last crucial feature is the topology of the connection matrix that determines the linkage between the elemental dynamical units. For instance, different collective behaviors are observed in networks of model neurons [6, 7] under varying connectivities, ranging from synchronization and coherence resonance to de-coherence [8]. Further, results from neuroscience suggest that perception and memory arise from synchronized networks [9].

A particular phenomenon of special significance in complex systems is the stabilization of steady states, and this has been observed in systems ranging from chemical reactions [10, 11] to biological oscillators [12, 13, 14, 15, 16]. Such fixed dynamics may be the desired target in certain cases, for instance in laser systems [17, 18, 19], where it leads to stabilization. In the biological context, some neurological diseases such as epilepsy lead to excessive neuronal excitation and so exploration of mechanisms that can suppress excitation is important for regulation of the disease [20]. On the other hand, the suppression of oscillations can also signal pathology, such as in neuronal disorders like Alzheimer or Parkinson's disease [21, 22, 23], where the focus is on prevention of fixed dynamics. Further, the suppression of oscillations is important in human-engineered systems, where much effort is focussed on control methods that can effectively and efficiently tame chaotic dynamics [24, 25, 26, 27, 28, 29, 30, 31]. For all these reasons, there has been considerable sustained research on suppression of chaotic oscillations in nonlinear systems over the years.

In this work we explore the behaviour of an ensemble of chaotic oscillators coupled only to an external chaotic system. So there is *no direct coupling amongst the oscillators*, and the interaction is mediated by coupling to the common external system [32]. So this

external system can be thought of as a pacemaker [16] of the group of oscillators (cf. Fig. 2.1 for a schematic). Note that the intrinsic dynamics of the external system can be *identical* to the group, or it can be an entirely *different* type of dynamical system.

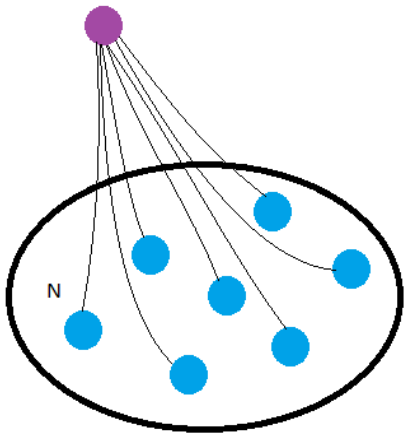

Figure 2.1: Schematic of a group of N oscillators coupled to an external oscillator.

Specifically, we first consider the example of N Rössler oscillators in a group, labelled by node index $i = 1, \ldots N$, with dynamics given by:

$$\begin{aligned} \dot{x_i} &= -(\omega + \delta(x_i^2 + y_i^2))\ y_i - z_i + \varepsilon\ (x_{ext} - x_i) \\ \dot{y_i} &= (\omega + \delta(x_i^2 + y_i^2))\ x_i + a\ y_i \\ \dot{z_i} &= b + z_i(x_i - c) \end{aligned} \tag{2.1}$$

where x_{ext} is a dynamical variable of the common external system to which the group is coupled *diffusively*.

The strength of coupling is given by ε.

When the external oscillator is also a Rössler oscillator, its governing equations are given by:

$$
\begin{aligned}
\dot{x}_{ext} &= -(\omega + \delta(x_{ext}^2 + y_{ext}^2))\ y_{ext} - z_{ext} + \frac{\varepsilon}{N}\sum_{j=1}^{N}(x_j - x_{ext}) \\
\dot{y}_{ext} &= (\omega + \delta(x_{ext}^2 + y_{ext}^2))\ x_{ext} + a\ y_{ext} \\
\dot{z}_{ext} &= b + z_{ext}(x_{ext} - c)
\end{aligned}
\tag{2.2}
$$

When the external oscillator is distinct from the group, for instance a Lorenz system, its dynamical equations are given by:

$$
\begin{aligned}
\dot{x}_{ext} &= \sigma\ (y_{ext} - x_{ext}) + \frac{\varepsilon}{N}\sum_{j=1}^{N}(x_j - x_{ext}) \\
\dot{y}_{ext} &= x_{ext}\ (r - z_{ext}) - y_{ext} \\
\dot{z}_{ext} &= x_{ext}\ y_{ext} - \beta\ z_{ext}
\end{aligned}
\tag{2.3}
$$

Parameters σ, β, r in the Lorenz system and parameters a, b, c, ω, δ in the Rössler oscillator, regulate the nature of the uncoupled dynamics, which can range from fixed points to chaos. In the sections below, we will present the spatiotemporal patterns arising in two distinct situations of interest: (a) the group of oscillators and the external oscillator are of identical type, and (b) the external chaotic system is distinct from the group of oscillators, and may even be hyper-chaotic.

2.2 Emergent Controlled Dynamics

Fig. 2.2 shows the bifurcation diagrams of the illustrative cases of an ensemble of chaotic Rössler oscillators coupled to (a) a chaotic external system that is identical (namely another Rössler oscillator) and (b) a chaotic external system that is dissimilar (namely, a Lorenz system). We find that a group of chaotic oscillators can be controlled to fixed points by the external *dissimilar* chaotic oscillator, when coupling is stronger than a critical value. However, when the chaotic oscillators are coupled to an external chaotic system of an *identical* type (namely all are Rössler oscillators), none of the oscillators are

controlled to fixed states, even for strong coupling.

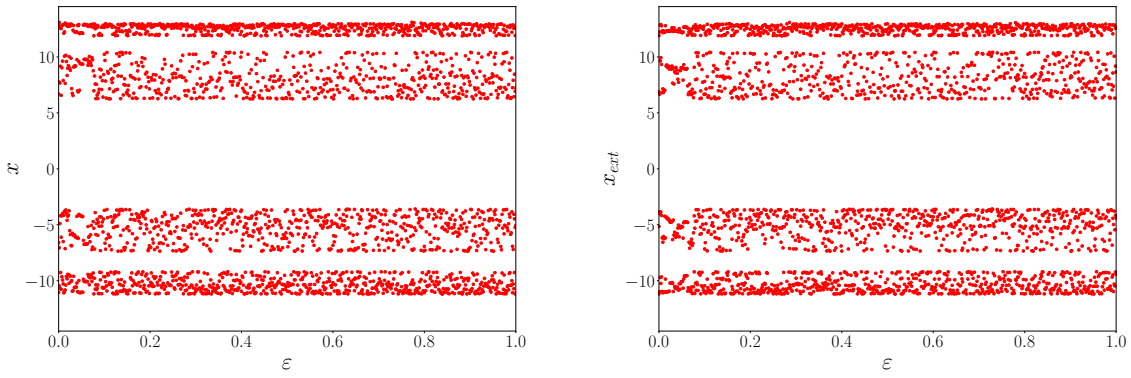

(a)

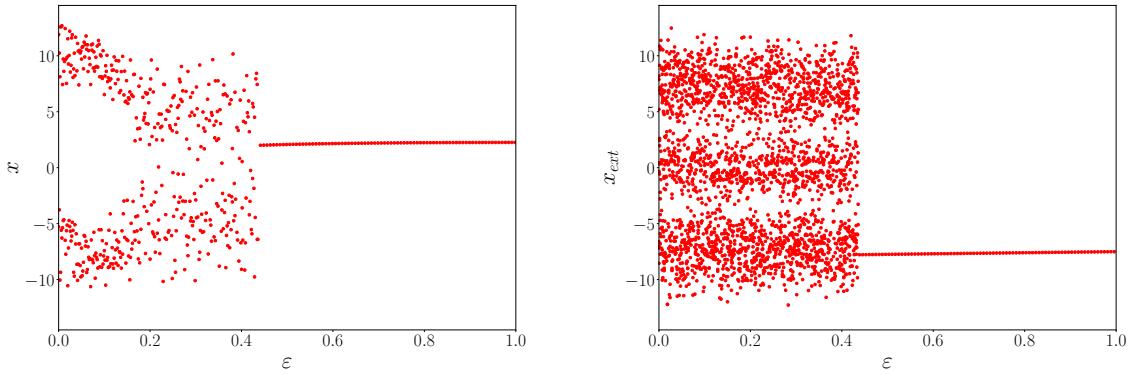

(b)

Figure 2.2: Bifurcation diagrams, with respect to the coupling strength ε, of one representative oscillator in the group (left) and an external oscillator (right). Here the group consists of chaotic Rössler oscillators with parameters $\omega = 0.41$, $\delta = 0.0026$, $a = 0.15$, $b = 0.4$ and $c = 8.4$ in Eqn. 2.1, and the external oscillator is: (a) a chaotic Rössler oscillator with parameters $\omega = 0.41$, $\delta = 0.0026$, $a = 0.15$, $b = 0.4$ and $c = 8.4$ in Eqn. 2.2, and (b) a chaotic Lorenz system with parameters $\sigma = 10.0$, $\beta = 8.0/3.0$ and $r = 25.0$ in Eqn. 2.3. In all the diagrams (including ones below) we display the x variable on the Poincare section of the phase curves of the oscillators at $y = y_{\text{mid}}$, where y_{mid} is the mid-point of the span of attractors along the y-axis.

Fig. 2.3 further illustrates this behaviour through phase portraits for representative Rössler oscillators from the group, for the case of coupling to (a) an identical external oscillator, and (b) a dissimilar external system. It is clear that for strong coupling the dynamics of the chaotic system is quenched to a fixed point when the external oscillator is dissimilar (cf. Fig. 2.3b), while coupling to a similar external oscillator does not suppress the chaos (cf. Fig. 2.3a).

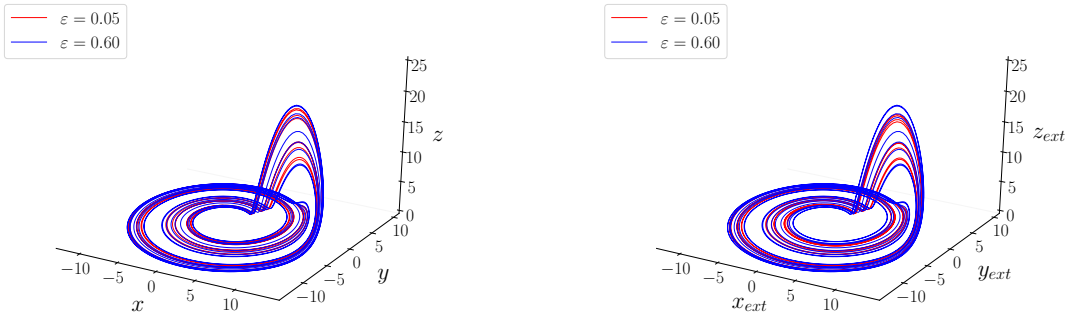

(a)

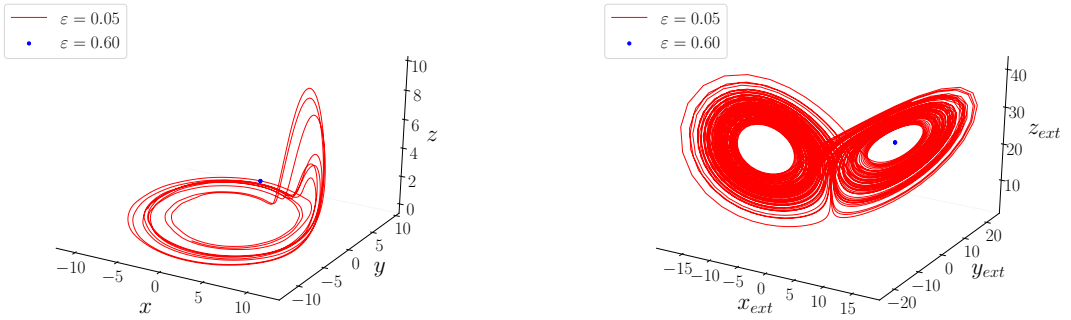

(b)

Figure 2.3: Phase portraits of a representative Rössler oscillator from the group (left) with parameters $\omega = 0.41$, $\delta = 0.0026$, $a = 0.15$, $b = 0.4$ and $c = 8.4$ in Eqn. 2.1, coupled to a common external system (right), at different coupling strengths ε. The panel (a) shows the case of coupling to an identical external Rössler oscillator, while panel (b) shows the case of coupling to a dissimilar chaotic oscillator, namely an external Lorenz system with parameters $\sigma = 10.0$, $\beta = 8.0/3.0$ and $r = 25.0$ in Eqn. 2.3.

When a group of chaotic Rössler oscillators is coupled on a common external chaotic Lorenz system, we find that there exists two steady states, as illustrated in Fig. 2.4. Depending on initial conditions, the system can go to either of the steady states. Linear stability analysis, via eigenvalues of the Jacobian, also corroborates the stabilization of the fixed points seen in the bifurcation diagrams (see Appendix for details).

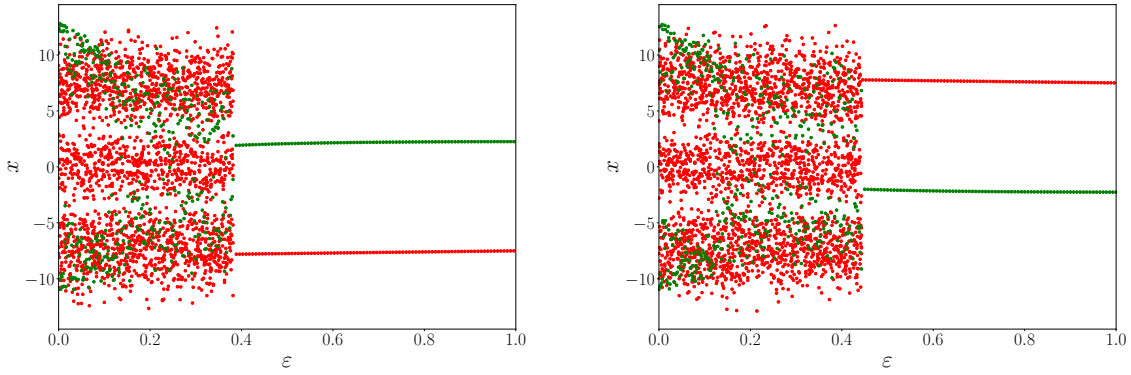

Figure 2.4: Bifurcation diagrams, with respect to the coupling strength ε, of one representative oscillator in the group (green) and an external oscillator (red), for the cases where the group of oscillators is comprised of chaotic Rössler oscillators with parameters $\omega = 0.41$, $\delta = 0.0026$, $a = 0.15$, $b = 0.4$ and $c = 8.4$ in Eqn. 2.1 and the external oscillator is a chaotic Lorenz system with parameters $\sigma = 10.0$, $\beta = 8.0/3.0$ and $r = 25.0$ in Eqn. 2.3.

2.3 Synchronization

We study the advent of synchronization in the group of oscillators, as a function of the coupling strength, for the case of identical and distinct external systems. Our focus is to ascertain what kind of external system facilitates synchrony, and which ones lead to control to steady states.

We calculate the synchronization error of the group of oscillators, averaged over time T, given by

$$Z = \frac{1}{T}\sum_{t}\sqrt{(\bar{x^2})_t - (\bar{x}^2)_t}$$

where $(\bar{x})_t = \frac{1}{N}\sum_{i=1}^{N} x_i$ and $(\bar{x^2})_t = \frac{1}{N}\sum_{i=1}^{N} x_i^2$ is the average value of x and x^2 of oscillators $i = 1, \ldots N$, at an instant of time t. Further we average Z over different initial states to obtain an ensemble averaged synchronization error $\langle Z \rangle$.

We display the average synchronization error defined above, in Fig. 2.5. It is clearly evident from the figure that the group of oscillators, *coupled only to a common external chaotic system*, get synchronized at sufficiently high coupling strengths. This trend holds for both identical and distinct external oscillators, suggesting that coupling to an external chaotic oscillator of wide-ranging dynamical types can induce synchronization. The critical coupling at which synchronization occurs is higher when the common external

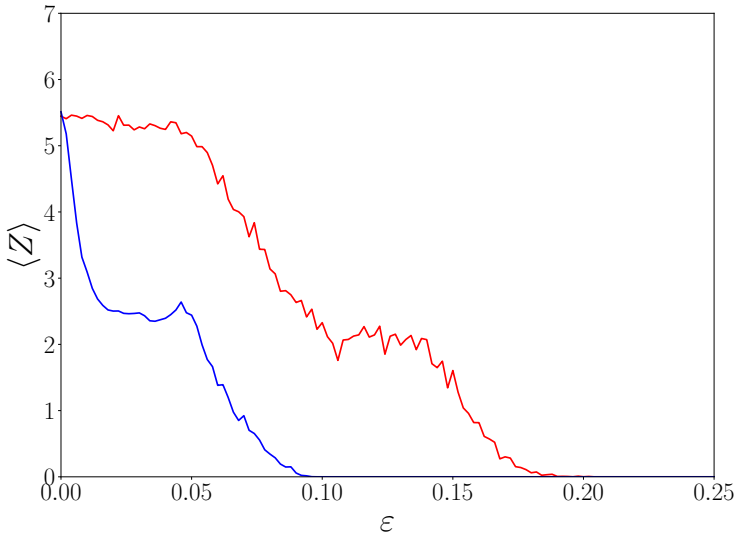

Figure 2.5: Synchronization error $\langle Z \rangle$ of the chaotic Rössler oscillators in the group with parameters $\omega = 0.41$, $\delta = 0.0026$, $a = 0.15$, $b = 0.4$ and $c = 8.4$ in Eqn. 2.1, averaged over 100 different initial conditions, with respect to coupling strength ε, for the case where the common external system is an identical chaotic Rössler oscillator (blue) with parameters $\omega = 0.41$, $\delta = 0.0026$, $a = 0.15$, $b = 0.4$ and $c = 8.4$ in Eqn. 2.2 and a chaotic Lorenz attractor (red) with parameters $\sigma = 10.0$, $\beta = 8.0/3.0$ and $r = 25.0$ in Eqn. 2.3.

oscillator is distinct from the group.

Interestingly, as coupling strength increases further, the oscillators are controlled to steady states, when the external oscillator is *dissimilar*. So an identical common external oscillator induces synchronization at weaker coupling strengths than a dissimilar external oscillator, but control to steady states occurs *only* when the external oscillator is distinct from the group.

2.4 Basin Stability of the Spatiotemporal Fixed Point

We now quantify the efficacy of control to steady states by finding the fraction BS_{fixed} of initial states that are attracted to fixed points, starting from generic random initial conditions. This measure is analogous to recently used measures of *basin stability* [3], and indicates the size of the basin of attraction for a spatiotemporal fixed point state. $BS_{fixed} \sim 1$ suggests that the fixed point state is globally attracting, while $BS_{fixed} \sim 0$ indicates that almost no initial states evolve to stable fixed states.

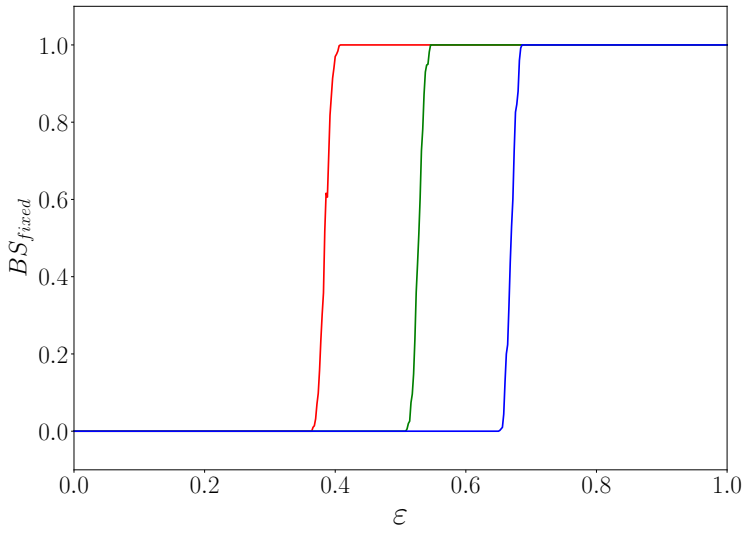

Figure 2.6: Dependence of the fraction of initial states BS_{fixed} attracted to the fixed point state, on the coupling strength ε, for a group of chaotic Rössler oscillators with parameters $\omega = 0.41$, $\delta = 0.0026$, $a = 0.15$, $b = 0.4$ and $c = 8.4$ in Eqn. 2.1, coupled to a common external chaotic Lorenz system with parameters $\sigma = 10.0$, $\beta = 8.0/3.0$ and 3 different values of parameter r in Eqn. 2.3: 24.7 (red), 25.0 (green) and 25.3 (blue). Note that there is no dependence of BS_{fixed} on the number of oscillators N in the group.

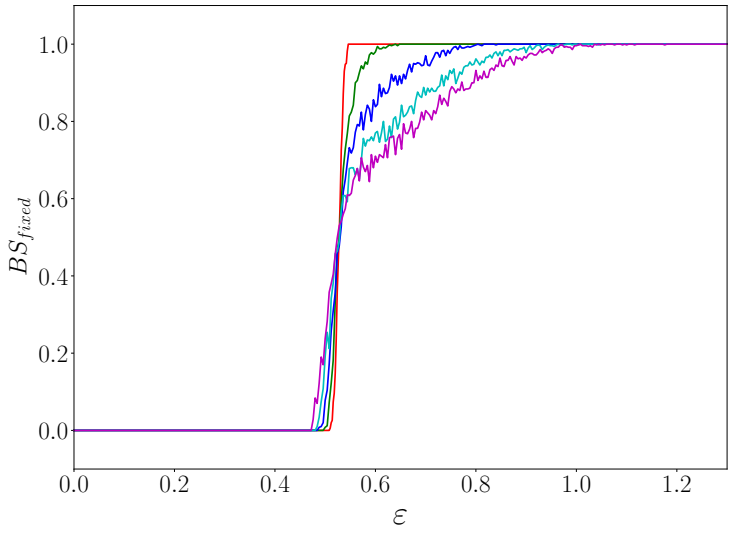

Figure 2.7: Dependence of the fraction of initial states BS_{fixed} attracted to the fixed point state, on the coupling strength ε, for a group of chaotic Rössler oscillators with parameters $\omega = 0.41$, $\delta = 0.0026$, $a = 0.15$, $b = 0.4$ and $c = 8.4$ in Eqn. 2.1, coupled to a common external chaotic Lorenz system with parameters $\sigma = 10.0$, $\beta = 8.0/3.0$ and $r = 25.0$ in Eqn. 2.3. In the 5 curves are obtained from initial states randomly distributed in a box of linear size $l = 2$ (red), 4 (green), 6 (blue), 8 (cyan), 10 (magenta) in the x, y and z coordinates.

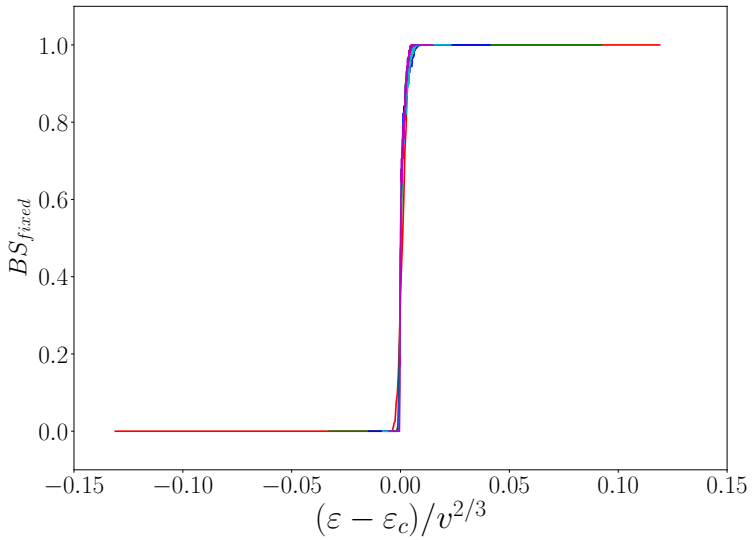

Figure 2.8: Dependence of the fraction of initial states BS_{fixed} attracted to the fixed point state, on the appropriate scaling of coupling strength ε, for a group of chaotic Rössler oscillators with parameters $\omega = 0.41$, $\delta = 0.0026$, $a = 0.15$, $b = 0.4$ and $c = 8.4$ in Eqn. 2.1, coupled to a common external chaotic Lorenz system with parameters $\sigma = 10.0$, $\beta = 8.0/3.0$ and $r = 25.0$ in Eqn. 2.3. For the 5 curves obtained in Fig. 2.7, we show data collapse with $v = l^3$, and $\varepsilon_c = 0.524$.

We show the dependence of this fraction BS_{fixed} in Figs. 2.6-2.8 for a group of chaotic Rössler oscillators coupled to an external chaotic Lorenz system as coupling strength is varied. It is evident that there is a sharp transition to complete control, where the spatiotemporal fixed point state is globally attracting, at sufficiently strong coupling. Namely, there is a critical coupling strength ε_c beyond which the intrinsic chaos of the oscillators is suppressed to fixed points, over a very large basin of initial states.

Note that qualitatively similar results, namely emergence of fixed point states at large enough coupling, are obtained over a wide range of parameters in Eqns. 2.1-2.3, indicating robustness of the phenomenon. However quantitatively, the precise value of ε_c may depend on the parameters of the system.

For instance, the onset of the fixed point state for Rössler oscillators coupled to an external chaotic Lorenz system, for different values of parameter c in Eqn. 2.1, is independent of the parameter, as this parameter influences the lyapunov exponent of the intrinsic dynamics of the Rössler oscillators very little. On the other hand, external Lorenz systems with varying parameter r in Eqn. 2.3 significantly affects ε_c (cf. Fig. 2.6). This can be rationalized by noting that the lyapunov exponent of the intrinsic dynamics of

the external system increases linearly with r, and it is clearly observed that as the lyapunov exponent of the external system increases, the transition shifts to higher coupling strengths. Namely, it takes stronger coupling to yield control to steady states as the common (dissimilar) external system gets more chaotic.

Lastly, note that we have not explicitly put in any feedback loops designed to achieve the steady states, as often used in control schemes relevant to engineered systems. Rather we have explored the naturally emergent behaviour of the system. Also interestingly, since the stabilization of the steady states is independent of system size, if this were to be used as a control strategy, arbitrarily large groups could potentially be controlled by just *one* external chaotic system.

2.5 Control to Steady States via an External Hyper-chaotic Oscillator

We have checked the generality of the results by considering a more stringent case of a group of chaotic oscillators coupled to an external hyper-chaotic oscillator, given by:

$$\begin{aligned} \dot{x}_{ext} &= (k'-2)x_{ext} - y_{ext} - G(x_{ext} - z_{ext}) + \frac{\varepsilon}{N}\sum_{j=1}^{N}(x_j - x_{ext}) \\ \dot{y}_{ext} &= (k'-1)x_{ext} - y_{ext} \\ \dot{z}_{ext} &= -w_{ext} + G(x_{ext} - z_{ext}) \\ \dot{w}_{ext} &= \beta' z_{ext} \end{aligned} \tag{2.4}$$

$$\text{where} \quad G(u) = \frac{1}{2}b'\{|u-1| + (u-1)\}$$

where k', β', b' are the parameters determining the dynamics of the oscillator.

We have coupled one variable (specifically, x_{ext}) of the hyper-chaotic external oscillator with one variable (specifically, x) of the group of chaotic Rössler oscillators.

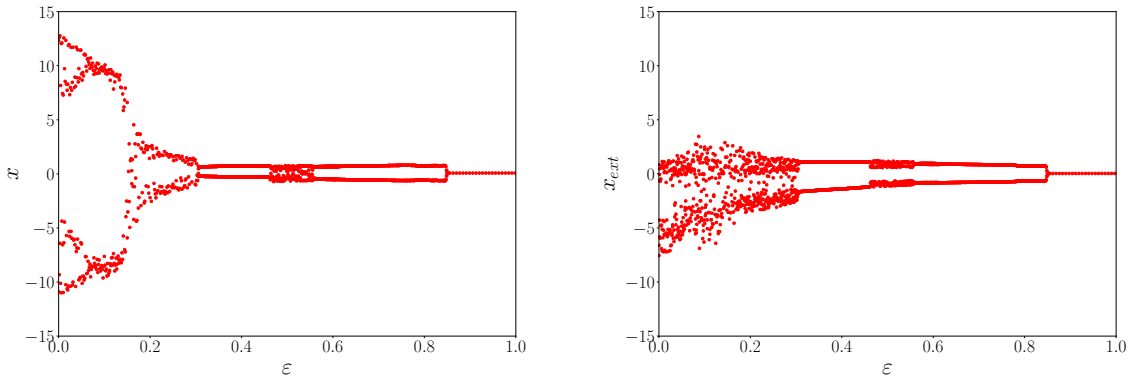

Figure 2.9: Bifurcation diagram, with respect to the coupling strength ε, of one representative oscillator of the group (left) and the external system (right), when the external system is hyper-chaotic with parameters $k' = 3.85$, $\beta' = 18.0$ and $b' = 88.0$ in Eqn. 2.4, and the group consists of chaotic Rössler oscillators with parameters $\omega = 0.41$, $\delta = 0.0026$, $a = 0.15$, $b = 0.4$ and $c = 8.4$ in Eqn. 2.1.

Interestingly, we again find that the intrinsically chaotic Rössler oscillators go to fixed points, when coupled to a common external hyper-chaotic oscillator, for sufficiently strong coupling (cf. Fig. 2.9). Further, it is apparent from Fig. 2.10 which displays the phase portraits of the Rössler oscillators at different ε, that the group of oscillators become regular when coupling strength is high.

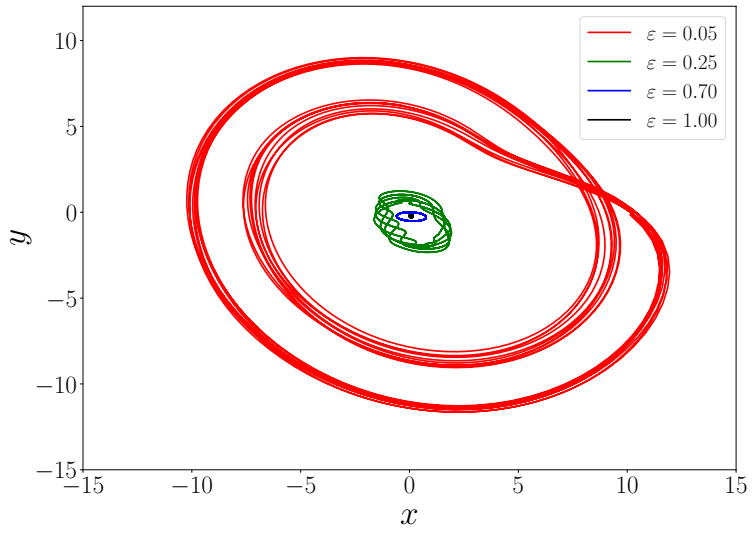

Figure 2.10: Phase portrait of a representative Rössler oscillator from the group with parameters $\omega = 0.41$, $\delta = 0.0026$, $a = 0.15$, $b = 0.4$ and $c = 8.4$ in Eqn. 2.1, coupled to a common external hyper-chaotic oscillator with parameters $k' = 3.85$, $\beta' = 18.0$ and $b' = 88.0$ in Eqn. 2.4, at different coupling strengths ε.

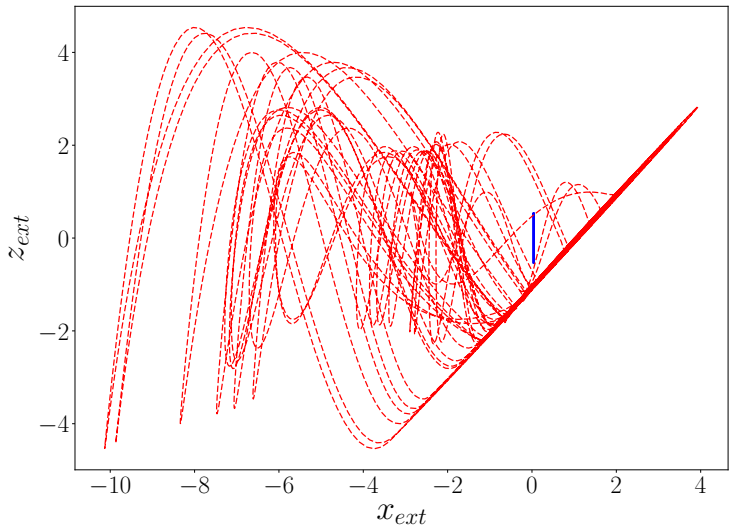

Figure 2.11: Phase portrait of the external hyper-chaotic oscillator with parameters $k' = 3.85$, $\beta' = 18.0$ and $b' = 88.0$ in Eqn. 2.4, for the case of an uncoupled external oscillator (red) and an oscillator with coupling to a group of chaotic Rössler oscillator with parameters $\omega = 0.41$, $\delta = 0.0026$, $a = 0.15$, $b = 0.4$ and $c = 8.4$ in Eqn. 2.1, with coupling strength $\varepsilon = 1.0$ (blue).

Fig. 2.11 shows the phase portrait for the external hyper chaotic oscillator. Again it is clear that at high coupling strengths, the dynamics of the hyper-chaotic system becomes regular. Further the size of the emergent external attractor is very small, though not a fixed point.

Note that when coupling strength $\varepsilon > \varepsilon_c$, the $(x_{ext} - z_{ext} - 1)$ term in Eqn. 2.4 becomes less than zero, implying that $G(x_{ext} - z_{ext})$ is always zero. So the dynamical equations for $\dot{x}_{ext}$ and $\dot{z}_{ext}$ becomes uncoupled, yielding two independent sub-sets of equations, with one coupled sub-set comprising of $\dot{x}_{ext}$ and $\dot{y}_{ext}$, and another coupled sub-set comprising of $\dot{z}_{ext}$ and $\dot{w}_{ext}$.

2.6 Stability Analysis

We investigate the linear stability of the steady state obtained when a group of intrinsically chaotic Rössler oscillators is coupled to a common external intrinsically chaotic Lorenz system, via the eigenvalues of the Jacobian matrix evaluated at those fixed points. Specifically, the Jacobian for N number of oscillators and an external oscillator is given

by $3(N+1) \times 3(N+1)$ matrix. Calculating each term using Eqns. (2.1) and (2.3), we obtain the Jacobian matrix to be:

$$J = \begin{pmatrix} -\sigma-\varepsilon & \sigma & 0 & \frac{\varepsilon}{N} & 0 & 0 & . & . & . & . \\ r-z_0 & -1 & -x_0 & 0 & 0 & 0 & . & . & . & . \\ y_0 & x_0 & -\beta & 0 & 0 & 0 & . & . & . & . \\ \varepsilon & 0 & 0 & -2\delta x_1 y_1 - \varepsilon & -\omega - \delta(x_1^2 + 3y_1^2) & -1 & . & . & . & . \\ 0 & 0 & 0 & \omega + \delta(3x_1^2 + y_1^2) & 2\delta x_1 y_1 + a & 0 & . & . & . & . \\ 0 & 0 & 0 & z_1 & 0 & x_1 - c & . & . & . & . \\ . & . & . & . & . & . & . & . & . & . \\ . & . & . & . & . & . & . & . & . & . \\ . & . & . & . & . & . & . & . & . & . \\ . & . & . & . & . & . & . & . & . & . \end{pmatrix}$$

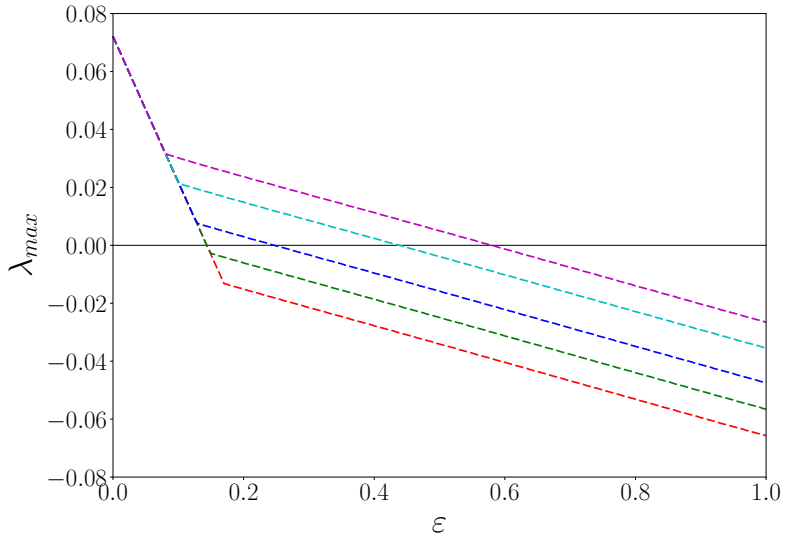

Figure 2.12: Maximum real part λ_{max} of the eigenvalues of the Jacobian at the fixed points, as a function of coupling strength ε, for the external Lorenz system having parameters $\sigma = 10.0$, $\beta = 8.0/3.0$ and (bottom to top) $r = 24.7, 25.0, 25.3, 25.7, 26.0$ in Eqn. 2.3 and group of chaotic Rössler oscillator with parameters $\omega = 0.41$, $\delta = 0.0026$, $a = 0.15$, $b = 0.4$ and $c = 8.4$ in Eqn. 2.1.

At each coupling strength, there is a set of $3(N+1)$ eigenvalues of the Jacobian. We show the maximum real part λ_{max} of the eigenvalues as a function of coupling strength ε in Fig. 2.12. Naturally, since the group of oscillators and the external oscillator are

intrinsically chaotic, $\lambda_{max} > 0$ for $\varepsilon = 0$. However, it is clear that at a critical value of coupling ε_c all eigen values are negative, indicating that all the oscillators in the group and the external system go to stable fixed points (cf. Fig. 2.12).

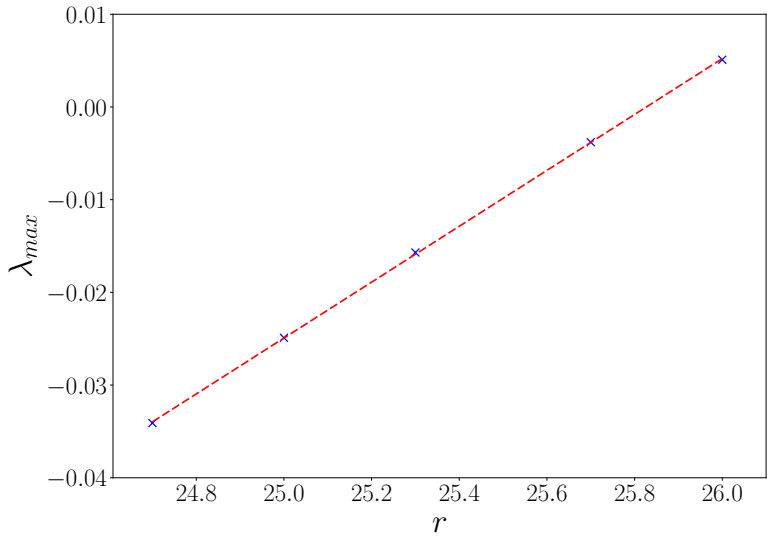

Figure 2.13: Dependence of λ_{max} on parameter r of the external Lorenz system, at fixed coupling strength ($\varepsilon = 0.5$ here), for the external Lorenz system with parameters $\sigma = 10.0$ and $\beta = 8.0/3.0$ in Eqn. 2.3 and group of chaotic Rössler oscillator with parameters $\omega = 0.41$, $\delta = 0.0026$, $a = 0.15$, $b = 0.4$ and $c = 8.4$ in Eqn. 2.1.

Note that the ε_c obtained through linear stability analysis is smaller than that observed from generic random initial states, as displayed in the bifurcation plots. So we undertook additional numerical simulations from initial states sufficiently close to the fixed point solutions and verified that for such close-by initial conditions the fixed point state is indeed stable at lower coupling strengths, in accordance with that seen in Fig. 2.12.

Further, from Fig. 2.13 it is clear that λ_{max} increases linearly with increasing parameter r in the external Lorenz system (cf. Eqn. 2.3). This supports the numerical observations that the *critical coupling strength* ε_c *increases linearly with* r, as displayed in Fig. 2.6.

2.7 Conclusions

We investigated the behaviour of an ensemble of uncoupled chaotic oscillators coupled diffusively to an external chaotic system. The common external system may be similar or

dissimilar to the group. We explored all possible scenarios, with the intrinsic dynamics of the external system ranging from chaotic to hyper-chaotic. Counter-intuitively, we found that an external system manages to successfully steer a group of chaotic oscillators on to steady states at sufficiently high coupling strengths when it is *dissimilar* to the group, rather than identical. So while the group of oscillators coupled to an identical external system synchronizes readily, surprisingly enough, control to fixed states is achieved *only* if the external oscillator is dissimilar. We indicate the generality of this phenomenon by demonstrating the suppression of chaotic oscillations by coupling to an external hyper-chaotic system.

Further, for the case of coupling to a non-identical external system, we quantified the efficacy of control by estimating the fraction of generic random initial states where the intrinsic chaos of the oscillators is suppressed to fixed points, a measure analogous to basin stability. We showed that there was a sharp transition to complete control, where the spatiotemporal fixed point is a global attractor, after a critical coupling strength.

In summary, our results demonstrate robust control of a group of chaotic oscillators to fixed points, by diffusive coupling to a dissimilar external chaotic system. This suppression of chaos occurs for arbitrarily large groups of chaotic oscillators at the same critical coupling strength, indicating that coupling to just *one* external chaotic system can suppress the intrinsic chaos of a *large* set of chaotic oscillators. We thus suggest a way in which chaos in natural systems may potentially be tamed, and our observations may also be used in design of potent control strategies in engineering contexts.

Chapter 3

Control of hierarchical networks by coupling to an external chaotic system

Adapted from the work published in :

Chaurasia, S. S., Sinha, S., "Control of hierarchical networks by coupling to an external chaotic system", ***Europhysics Letters*** 125., (2019) 50006

3.1 Introduction

Science of complex systems is an active area of research that has helped in understanding large interactive systems ranging from man-made systems to natural systems, such as Josephson junction arrays [33], chemical reactions [34], semiconductor lasers [35], power grids [36, 37], neurons [38] and circadian pacemakers [39]. These complex systems typically consist of oscillators, whose intrinsic dynamics may be periodic, quasi-periodic or chaotic. On coupling such oscillators one obtains a variety of spatiotemporal patterns, such as synchronization [40, 41].

An important specific research direction involves the control of spatiotemporal patterns. Of particular significance is the suppression of chaos to steady states [42, 43, 44, 45, 46, 47], namely the stabilization of steady states in complex systems comprised of intrinsically chaotic sub-systems. Such fixed point dynamics serve as a target of control mechanisms, ranging from the stabilization of coupled lasers to control of neuronal disorders such as Alzheimer's and Parkinson's disease [21, 22, 23]. Given its wide potential applications, research on the control of chaotic oscillations has seen intense activity over the years.

In this direction it had been demonstrated recently that chaos in an ensemble of oscillators could be suppressed through coupling to an external dissimilar chaotic system [48]. Here we will demonstrate a very significant generalization of the idea, to the *control of an entire hierarchical network by coupling to a single external chaotic system*, indicating the enormous scope of controlling large networks of chaotic systems through a single external system.

Hierarchical networks [49] combine properties of scale-free topology and high clustering of the nodes, and describe connections characteristic of many real-life networks ranging from metabolic networks to webpage and social networks. In particular we consider a generic hierarchical network (see schematic in Fig. 3.1), with intrinsically chaotic oscillators at different levels of the hierarchy. We consider level 0 to represent an *external system*, which may be *dissimilar* to all other oscillators in the network. The oscillators at each level of hierarchy are connected to one oscillator in the level above it and a cluster of oscillators in the level below it in the hierarchy. For instance in the example illustrated in the schematic, each of the three oscillators at level 1 are connected to the oscillator at level 0 (i.e. one level above in the hierarchy) and to the three oscillators at level 2 (i.e. one level below in the hierarchy).

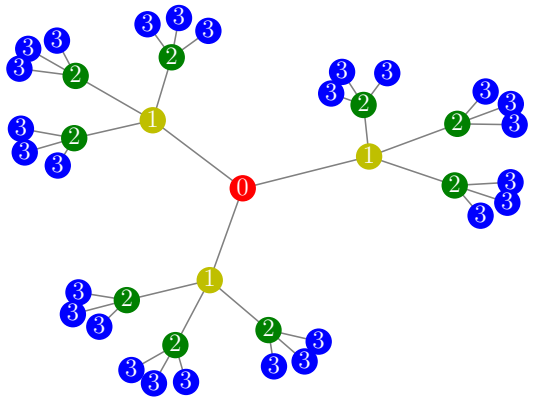

Figure 3.1: Schematic diagram of a hierarchical network with three levels of hierarchy, derived in an iterative way by replicating the initial cluster. The tiers in the hierarchy are labelled by $l = 0, 1, 2, 3$ and displayed in distinct colours.

The number of oscillators at different levels of the hierarchy is denoted by N_l, with level 0 of the network having *one* oscillator (i.e. $N_0 = 1$), and the state variables of the i^{th} oscillator at level l of the hierarchical network is denoted by $\mathbf{X}_i^{(l)}$, with $i = 1, \ldots N_l$.

In this work we will consider representative 3-dimensional systems, i.e $\mathbf{X}_i^{(l)} \equiv \{x_i^{(l)}, y_i^{(l)}, z_i^{(l)}\}$, with the dynamics of the oscillators at different levels $l = 0, \ldots N$ of the hierarchy given as follows:

$$\begin{aligned}
\frac{dx_i^{(l)}}{dt} &= f_l(\mathbf{X}_i^{(l)}) + \varepsilon[(\langle x^{(l+1)}\rangle - x_i^{(l)}) + (x_j^{(l-1)} - x_i^{(l)})] \\
\frac{dy_i^{(l)}}{dt} &= g_l(\mathbf{X}_i^{(l)}) \\
\frac{dz_i^{(l)}}{dt} &= h_l(\mathbf{X}_i^{(l)})
\end{aligned} \tag{3.1}$$

where $\langle x^{(l+1)}\rangle = \frac{1}{N_{l+1}} \sum x_i^{(l+1)}$ is the mean-field of the x-variable of the oscillators at level $l+1$ of the hierarchy, with the sum running over all the nodes at level $l+1$ connected to level l. The index j denotes the node at the previous level $l-1$ connected to the oscillator at level l. So each oscillator at level l of the hierarchy couples via the mean-field of the oscillators below it in the hierarchy (i.e. at level $l+1$) and diffusively to the parent node at level $l-1$. The coupling strength is given by the real positive constant ε.

The two extremal levels, $l = 0$ (namely the *external system*) and $l = k$, have no

oscillators at the $l-1$ and $l+1$ levels respectively. So the first dynamical equation of Eqn. 3.1 for the zeroth level is $\frac{dx_0}{dt} = f_0(\mathbf{X}_0) + \varepsilon(\langle x^{(1)} \rangle - x_0)$ and for the last level $l = k$ is $\frac{dx_i^{(k)}}{dt} = f_k(\mathbf{X}_i^{(k)}) + \varepsilon(x_j^{(k-1)} - x_i^{(k)})$

We consider all oscillators in the network at levels $l = 1, \ldots k$ to be Rössler oscillators in the chaotic region, with dynamical equations [50]:

$$\begin{aligned} f_l(x, y, z) &= -(\omega + \delta(x^2 + y^2))\ y - z \\ g_l(x, y, z) &= (\omega + \delta(x^2 + y^2))\ x + a\ y \\ h_l(x, y, z) &= b + z(x - c) \end{aligned} \tag{3.2}$$

Only the single oscillator at the zeroth level $l = 0$, is considered to be dissimilar, and in particular is a Lorenz system in the chaotic region. So at level 0 of the hierarchical network the intrinsic dynamical equations are:

$$\begin{aligned} f_0(x, y, z) &= \sigma\ (y - x) \\ g_0(x, y, z) &= x\ (r - z)\ -\ y \\ h_0(x, y, z) &= x\ y\ -\ \beta\ z \end{aligned} \tag{3.3}$$

Specifically, we consider the parameters of the Rössler oscillators to be $\omega = 0.41$, $\delta = 0.0026$, $a = 0.15$, $b = 0.4$ and $c = 8.4$ in Eqn. 3.2, and the parameters of the Lorenz system to be $\sigma = 10.0$, $\beta = 8.0/3.0$, and $r = 25.0$ in Eqn. 3.3. These parameter sets ensure that each oscillator is in the *chaotic* region when uncoupled. So in this hierarchical network, the external system at level $l = 0$ is a chaotic Lorenz system, while the rest of the oscillators at levels $l = 1, \ldots k$ are chaotic Rössler oscillators.

3.2 Emergent Controlled dynamics

Fig. 3.2 shows the bifurcation diagram of one representative oscillator from each level of hierarchy $l = 0, 1, 2, 3$ in the network shown schematically in Fig. 3.1. The emergent behaviour is qualitatively the same for any number N_l of oscillators attached to level l. At very low coupling strengths all the oscillators yield their intrinsic chaotic dynamics. However, beyond a critical coupling strength ($\varepsilon_c \sim 0.4$), there is sudden transition from large chaotic oscillations to steady states. The chaos is suppressed to different fixed points at the different levels of hierarchy, though the emergent steady state is the same for all

oscillators at a particular level.

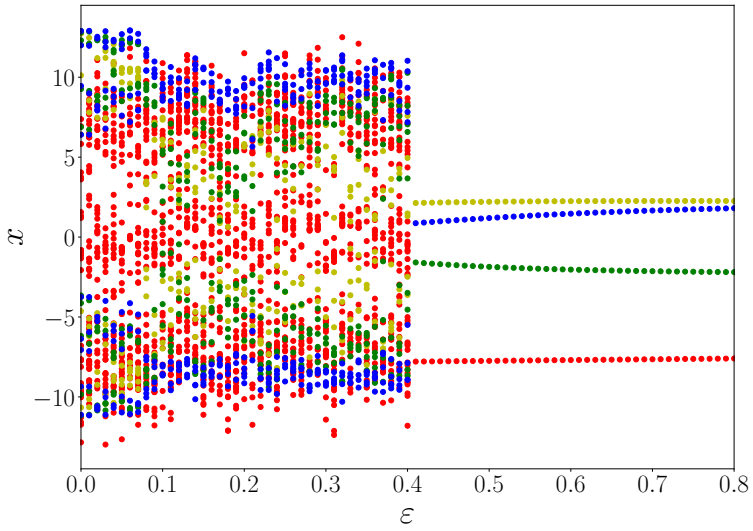

Figure 3.2: Bifurcation diagram, with respect to coupling strength ε, of one representative oscillator from the three levels of hierarchy, and the external system. Colours correspond to the hierarchy level of the oscillators, as given in Fig. 3.1. In all bifurcation diagrams in this work, we show the x-variable of the Poincare section of the phase curves of the oscillators at $y = y_{mid}$, where y_{mid} is the mid-point along y-axis of the span of the oscillator.

Fig. 3.3 shows the projection of phase portraits on the $x-y$ plane of one representative oscillator from each level of hierarchy at intermediate coupling strength $\varepsilon = 0.2$. The colours correspond to the hierarchy level as illustrated in the schematic diagram. It is evident that the oscillators at the level closest to the external system are most distorted. At levels further from the external system (i.e. for larger l), the oscillations remain closer to their intrinsic dynamics. The dots in the figure show the fixed points obtained at high coupling strength ($\varepsilon = 0.6$).

So we find that the chaotic oscillators at *all levels of hierarchy* can be controlled to a steady state, at sufficiently high coupling strengths, by a single external chaotic Lorenz system. The results are unchanged on increasing the number of oscillators at a level N_l, indicating that the control is effective *independent of system size*.

In order to ascertain the robustness of the control to steady states, we explore the dynamics under parametric perturbations. Fig. 3.4 displays representative results, and clearly shows that the emergent fixed point is robust under fluctuations in parameters, at all levels of hierarchy.

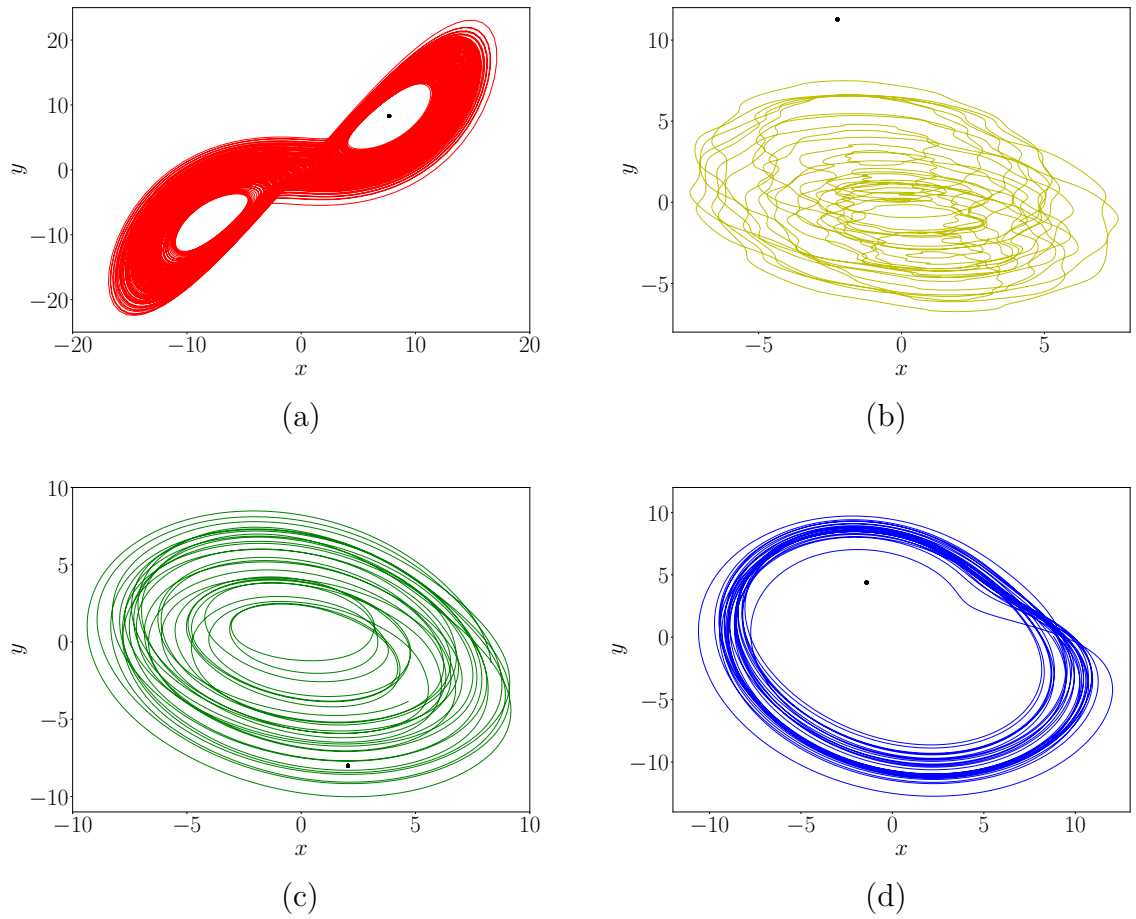

Figure 3.3: Phase portraits of (a) the external system and (b, c and d) one representative oscillator from each level of hierarchy, for $\varepsilon = 0.2$. The dots are the fixed points obtained for $\varepsilon = 0.6$. The colours represent the different hierarchy levels as given in Fig. 3.1.

Further, we explored the dynamics of the network with increasing levels of hierarchy and increasing number of elements at each level of the hierarchy. We found that the global control of the network to steady states, mediated by a single external system, remained effective, even for large number of hierarchy levels. Note that the information transfer here is a two-way process, and so the controlled states may be de-stabilized by perturbations in levels both above and below it in the hierarchy. So the fact that the chaos suppression is robust under the influence of a *single* dissimilar external system, even when the number of hierarchy levels increases, is indeed quite remarkable.

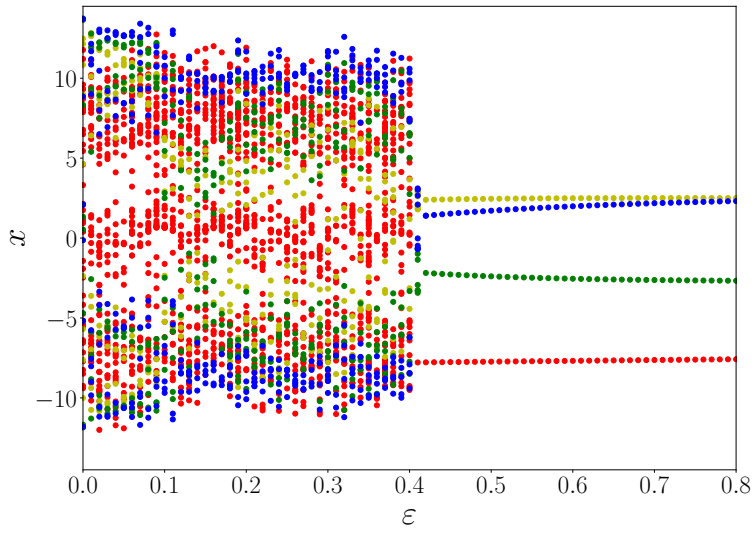

Figure 3.4: The effect of parametric perturbations on the bifurcation diagram in Fig. 3.2. The figure shows the dynamics with respect to coupling strength ε, of one representative oscillator from the three levels of hierarchy, and the external system, in colors given by the scheme in Fig. 3.1.

3.3 Synchronization at a hierarchy level

It is evident from Fig. 3.2 that the oscillators at each level of hierarchy evolve to different fixed points, i.e. there is no synchronization across different levels, though there is synchronization within a level. Here we examine the advent of the intra-level synchronization within a hierarchy level in the network, as a function of coupling strength. In order to do so, we calculate the synchronization error of the oscillators at a particular level l of the hierarchical network, averaged over time T, given as:

$$Z = \frac{1}{T}\sum_{t}\sqrt{(\bar{x^2})_t - (\bar{x}^2)_t} \tag{3.4}$$

where $(\bar{x})_t = \frac{1}{N_l}\sum_{i=1}^{N_l} x_i^{(l)}$ and $(\bar{x^2})_t = \frac{1}{N_l}\sum_{i=1}^{N_l}(x_i^{(l)})^2$ are the average value of x and x^2 of the oscillators, at an instant of time t, at level l of the hierarchy. Further we average Z over different initial states to obtain an ensemble averaged synchronization error $\langle Z\rangle$.

Fig. 3.5 shows the variation of the ensemble-averaged synchronization error $\langle Z\rangle$ of the different levels in the hierarchy with respect to coupling strength. It is evident that oscillators within each level of hierarchy are also synchronized when the oscillations are

suppressed, i.e oscillators at the same level evolve to the same fixed points, even though there is *no direct coupling between them.*

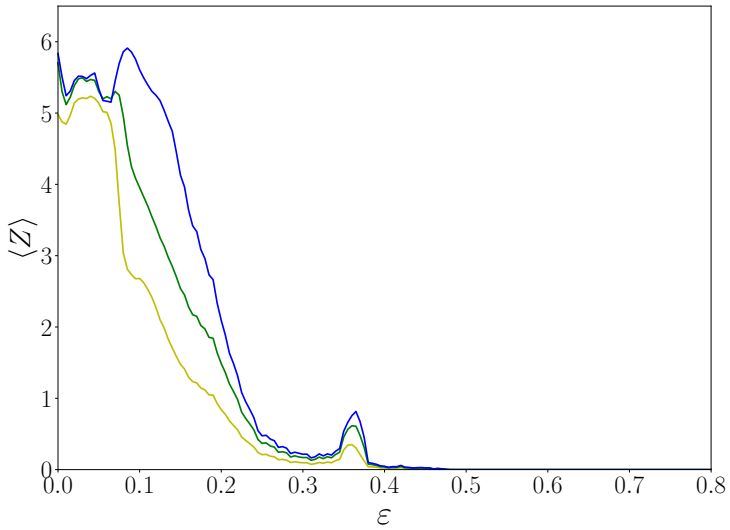

Figure 3.5: Synchronization error $\langle Z \rangle$ of the Rössler oscillators, with respect to coupling strength, averaged over 1000 initial conditions. The colours correspond to the different hierarchy levels, as given in Fig. 3.1.

3.4 Basin Stability of Steady States

The commonly employed linear stability analysis, based on the linearization in the neighbourhood of fixed points, provides only local information about the stability at the fixed point. It cannot accurately indicate the stability for large perturbations, nor indicate the size of the basin of attraction of the dynamics, especially in the presence of other competing attractors in phase space.

Here we quantify the efficacy of control to steady states by sampling a large set of random initial conditions, spread uniformly over a volume of phase space and estimating the fraction BS_{fixed} of initial states attracted to fixed points. This measure is analogous to recently used measures of basin stability [3, 51] and indicates the size of the basin of attraction for the steady state. $\mathrm{BS}_{fixed} \sim 1$ suggests that the fixed point state is *globally attracting*, while $\mathrm{BS}_{fixed} \sim 0$ indicates that almost no initial state evolves to stable fixed points. *So this measure truly reflects the reliability of control to steady states from generic initial states.*

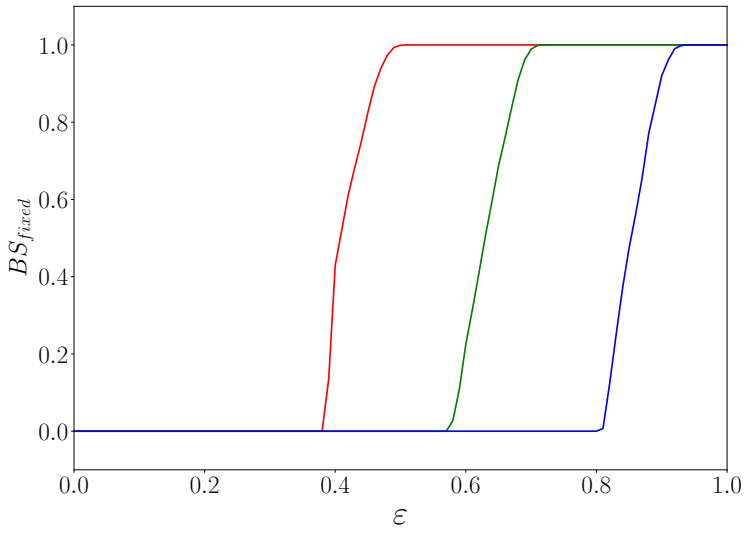

Figure 3.6: Dependence of the fraction of initial conditions attracted to the spatiotemporal fixed point, BS_{fixed}, on the coupling strength ε, averaged over 5000 initial conditions, for three different parameters in Eqns. 3.3: $r = 25$ (red), $r = 25.5$ (green) and $r = 26$ (blue).

We show the variation of BS_{fixed} as a function of coupling strength (cf. Fig. 3.6). It is clear that there is a lower critical value of coupling for which the system does not evolve to the fixed point state for any initial condition, while there is an upper critical value of coupling beyond which $\mathrm{BS}_{fixed} \sim 1$, suggesting that the network gets attracted to a spatiotemporal fixed point for all initial conditions for sufficiently high coupling strengths. In the intermediate range of coupling strengths, the network has a finite probability to get attracted to the spatiotemporal fixed point state from a generic random initial state, as indicated by $\mathrm{BS}_{fixed} > 0$. The values of the critical coupling strengths are dependent on the specifics of the external system, but the qualitative behaviour is similar for all, with global control arising when the hierarchical network is coupled strongly enough to a dissimilar external oscillator.

3.5 Stability Analysis

Now we demonstrate the stability of the steady state through linear stability analysis of the fixed point solution as a function of the coupling strength ε. Fig. 3.7(b) shows the maximum eigenvalue of the Jacobian (J) obtained from the dynamical equations of Eqn. 3.1 for a representative hierarchical network with 2 levels, with each node at each

level coupled to two nodes at the next level.

$$J = \begin{bmatrix} -\sigma-\varepsilon & -\sigma & 0 & \varepsilon/2 & 0 & 0 & . & . & . \\ r-z_0 & -1 & -x_0 & 0 & 0 & 0 & . & . & . \\ y_0 & x_0 & -\beta & 0 & 0 & 0 & . & . & . \\ \varepsilon & 0 & 0 & -2\delta x_1 y_1 - 2\varepsilon & -\omega - \delta x_1^2 - 3\delta y_1^2 & -1 & . & . & . \\ 0 & 0 & 0 & \omega + 3\delta x_1^2 + \delta y_1^2 & 2\delta x_1 y_1 + a & 0 & . & . & . \\ 0 & 0 & 0 & z_1 & 0 & x_1 - c & . & . & . \\ . & . & . & . & . & . & . & . & . \\ . & . & . & . & . & . & . & . & . \\ . & . & . & . & . & . & . & . & . \end{bmatrix}_{21\text{x}21}$$

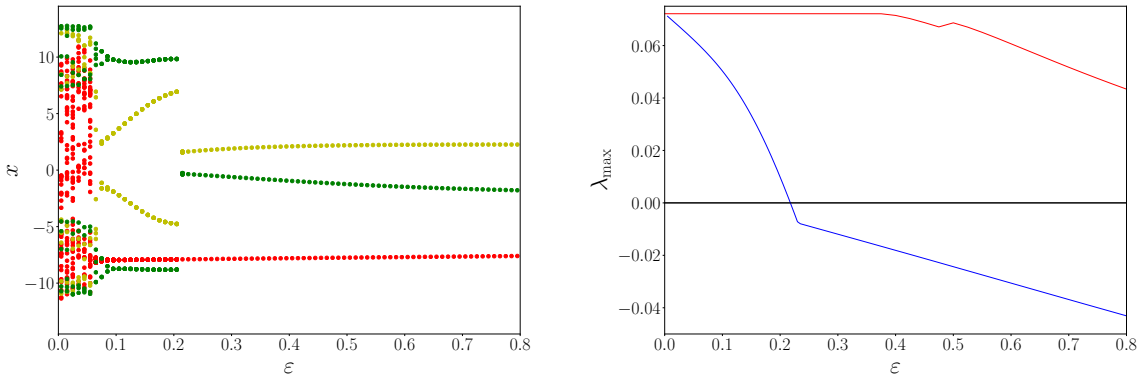

(a) (b)

Figure 3.7: (a) Bifurcation diagram, with respect to coupling strength ε, of one representative oscillator from the two levels of hierarchy, and the external system. Colours correspond to the hierarchy level of the oscillators, as given in Fig. 3.1 and (b) maximum eigenvalue of Jacobian, with respect to coupling strength ε, of the whole system around fixed point, when external system is chaotic Lorenz oscillator (blue) and chaotic Rössler oscillator (red).

It is clearly evident from Fig. 3.7(b) that the fixed point of the system becomes stable around $\varepsilon \sim 0.2$, as the maximum eigenvalue (λ_{max}) attains a negative value. Fig. 3.7(a) shows the bifurcation diagram with initial conditions in the neighbourhood of the fixed point, and we find complete agreement of the numerics with the analytical results. Notice that the suppression of the oscillations occur at a lower coupling strength when the initial state is close to the fixed point solution, than the coupling strength necessary for a generic

random state to be controlled to a steady state. The latter is around $\varepsilon \sim 0.4$ as evident from the basin stability estimates in Fig. 3.6. This indicates that obtaining control that is effective for a large set of initial conditions requires stronger coupling strength than that dictated by linear stability analysis. This further underscores the importance of global stability measures such as Basin Stability in designing control.

3.6 Generality of the results

We have also investigated the dynamics of the hierarchical network when the external system is a Rössler system with parameters that are different from those of all the other oscillators, i.e. the dynamical equations are the same, but the parameters of the oscillator at level 0 are different from all the others in the hierarchical network. We again find that hierarchical network does get controlled, but the chaos suppression now occurs at much higher coupling strengths. For instance, as evident from Fig. 3.8a, the steady states emerge around $\varepsilon \sim 2$ while it emerges around $\varepsilon \sim 0.4$ when the external system is a chaotic Lorenz oscillator. The critical coupling strength is especially high when the external oscillator is *not* a chaotic system. For instance, when the intrinsic dynamics of the external system is a limit cycle (cf. Fig. 3.8b) the coupling strength necessary to effect control to steady states in the hierarchical network is greater than $\varepsilon \sim 3$. So we deduce that *control to steady states is most efficient and occurs at lowest coupling strengths when the external system is chaotic and dissimilar.*

Next we examine a hierarchical network of chaotic Rössler oscillators coupled to an external *hyper-chaotic oscillator* at level 0. The specific hyper-chaotic system chosen was:

$$\begin{aligned} f_{ext}(x,y,z) &= (k'-2)x - y - G(x-z) \\ g_{ext}(x,y,z) &= (k'-1)x - y \\ h_{ext}(x,y,z) &= -w + G(x-z) \\ h'_{ext}(x,y,z) &= \dot{w} = \beta' z \end{aligned} \tag{3.5}$$

where $G(u) = \frac{1}{2}b'\{|u-1| + (u-1)\}$ and k', β', b' are the parameters which determine the oscillator dynamics. This system has efficient electronic circuit analogs, and thus lends itself to experimental verification [46]. From Fig. 3.9 and Fig. 3.10, it is evident that an external hyper-chaotic system is also capable of chaos suppression, with the controlled dynamics being limit cycles here.

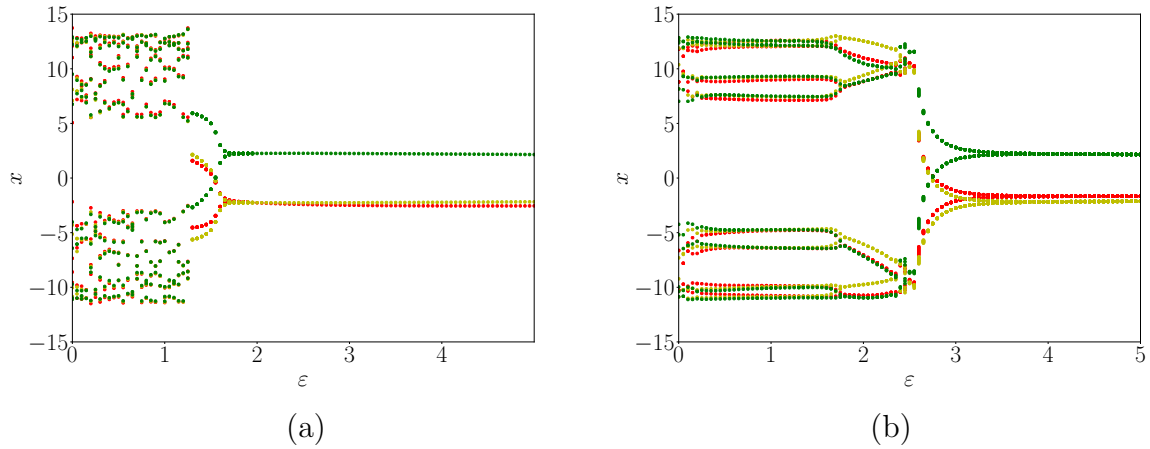

Figure 3.8: Bifurcation diagram, with respect to coupling strength ε, of one representative oscillator from each hierarchy level, with the external system being a Rössler system whose intrinsic dynamics is (a) chaotic and (b) periodic. Colours correspond to the hierarchy level of the oscillators.

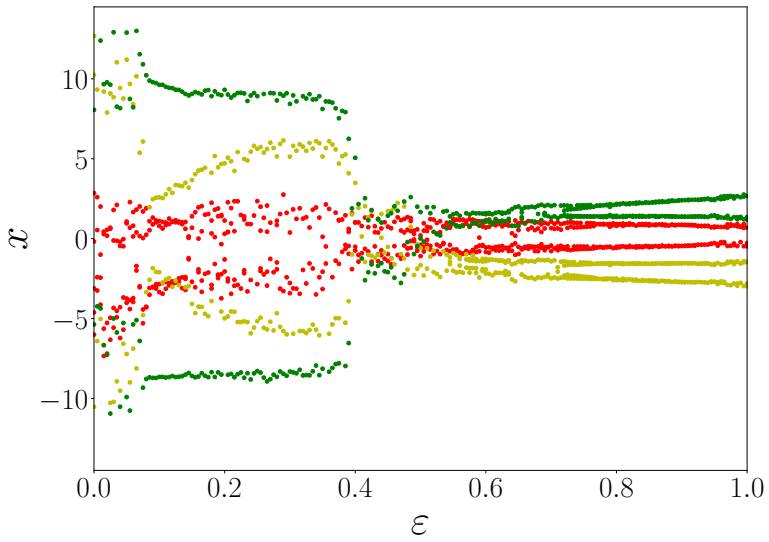

Figure 3.9: Bifurcation diagram, with respect to coupling strength ε, of one representative oscillator from each hierarchy level. Here the external system is a hyper-chaotic oscillator, described by Eqn. 3.5 with parameters $k' = 3.85$, $\beta' = 18.0$, $b' = 88.0$. The colours correspond to the hierarchy level of the oscillators.

Lastly, we investigate the effect of an external linear oscillator on a hierarchical network of chaotic oscillators. Representative results are shown in Fig. 3.11. We find that an external linear oscillator too can suppress the chaos to steady states, in all hierarchy levels, when the coupling strength is sufficiently high. Further Fig. 3.12 shows the dependence on the basin stability for different frequencies of the external linear oscillator. It is

evident from the figure that the suppression of oscillations is stable in a larger window of coupling strengths for higher frequency of the external oscillator.

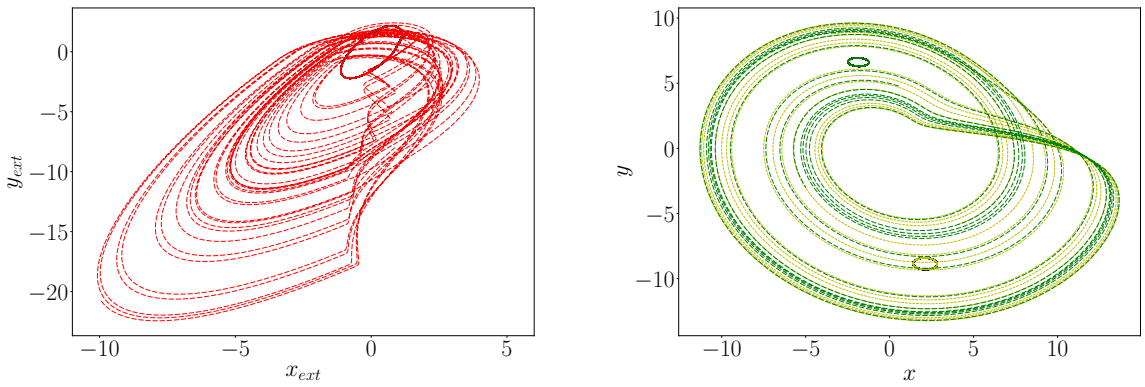

Figure 3.10: Phase portraits of the hyper-chaotic external system (left) and one representative oscillator from each level of hierarchy (right), for $\varepsilon = 0.0$ and 0.9, which correspond to chaotic and one period oscillations respectively. The parameters for hyper-chaotic external system are $k' = 3.85$, $\beta' = 18.0$, $b' = 88.0$ and the colours correspond to the hierarchy level of the oscillators.

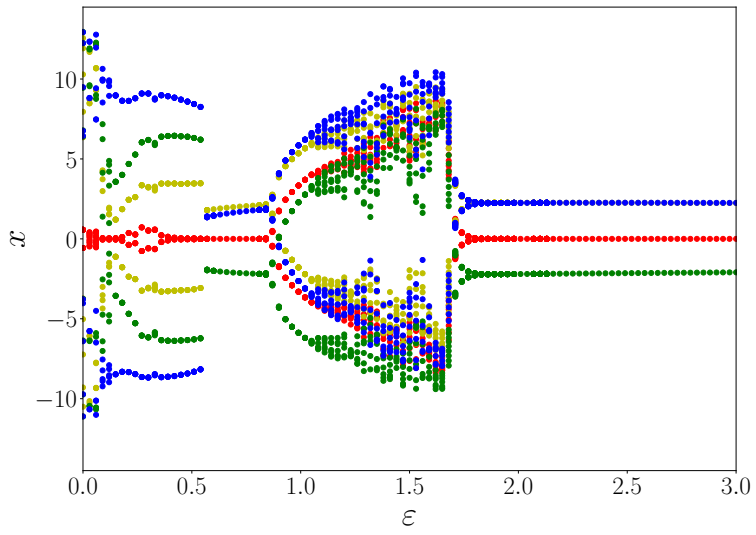

Figure 3.11: Bifurcation diagram, with respect to coupling strength ε, of one representative oscillator from the three levels of hierarchy, and the external system. Here the external system is a linear harmonic oscillator. Colours correspond to the hierarchy level of the oscillators, as given in Fig. 3.1.

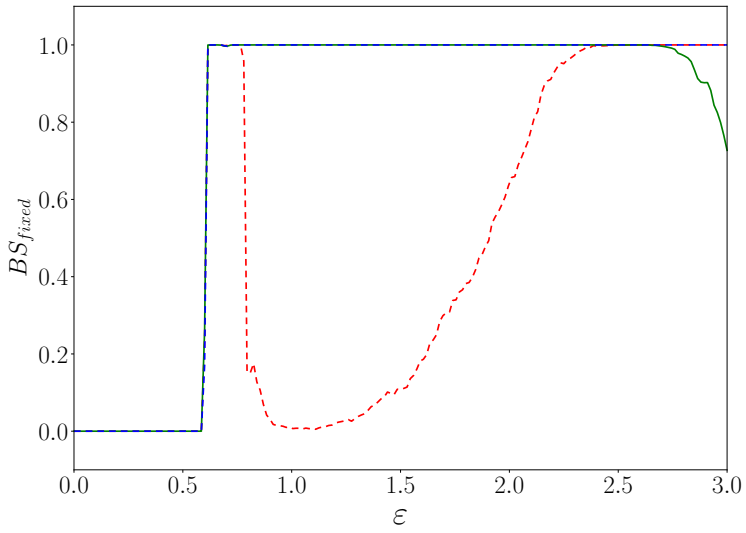

Figure 3.12: Dependence of the fraction of initial conditions attracted to the spatiotemporal fixed point, BS_{fixed}, on the coupling strength ε, averaged over 5000 initial conditions, for three different frequencies of external linear oscillator: $\omega = 1.0$ (red), $\omega = 2.0$ (green) and $\omega = 3.0$ (blue).

So we have explicitly demonstrated that a hierarchical network of intrinsically chaotic systems can be effectively driven to regular states by coupling to a single external system that may be linear, chaotic or hyperchaotic. This suggests that the potential scope of this control mechanism is considerably wide.

3.7 Conclusions

We investigated the behaviour of a hierarchical network of chaotic oscillators, where at the zeroth level of the hierarchy we have *one chaotic external system that is dissimilar to the rest of the oscillators in the network*. Remarkably, this external system managed to successfully steer the chaotic oscillators at all levels of the hierarchy onto steady states, at sufficiently high coupling strengths. So this suggests a potent method to efficiently control chaotic dynamics in a hierarchical network to stable steady states, by simply coupling to an external chaotic system.

3.8 Appendix

In this appendix, we consider a different coupling from in Eqn. 3.1. The number of oscillators at different levels of the hierarchy is denoted by N_l, with level 0 of the network having *one* oscillator (i.e. $N_0 = 1$), and the state variables of the i^{th} oscillator at level l of the hierarchical network is denoted by $\mathbf{X}_i^{(l)}$, with $i = 1, \ldots N_l$.

Again we will consider representative 3-dimensional systems, i.e $\mathbf{X}_i^{(l)} \equiv \{x_i^{(l)}, y_i^{(l)}, z_i^{(l)}\}$, with the dynamics of the oscillators at different levels $l = 0, \ldots N$ of the hierarchy given as follows:

$$\begin{aligned}
\frac{dx_i^{(l)}}{dt} &= f_l(\mathbf{X}_i^{(l)}) + \varepsilon \left[\frac{1}{N_{l+1}+1} \left(x_j^{(l-1)} + \sum x_i^{(l+1)} \right) - x_i^{(l)} \right] \\
\frac{dy_i^{(l)}}{dt} &= g_l(\mathbf{X}_i^{(l)}) \\
\frac{dz_i^{(l)}}{dt} &= h_l(\mathbf{X}_i^{(l)})
\end{aligned} \tag{3.6}$$

Here $\frac{1}{N_{l+1}} \sum x_i^{(l+1)}$ is the mean-field of the x-variable of the oscillators at level $l+1$ of the hierarchy, with the sum running over all the nodes at level $l+1$ connected to level l. The index j denotes the node at the previous level $l-1$ connected to the oscillator at level l. So each oscillator at level l of the hierarchy couples via the mean-field of the oscillators below (i.e. at level $l+1$) and above (i.e. at level $l-1$) in the hierarchy. The coupling strength is given by the real positive constant ε. Specifically we will consider Lorenz oscillator as the external system and Rössler oscillators in the rest of the network.

It is evident from Fig. 3.13 that increasing the number of oscillators at level 2 of the hierarchy increases the required coupling strength to suppress the oscillations to fixed points. However one observes that the chaotic dynamics is controlled to regular limit cycle oscillations even when the number of oscillators increased (cf. Fig. 3.13c and d). In the coupling form in Eqn.3.6, note that the effective contribution of the oscillator in the level above reduces with increasing oscillators in the hierarchy level below, as the interaction is through the mean-field of the state of oscillators in the level $l+1$ and $l-1$. This implies that the flow of information from the external system decreases with increasing levels. So the nature of the controlled regular dynamics depends upon the specific form of coupling and the underlying hierarchical connectivity network. However importantly, we find that the chaotic dynamics is always controlled to regular limit cycles or fixed points for sufficiently high coupling strength in a wide range of systems.

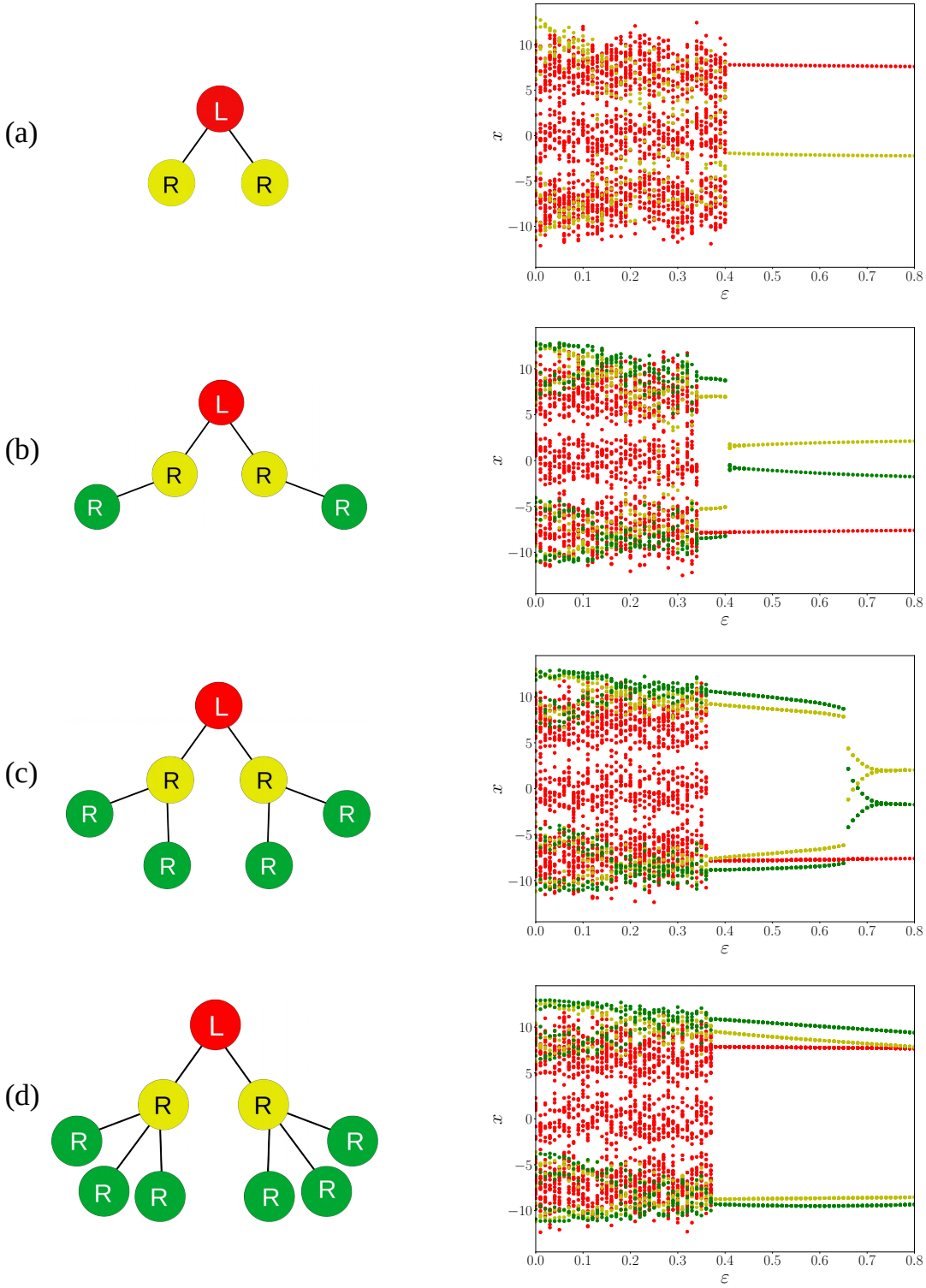

Figure 3.13: Bifurcation diagrams on the right, with respect to coupling strength ε, of one representative oscillator from the all levels of hierarchy, and the external system. Colours correspond to the hierarchy level of the oscillators as shown in the schematic diagrams on the left.

Chapter 4

Environment-induced symmetry breaking in the basin stability of the oscillation-death state

Adapted from the work :

Chaurasia, S. S., Yadav, M., Sinha, S., "Environment-induced symmetry breaking of the oscillation-death state", ***Phys. Rev. E*** 98., (2018) 032223

and

Yadav, M., **Chaurasia, S. S.**, Sinha, S., "Asymmetry in the basin stability of oscillation death states under variation of environment-oscillator links", (To appear in ***NODYCON 2019 Springer Proceedings***).

4.1 Introduction

Complex systems has been a very active area of research over the past few decades, initiated by the discovery that even systems with low degrees of freedom can show a wide range of dynamical patterns. For instance, two or more oscillators, when coupled to each other can show completely synchronized oscillations, in-phase or antiphase synchronized oscillations, oscillation quenching to homogeneous steady states or inhomogeneous steady states, with transitions between different dynamical behaviours obtained by parameter tuning.

In general, oscillation quenching is categorized into homogeneous steady state (HSS) or amplitude death (AD) and inhomogeneous steady state (IHSS) or Oscillation death (OD) [52]. AD refers to the situation where the coupled oscillator systems, under oscillation quenching, evolve to the same fixed point. This type of quenching is relevant in laser systems [17, 18, 19], and is important in situations involving stabilization to a particular fixed point. A lot of mechanisms leading to amplitude death have been found, such as time-delay in the coupling [53, 54], coupling via conjugate variables [55], introduction of large variance of frequencies [56] and coupling to a dissimilar external oscillator [48]. However, oscillation quenching can give rise to oscillation death, a phenomenon that is completely different from AD. Here the oscillators split into two sub-groups, around an unstable fixed point via pitchfork bifurcations, generating a set of stable fixed points. Oscillation death is very relevant to biological systems, as this oscillation quenching mechanism can lead to the emergence of inhomogeneity in homogeneous medium. So, for instance, OD has been interpreted as a mechanism for cellular differentiation [57, 58]. Thus a lot of research effort has centered around transitions from AD to OD [59, 60], and mechanisms that steer the dynamics to the OD state have been investigated. For example, OD can be achieved via parametric modulation in coupled non-autonomous system [61], parameter mismatch (i.e. detuning of parameters) in coupled oscillators [13, 62] and the introduction of local repulsive links in diffusively coupled oscillators [63]. In a complementary direction, some studies have also shown how OD states are eliminated when gradient coupling is introduced in delay induced OD [64].

Our work here focuses on oscillation quenching mechanisms that give rise to inhomogeneous steady states. Our test bed will be a group of oscillators, coupled to a common external system, which is dynamically very distinct from the oscillators. This common external system provides a common "environment" and allows a group of oscillators to be indirectly coupled via an external common medium. When uncoupled, the oscillators

have equal probability to go to either of the OD states. However, we will show that this system displays *symmetry breaking in the basin stability of OD states* when coupled. That is, a specific oscillator-death state is preferentially achieved. This state selection leads to asymmetric distribution of OD states in the ensemble of oscillators, suggesting a natural mechanism that allows the emergence of a favored set of fixed points. Further, we will explore the effect of the oscillator group connecting to the environment through links that switch on and off. We will demonstrate that blinking oscillator-environment connections will remarkably work toward partial restoration of the symmetry of the oscillator-death states, though the presence of some blinking connections reduces the symmetry of the dynamical equations. We then go on to investigate the dynamics as the environment-oscillator links are disconnected one by one. We will show how cutting off the environment-oscillator links leads to a restoration of symmetry in the distribution of OD states. We will further demonstrate that one can use the external medium coupling strength and the environmental damping constant to control the distribution of oscillators in the different OD-states for a given fraction of environment-oscillator links.

4.2 Oscillators Coupled via Common Environment

In the context of many real world systems, interactions can occur through a common medium. For instance, chemical oscillations of catalyst-loaded reactants have been found in a medium of catalyst-free solution, where the coupling is through exchange of chemicals with the surrounding medium [65]. Similarly, in the context of genetic oscillators coupling occurs by diffusion of chemicals between cells and extracellular medium [66, 67, 68, 69]. Further, in a collection of circadian oscillators, the concentration of neurotransmitter released by each cell can induce collective behaviour [70, 71].

In general, such cases occur due to the common medium, referred to as a *common environment*, interacting with the dynamical systems. So a model system mimicking this scenario consists of N identical oscillator systems $\mathbf{x}_i$, $i = 1, \ldots, N$ coupled through a (possibly time-varying) environment, denoted by variables $\mathbf{u}$, whose most general dynamical equations is given as:

$$\dot{\mathbf{x}_\mathbf{i}} = f_\mathbf{x}(\mathbf{x}_i) + \varepsilon_{\text{ext}}\ g(\mathbf{u}) \tag{4.1}$$

and

$$\dot{\mathbf{u}} = f_\mathbf{u}(\mathbf{u}) + \varepsilon_{\text{ext}}\ h(\mathbf{x}_1, \mathbf{x}_2, \ldots, \mathbf{x}_n) \tag{4.2}$$

where $\mathbf{x_i}$ and $\mathbf{u}$ are the variables of the oscillators and the environment respectively [72]. For instance, in the case of biological cells, this would be a vector whose components are the concentrations of various biochemical species in cell and a vector of concentrations of the relevant biochemical species in the exterior of the cells respectively. The coupling parameter ε_{ext} would reflect the ratio of the total intracellular volume to the volume of the environment. The interaction of cells and environment may occur through the diffusion and transport of chemical species across the cell membranes or through the effects of the activation of receptors on the cell membrane. Now a variety of models of biochemical oscillators coupled through an environment are described by equations of this form [65, 66, 67, 68, 69, 70, 71, 73, 74, 75, 76, 77, 78, 79]. So this framework unifies many specific models of particular systems [72], and allows us to obtain some basic general results which potentially apply to all of them.

Specifically in this work we will consider a collection of Stuart-Landau oscillators [1] whose coupling is mediated via a common external environment. The Stuart-Landau oscillator is a generic two-dimensional oscillator of broad relevance. Complex systems often undergo Hopf bifurcations and sufficiently close to such a bifurcation point, the variables which have slower time-scales can be eliminated. This leaves us with a couple of first order ordinary differential equations, popularly known as the Stuart-Landau (SL) system.

So in this work we consider a group of N globally coupled SL oscillators (i.e. $\mathbf{x}_i = (x_i, y_i)$ in Eqn. 4.1), with the oscillators within the group are coupled via the mean field $\bar{x}$ of the x-variable. Additionally, this oscillator group also couples to an external common environment, denoted by a single-variable u. The environment exponentially decays to zero, with decay constant k, when uncoupled from the oscillator group, namely $f_u = -ku$ in the general dynamical equations. When coupled to the oscillators, the environment provides an input to the oscillators, as well as receives a feedback proportional to the mean field $\bar{y}$ of the y-variables of the oscillators. The strength of this feedback from the external system is given by the coupling strength ε_{ext}. So the complete dynamics of the group of oscillators, along with the external environment, is then given by the following evolution equations:

$$\begin{aligned} \dot{x}_i &= (1 - x_i^2 - y_i^2)x_i - \omega y_i + \varepsilon_{\text{intra}}(q\bar{x} - x_i) \\ \dot{y}_i &= (1 - x_i^2 - y_i^2)y_i + \omega x_i + \varepsilon_{\text{ext}} u \\ \dot{u} &= -ku + \varepsilon_{\text{ext}}\bar{y} \end{aligned} \tag{4.3}$$

Here ω is the angular frequency of oscillator and $\varepsilon_{\text{intra}}$ reflects the strength of intra-group coupling, with $\bar{x} = \frac{1}{N}\sum_{i=1}^{N} x_i$ and $\bar{y} = \frac{1}{N}\sum_{i=1}^{N} y_i$. In this coupling scheme, q is a control parameter for the mean-field interaction, describing the influx and consequent influence of the mean field in the oscillator group. A similar type of coupling mechanism was suggested in the context of intercell communication of synthetic gene oscillators via a small autoinducer molecule [75]. As q tends to zero, the effect of the mean-field interaction decreases, suppressing the oscillations of the coupled systems. The limit $q = 0$ indicates no interaction between the oscillators (i.e. they are simply uncoupled oscillators with self-feedback), while the limit $q = 1$ maximizes the interaction with the mean field. At intermediate values of q the oscillators are driven to AD/OD states.

So in our system the common external environment provides an *indirect coupling* conjoining the different oscillators in the group, in addition to the direct coupling within the group. Studies on the effect of an external environment on coupled Stuart-Landau oscillators have revealed phenomena such as the revival of oscillations in a group of oscillators at steady state by coupling to an oscillating group via a common environment [80], phase-flip transitions in a system of oscillators diffusively coupled to the environment [81] and co-existence of in-phase oscillations and oscillation death in environmentally coupled oscillators [82].

In this work we will first explore in Section 4.3 the symmetry-breaking effect of the common external environment on the oscillatory patterns. Further, we will explore the spatiotemporal effects of the time variation and complete disconnection of the oscillator-environment links in Section 4.4 and section 4.5 respectively. Lastly in Section 4.6, we will demonstrate that a constant common environment also leads to pronounced symmetry breaking in the Oscillator Death states, suggesting the generality of our central result.

4.3 Symmetry Breaking in the Oscillator Death States

We first present the bifurcation sequence of the oscillators as a function of the oscillator-environment coupling strength ε_{ext}. The values of $\varepsilon_{\text{intra}}$ and q are fixed at 6.0 and 0.4 so that oscillators are in the oscillation death (OD) state in the absence of coupling to the environment. Here one of the oscillator death states has positive x and negative y, and the other oscillator death state has and negative x and positive y (cf. Fig. 4.1). We call the steady state solution with $x > 0$ the "positive state" and the steady state with $x < 0$ the "negative state". In the bifurcation diagram in Fig. 4.1, the size of the

symbols represent the probability of being in that state, with the probability estimated by sampling over a large number of initial states.

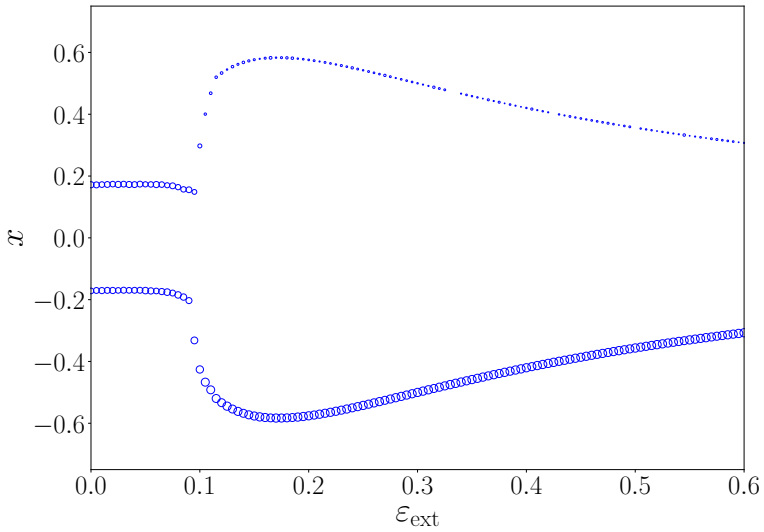

Figure 4.1: Bifurcation diagram of x of one of the Stuart-Landau oscillator in a group, with respect to the coupling strength ε_{ext} of the group with the environment (cf. Eqn. 4.3). The diagram displays the superposition of the system evolving from a large range of random initial states, with $x_i, y_i \in [-1, 1]$ and the environmental variable $u \in [0, 1]$. The size of the circle represent the probability of being in that state (positive or negative). Here we consider the Stuart-Landau oscillators with parameters ω=2.0, $q = 0.4$ and $\varepsilon_{\text{intra}} = 6.0$ (namely in the Oscillator Death region when uncoupled to the environment). The environmental damping constant $k = 0.01$ and the system size $N = 20$.

It is evident from the figure that in the absence of coupling to an external environment, the states of the group of oscillators are symmetrically distributed between the positive and negative states. That is, starting from generic random initial conditions, the group of oscillators will have equal probability to evolve to a positive state or a negative state. So one typically observes an equi-distribution of positive and negative oscillators in a group of Stuart-Landau oscillators in the oscillator death regime, when uncoupled to the environment. This is evident from the bifurcation diagram, which shows equal probability to be in either of the two OD states at $\varepsilon_{\text{ext}} = 0$ (as reflected by symbols of the same size in the positive and negative states in the figure at $\varepsilon_{\text{ext}} = 0$). This behaviour is also clear from the time series of the oscillator group displayed in Fig. 4.2a and histogram 4.3.

Interestingly however, when the oscillator group is coupled to the external environment we observe *symmetry breaking in the basin stability of Oscillator Death states.*

Namely, the group of oscillators in the presence of the environment, preferentially go to one of the oscillator death state. So, typically we do not obtain an equal number of positive and negative states. Rather there is now a *pronounced prevalence of one of the Oscillator Death states.*

This is evident from the bifurcation diagram, which shows unequal probability to be in the OD states, especially at large ε_{ext} ($\varepsilon_{\text{ext}} > 0.1$). This is reflected by symbols of the different sizes in the positive and negative states in the figure at large ε_{ext}. Namely, it is clear that for high coupling strengths an oscillator in the system has a much higher probability of evolving to the negative OD state, as evident from the significantly larger symbols for the negative states vis-a-vis those representing the positive OD states.

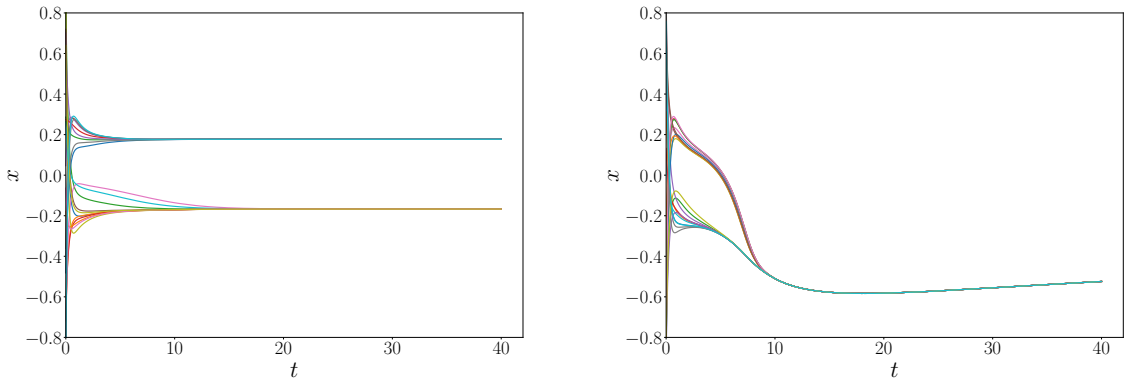

Figure 4.2: Time series of twenty oscillators in the group (shown in distinct colours), (a) in the absence of coupling to an external environment and (b) when the group is connected to the external environment with coupling strength $\varepsilon_{\text{ext}} = 0.6$, and $k = 0.01$.

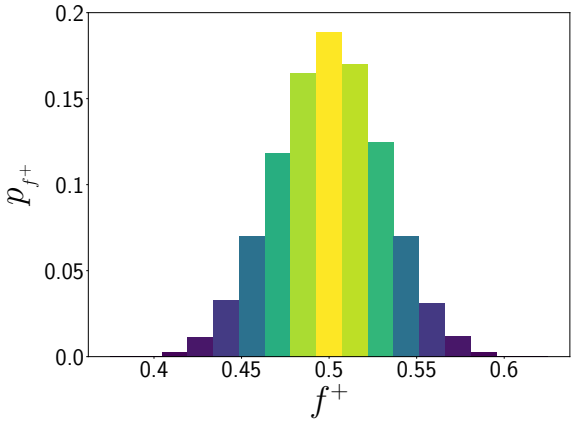

Figure 4.3: Histogram showing the probability of the fraction of oscillators in positive state when the coupling of the oscillator group to the environment $\varepsilon_{ext} = 0$.

This behaviour is also clear from the time series of the oscillator group displayed in Fig. 4.2b, which shows the oscillators preferentially evolving to one of the two OD solutions. Interestingly, note that for a specific initial state *all* oscillators may go to negative OD states in the symmetry-broken parameter region, as seen in Fig. 4.2b. Typically, for low values of damping constant k, a large majority of initial conditions evolve to a state where all oscillators go to one of the OD states (cf. Fig. 4.2b), while for larger k most initial conditions yield a state where oscillators occupy both OD states, but with one state preferentially occupied yielding significant asymmetry as well.

Global Stability of the Oscillator Death States:

Now linear stability analysis shows that the both the OD states are stable, which is consistent with the bifurcation diagram in Fig. 4.1. However, the significant question here is the following: Which state does an oscillator in the system evolve to, starting from initial states that are far from the state? This depends on the relative sizes of the basins of attraction of the states. So we need to consider the *global stability* of the OD states in order to understand the symmetry-breaking that emerges in the system.

In order to gauge the global stability of an Oscillator Death state, say the positive state, we use the concept of Basin Stability. We choose a large number of random initial conditions, uniformly spread over phase space volume. For each initial state, we calculate the fraction f^+ of oscillators that evolve to the positive OD state. The average of f^+ over random initial conditions $\langle f^+ \rangle$ yields an estimate of the Basin Stability of the positive state, and indicates the probability of obtaining the positive oscillator death state in a group of oscillators starting from random initial conditions in the prescribed volume of phase space. The most symmetric distribution, namely half the oscillators in the positive state and the other half in the negative state, leads to a Basin Stability measure of 0.5. *Deviations from* 0.5 *indicate asymmetry in the distribution of oscillator death states*, with a prevalence of the positive or negative state. So the quantity $\langle f^+ \rangle$ serves as an order parameter for symmetry-breaking of the Oscillator Death states.

It is clearly evident from Fig. 4.4 that there is a sharp transition from a reasonably symmetric state (where $\langle f^+ \rangle$ is close to 0.5) to a completely asymmetric state characterized by $\langle f^+ \rangle \sim 0$ as ε_{ext} increases. This suggests that the external environment plays a key role in breaking the symmetry of the Oscillator Death state, as this phenomenon emerges only when the oscillator-environment coupling is sufficiently strong, with the sudden onset of asymmetry in the group of oscillators occurring at a critical coupling strength. Further, it is clear from Fig. 4.4 that the symmetry breaking of the Oscillator

Death states is independent of system size N, over a large range of system sizes.

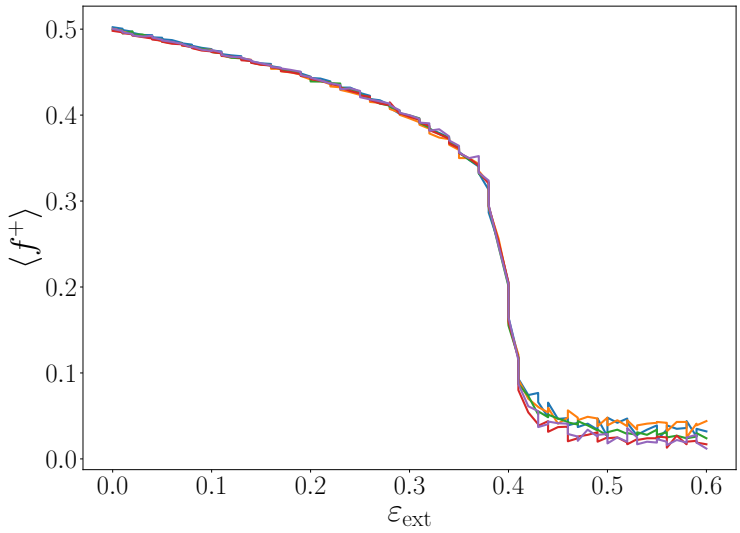

Figure 4.4: Basin Stability of the positive Oscillator Death state of coupled oscillators with ε_{ext}, where groups of oscillators of different sizes N=40, 60, 80, 100, 120 are shown in different colours. Here the damping constant of the external environment is $k = 0.2$.

Lastly, we analyze the effect of this symmetry-breaking induced by the external environment. Now, the external system is a damped system influenced by the mean field of the group of oscillators, and it settles down to a fixed point $u^\star$ when the OD state becomes stable. This is easily seen as follows: when the OD state is stable, $\bar{y}$ is a constant. So the steady state solution of u is given by $\varepsilon_{\text{ext}}\bar{y}/k$. Denoting the x variable of the positive OD state by x^+ and the y-variable as y^+, and denoting the x variable of the negative OD state by x^- and the y-variable as y^-, we have

$$\bar{y} = \{f^+ y^+ + (1 - f^+)y^-\},$$

yielding

$$u^\star = \frac{\varepsilon_{\text{ext}}\{y^+(2f^+ - 1)\}}{k}.$$

Further, from linear stability analysis of the dynamics of the external system one can see that $u^\star$ is a stable steady state, as the derivative of the vector field governing $\dot{u}$ is $-k$ which is always negative for a damped external system.

It is also clearly evdient from this analysis that if the probabilities of obtaining the positive and negative OD states are equal, i.e. $f^+ = 0.5$, then $u^\star = 0$. If the asymmetry is extreme and $f^+ \sim 0$ we have $u^\star = -\{\varepsilon_{\text{ext}} y^+\}/k$. Since the positive OD state has $x^+ > 0$ and $y^+ < 0$, $u^\star$ is positive. Also notice that the value of $u^\star$ is inversely proportional to

damping constant k (cf. Fig. 4.5). So a strongly damped environment evolves to $u^\star$ close to zero, as is intuitive.

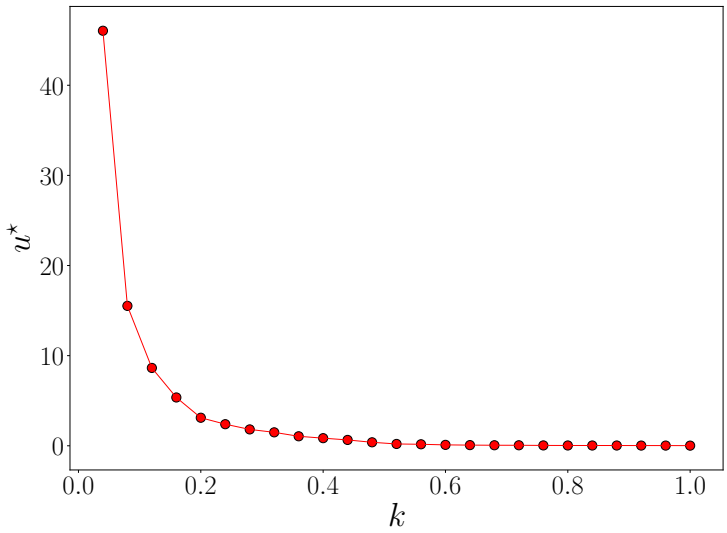

Figure 4.5: Environmental steady state $u^\star$ with respect to damping constant k. Here the number of oscillators in the group $N = 20$ and coupling strength of oscillators with external environment $\varepsilon_{\text{ext}} = 0.6$.

One can thus conclude that the state of the environment $u^\star$ is *strongly correlated to the asymmetry*. In fact, simply observing $u^\star$ tells us if the symmetry-breaking in the group of oscillators is pronounced or not.

Note that the above can also be rationalized by the fact that the damping constant k controls how fast the external system decays. For high k, the intrinsic damping of the environment is much more significant than the influence of the oscillator group, and so the external system rapidly decays to $u^\star = 0$. However, for very small damping k, the feedback from the oscillator group drives the environmental variable to a finite steady state (cf. Fig. 4.5), which in turn drives the asymmetry in the OD state.

4.4 Effect of Blinking Connections

In the section above we considered the effect of the external environment on a group of oscillators, when the external system was connected to all oscillators at all times, and we clearly demonstrated that this lead to marked asymmetry in Oscillator Death states. This is in contradistinction to the case where the group of oscillators are not connected

to an external system, which leads to complete symmetry in the Oscillator Death states. Now we will consider the effect of oscillator-environment connections blinking on-off, and explore the effect of such time-varying links on the symmetry of the Oscillator Death states.

In order to model connections to the environment blinking on and off, we consider a time-dependent oscillator-environment coupling strength in Eqn. 4.3, with the feedback from the oscillator group to the external system given by $\bar{y} = \frac{1}{N}\sum_{i=1}^{N} g_i(t)y_i$. If the connection of an oscillator to the environment is constant, $g_i(t) = 1$ for all t. Such a link is considered a time-invariant *non-blinking connection*. If the connection of the i^{th} oscillator in the group and the external system periodically switches on and off, namely the link is a *blinking connection*, $g_i(t)$ is a square wave. When oscillator i in the group is connected to environment $g_i(t) = 1$, otherwise $g_i(t) = 0$. So $g_i(t)$ switches between 0 (off) and 1 (on), with time period T_{blink} which provides a measure of the time-scale at which the links vary. Here we will principally consider rapidly switching links, i.e. low T_{blink}.

One of the most important parameters in this time-varying scenario is the fraction of blinking oscillator-environment connections in the group, which we denote by f_{blink}. If all oscillators are connected to the external, then $f_{\text{blink}} = 0$ and if all connections are blinking, then $f_{\text{blink}} = 1$. Here we will study the entire range $0 \leq f_{\text{blink}} \leq 1$, and gauge the effect of the fraction of blinking connections on the symmetry of OD state. Notice that the presence of connections switching on-off in a sub-set of oscillators results in the dynamical equations of the oscillator groups being less symmetric, as the group splits into two sub-sets having distinct dynamics. So it is most relevant to investigate if this lack of symmetry in the dynamical equations leads to more asymmetry in the steady states. However, what we will demonstrate in this Section is the following result: counter-intuitively, blinking links partially *restore* the symmetry of the emergent Oscillator Death states.

Fig. 4.6 shows the Basin Stability of the positive oscillator death state, as a function of the fraction f_{blink} of oscillators with blinking connections to the environment. We find that when there are no blinking links, namely the connections of the oscillators to the external system are always on, the emergent state is the *most asymmetric*. That is, the deviations of the Basin Stability from 0.5 is the most pronounced for $f_{\text{blink}} = 0$. Increasing the number of blinking connections reduces the asymmetry and restores the symmetry of the oscillator death states to a large extent, yielding states that are almost equi-distributed between positive and negative states. The transition from the asymmetric state (where

$\langle f^+ \rangle \sim 0$) to a more symmetric state (where $\langle f^+ \rangle$ is significantly different from 0) occurs sharply at a critical fraction of blinking links, which we denote by f^c_{blink}. Further, it is evident from Fig. 4.6 that the symmetry breaking dynamics of the system, and f^c_{blink} in particular, is independent of number N of oscillators in the group.

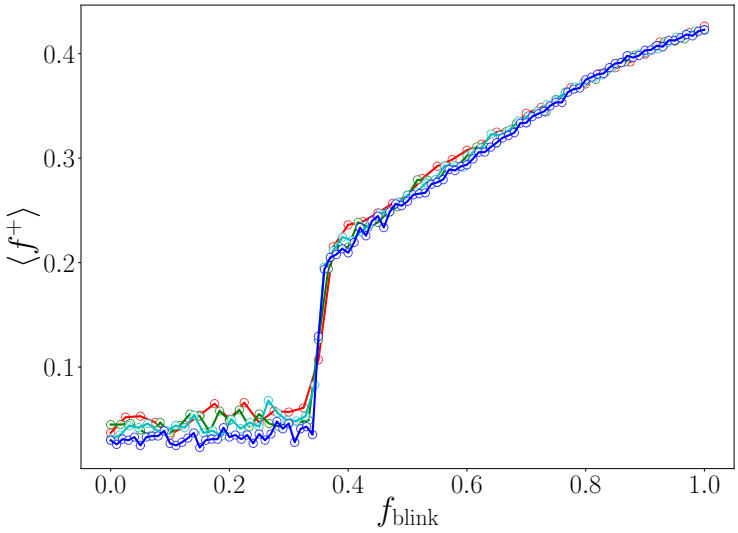

Figure 4.6: Dependence of the Basin Stability of the positive Oscillator Death state $\langle f^+ \rangle$, on the fraction of oscillators f_{blink} with blinking oscillator-environment connections in the group. Different system sizes $N = 40, 60, 64, 100$ are shown in different colours. Here the time period of the on-off blinking $T_{\text{blink}} = 0.02$, oscillator-environment coupling strength $\varepsilon_{\text{ext}} = 0.5$ and the damping constant of the environment $k = 0.2$.

Fig. 4.7 and Fig. 4.8 shows the dependence of the Basin Stability of the positive Oscillator Death state on the fraction of oscillators with blinking oscillator-environment connections f_{blink}, and the oscillator-environment coupling strength ε_{ext}. It is evident that for weaker coupling strengths the group of oscillators evolve to the positive and negative OD states with almost equal probability, i.e. $\langle f^+ \rangle$ is quite close to 0.5. On the other hand, for strong coupling strengths, there is a sharp transition from a very asymmetric situation (where $\langle f^+ \rangle \sim 0$) at low f_{blink}, to a more balanced situation (where $\langle f^+ \rangle$ is closer to 0.5) at high f_{blink}. Further, one observes that a system with a large fraction of blinking connections does not become markedly asymmetric even for large coupling strengths, i.e. $\langle f^+ \rangle$ is not close to 0 even for ε_{ext} close to 1. However, in a system with few blinking connections, there is a sharp transition to asymmetry for sufficiently high coupling strengths.

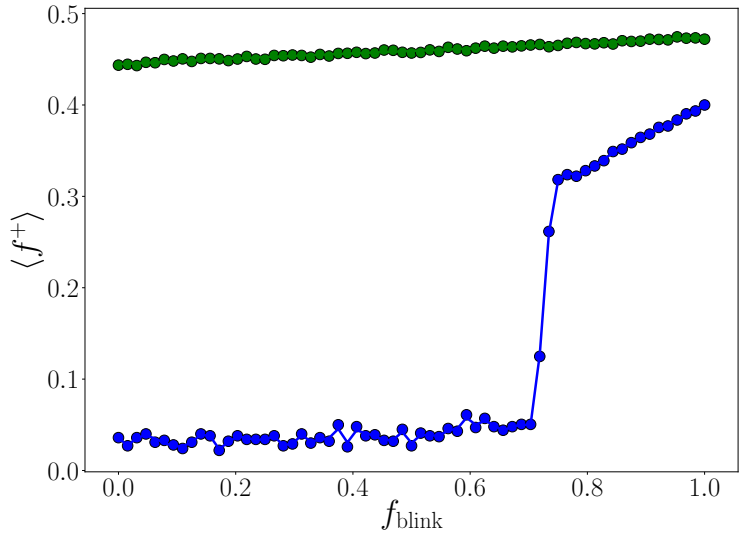

Figure 4.7: Basin Stability of the positive Oscillator Death state, as a function of fraction of oscillators with blinking oscillator-environment connections f_{blink}, for coupling strength $\varepsilon_{\text{ext}} = 0.2$ (green) and $\varepsilon_{\text{ext}} = 0.6$ (blue). Here the time period of blinking $T_{\text{blink}} = 0.02$, the damping constant of the environment $k = 1.0$ and $N = 64$.

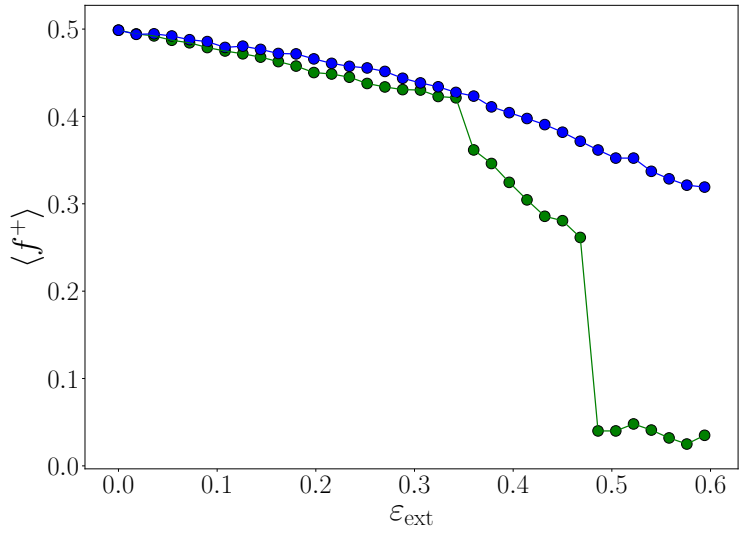

Figure 4.8: Basin Stability of the positive Oscillator Death state, as a function of oscillator-environment coupling strength ε_{ext}, for $f_{\text{blink}} = 0.25$ (green) and $f_{\text{blink}} = 0.75$ (blue). Here the time period of blinking $T_{\text{blink}} = 0.02$, the damping constant of the environment $k = 1.0$ and $N = 64$.

We will now focus on the effect of the dynamical features of the common environment on symmetry breaking of the OD state. Note that the common environment, when

uncoupled to the oscillator group, is an exponentially decaying system $u = u_0 e^{-kt}$, where u_0 is the amplitude at time $t = 0$ and k is the damping rate.

Fig. 4.9 shows the probability of obtaining the positive Oscillator Death state, as the fraction of oscillators with blinking connections is varied, for different environmental damping constants k. It is evident that at high environmental damping rates, the effect of environment is less pronounced, and the Oscillator Death states are selected with almost equal probability. However, there is pronounced asymmetry in OD states when the damping rate of the environment is low, with critical f^c_{blink} tending to 1 as k increases.

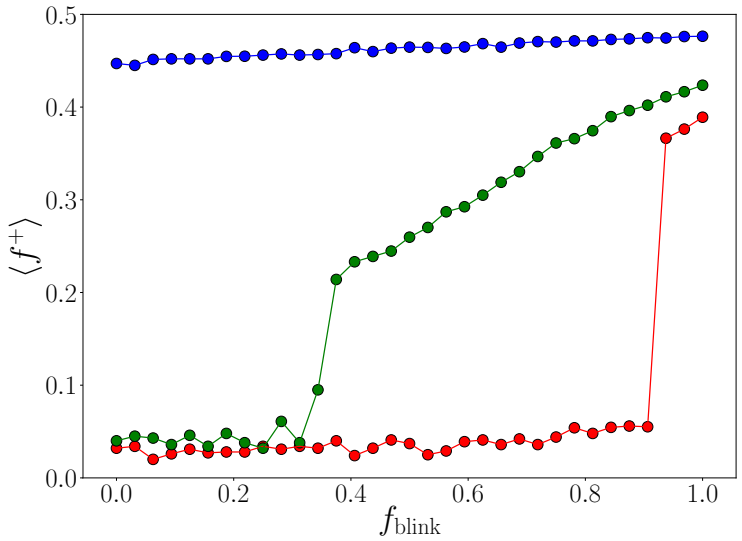

Figure 4.9: Basin Stability of the positive Oscillator Death state on the fraction of oscillators with blinking connections f_{blink}, for environmental damping constant $k = 0.1$ (red), $k = 0.2$ (green) and $k = 1.0$ (blue). The time period of blinking $T_{\text{blink}} = 0.02$, oscillator-environment coupling strength $\varepsilon_{ext} = 0.5$ and number of oscillators in the group $N = 64$. To estimate the Basin Stability we randomly sampled $u_0 \in (0, 1]$, for each k.

Further we estimate the probability of an oscillator to be in the positive Oscillator Death state, for the case of the sub-group of oscillators with blinking links to the environment (see Fig. 4.10a), and for the case of the sub-group of oscillators with static links to the environment (see Fig. 4.10b). For low environmental damping rates, there is a sharp boost in the probability of oscillators to be in the positive OD state in the sub-group of oscillators with blinking oscillator-environment connections, at a critical f^c_{blink} (e.g. $f^c_{\text{blink}} \sim 0.3$ for $k = 0.2$ and $f^c_{\text{blink}} \sim 0.9$ for $k = 0.1$.). For the case of the sub-group of oscillators with static oscillator-environment connections, the probability of obtaining the positive Oscillator Death state remains quite invariant. *This implies that the sub-group of oscillators with blinking connections to the environment is the group that is vital to the*

restoration of symmetry.

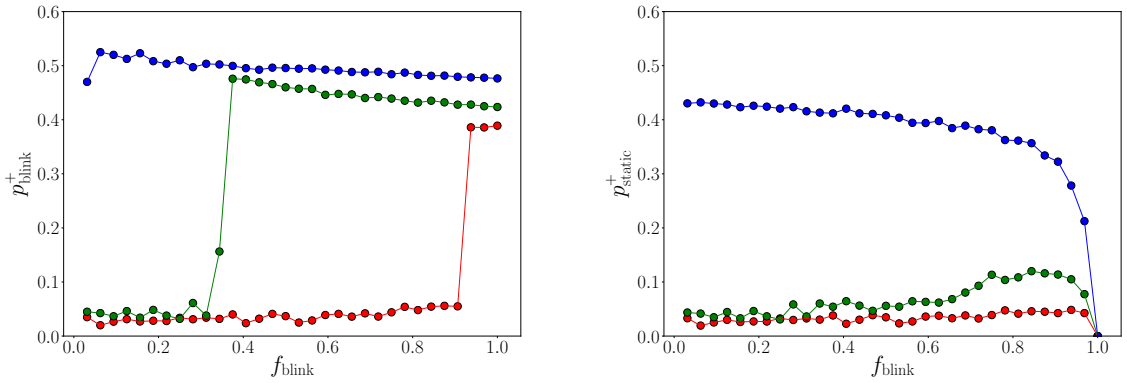

(a) (b)

Figure 4.10: Probability of obtaining the positive Oscillator Death state for the sub-group of oscillators with (a) blinking oscillator-environment connections, denoted by p^+_{blink}, and (b) static oscillator-environment connections denoted by p^+_{static}, as a function of the fraction of oscillators with blinking connections $f_{\rm blink}$. Here the time period of blinking $T_{\rm blink} = 0.02$, the oscillator-environment coupling strength $\varepsilon_{ext} = 0.5$, number of oscillators in the group $N = 64$, and the environmental damping constant k=0.1 (red), $k = 0.2$ (green) and $k = 1.0$ (blue).

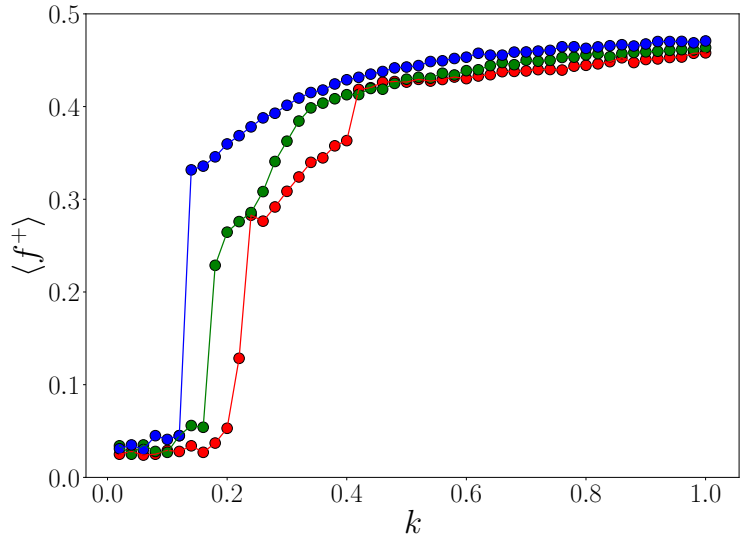

Figure 4.11: Basin Stability of the positive Oscillator Death state, as a function of the damping constant k of the environment. Here time period of blinking $T_{\rm blink} = 0.02$, oscillator-environment coupling strength $\varepsilon_{ext} = 0.5$ and the number of oscillators in the group $N = 64$ and the fraction of blinking oscillator-environment connections are: $f_{\rm blink} = 0.25$ (red), $f_{\rm blink} = 0.50$ (green) and $f_{\rm blink} = 0.75$ (blue).

Fig. 4.11 shows the dependence of the fraction of oscillators in the positive Oscillator Death state on the damping constant k of the environment, for different fractions of blinking connections. It is evident that at low damping constants, there are very few oscillators in the positive OD state. On increasing the damping constant of the environment there is a sharp jump in the fraction of oscillators in the positive OD state. So there is a sudden transition from a very asymmetric state, where the fraction of oscillators in the positive OD state is close to zero, to a more symmetric state, where this fraction is close to half. The critical k where this jump occurs depends upon the number of blinking oscillator-environment links. When there is a higher fraction f_{blink} of blinking connections in the system, the critical k is lower, i.e. the jump to a more symmetric situation occurs at lower damping constants.

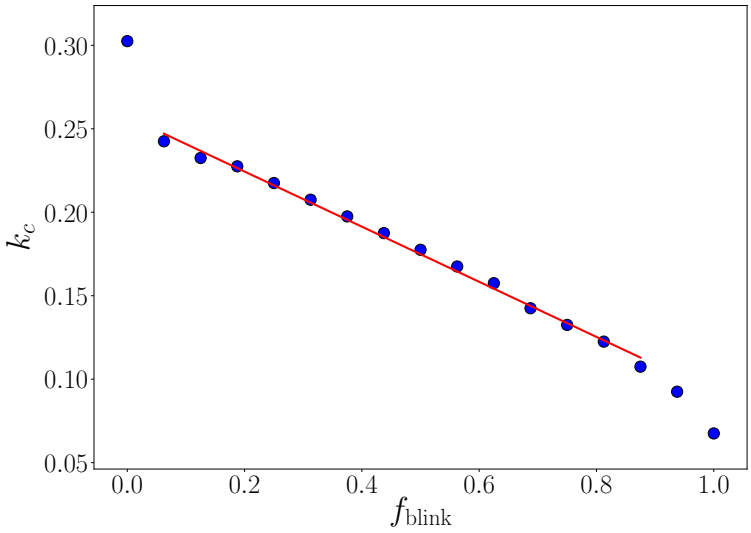

Figure 4.12: Critical value of damping constant k_c vs. fraction of blinking oscillator-environment connections f_{blink}. Here the time period of blinking $T_{\text{blink}} = 0.02$, oscillator-environment coupling strength $\varepsilon_{ext} = 0.5$ and number of oscillators in the group $N = 64$. The data points from numerical simulations are in blue, and the curve given by equation: $k_c = k_c^0 - c\ f_{\text{blink}}$, for $k_c^0 \approx 0.26$ and $c \approx 0.16$, is shown in red.

Further we estimate the value of damping constant k where $\langle f^+ \rangle$ crosses a threshold value of 0.1 (with no loss of generality), denoted by k_c. This critical value indicates the damping constant below which significant symmetry-breaking of the Oscillator Death states occurs. Fig. 4.12 shows critical k_c as a function of the fraction of blinking connections f_{blink}. The critical damping k_c decreases with increasing fraction of blinking connections f_{blink}. Specifically, in a large range of f_{blink} we find that k_c decreases linearly with f_{blink} (see Fig. 4.12). This demonstrates that low environmental damping favours

enhanced asymmetry, while more blinking connections tends to restore the symmetry of the OD states.

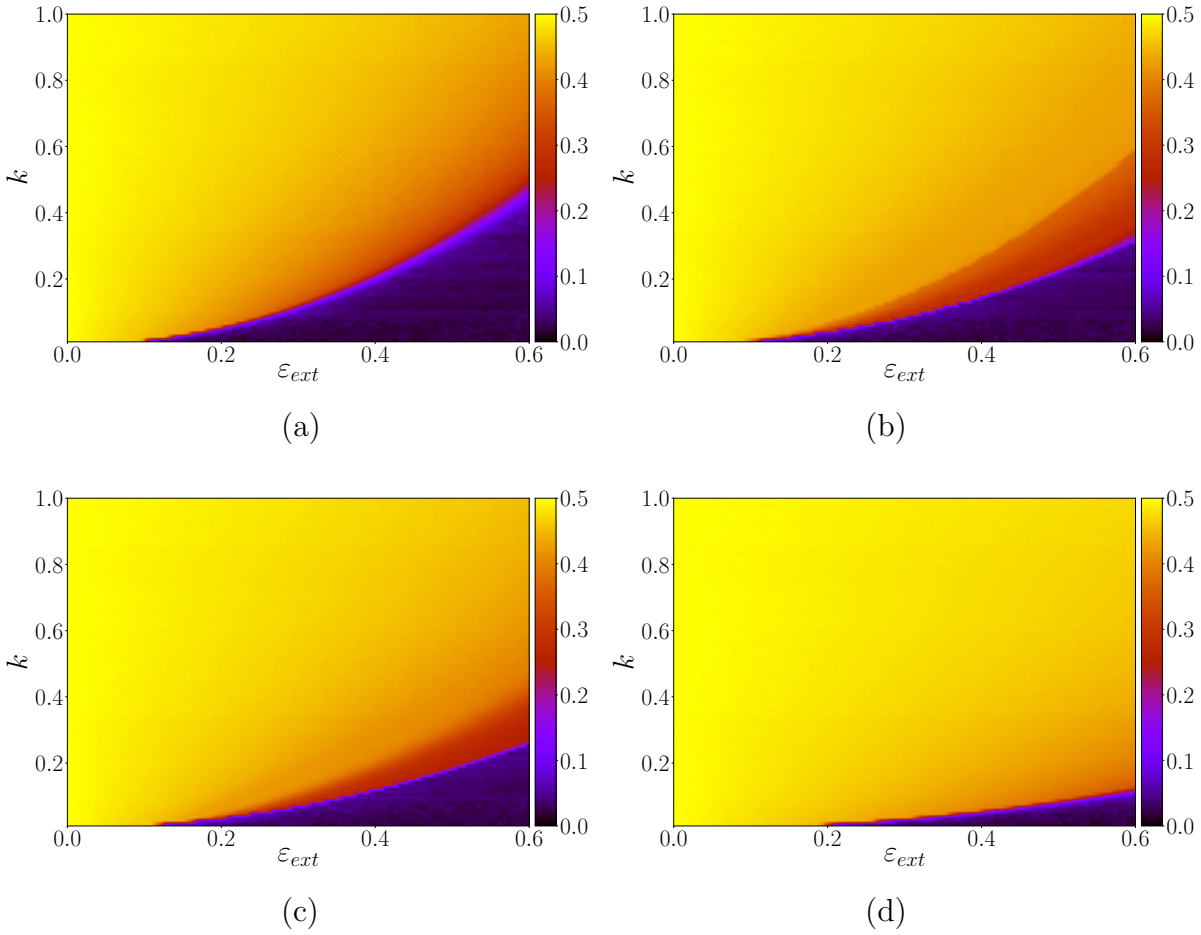

Figure 4.13: Basin Stability of the positive Oscillator Death in the parameter space of oscillator-environment coupling strength ε_{ext} and environmental damping constant k. The fraction of blinking oscillator-environment connections are: (a) $f_{\text{blink}} = 0.0$ (i.e. the static case), (b) $f_{\text{blink}} = 0.25$, (c) $f_{\text{blink}} = 0.50$, (d) $f_{\text{blink}} = 1.0$. The time period of blinking $T_{\text{blink}} = 0.02$ and the number of oscillators in the group $N = 64$.

The fraction of oscillators in the positive Oscillator Death state, in the parameter space of k and ε_{ext}, is displayed in Fig. 4.13, for different fraction of blinking oscillator-environment connections. The black regions in the figures represent the asymmetric state. Clearly, low environmental damping k and high oscillator-environment coupling ε_{ext} yields the greatest asymmetry in the emergent Oscillator Death states.

Now we focus on the line of transition from high $\langle f^+ \rangle$ to low $\langle f^+ \rangle$, shown in Fig. 4.14. We find that k is proportional to $\varepsilon_{\text{ext}}^2$ along the lines of transition, with the proportionality constant depending on the fraction of blinking oscillator-environment connections (see inset). Interestingly, comparing Fig. 4.12 and the inset of Fig. 4.14, reveals that both

have the same dependence on f_{blink}, and the proportionality constant is equal to $4k_c$. This implies that the line of transition to asymmetry in the space of k-ε_{ext} is given by:

$$k = 4k_c\ \varepsilon_{\text{ext}}^2 \tag{4.4}$$

where k_c is inversely proportional to the fraction of blinking connections f_{blink}.

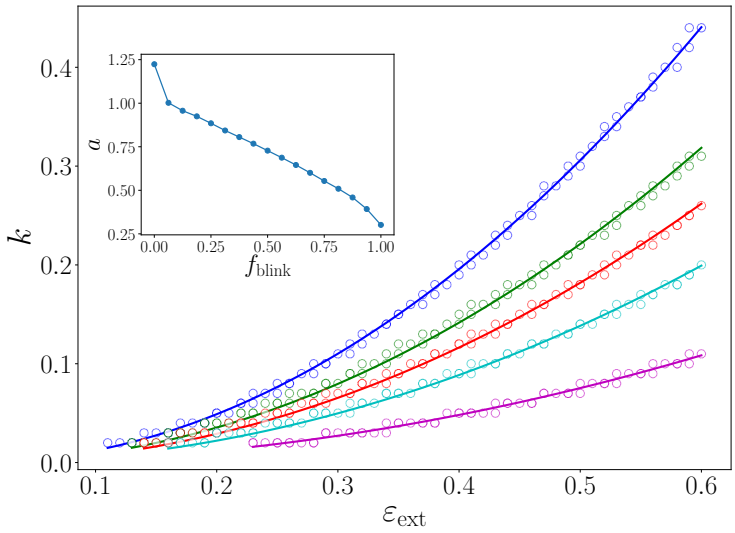

Figure 4.14: Transition line in Fig. 4.13, fitted to the curve (solid lines): $k = a\varepsilon_{\text{ext}}^2$, where the different curves correspond to $f_{\text{blink}} = 0.0, 0.25, 0.50, 0.75, 1.0$ from top to bottom. The inset shows the variation of a with f_{blink}.

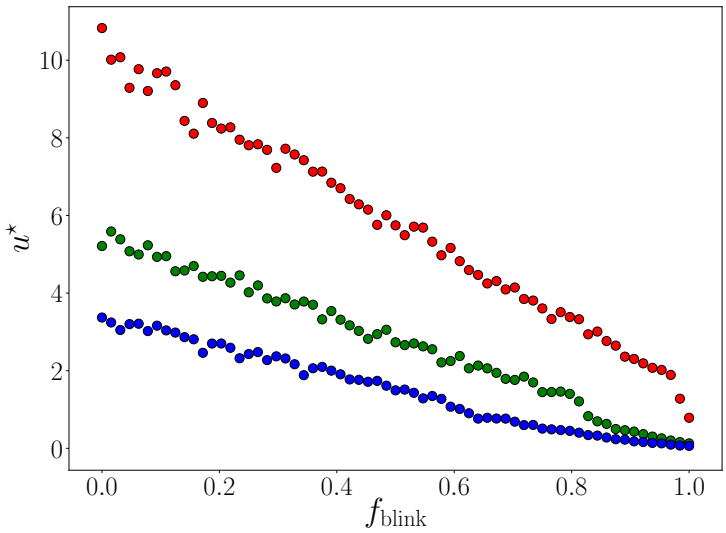

Figure 4.15: Environmental steady state $u^\star$ with respect to the fraction of oscillator-environment blinking connections, for damping constant $k = 0.08$ (red), 0.12 (green), 0.16 (blue). Here the number of oscillators in the group $N = 64$ and coupling strength of oscillators with external environment $\varepsilon_{\text{ext}} = 0.5$.

The environmental steady state $u^\star$ with respect to the fraction of oscillator-environment blinking connections, is shown in Fig. 4.15, for different damping constants. It is clear that as the fraction of blinking connections tends to one, the state of the environment $u^\star$ tends to zero. Consequently, the symmetry of the system is restored and the two OD states are almost equally preferred when almost all links are blinking.

Effect of the frequency of blinking on Oscillation Death:

In the results discussed above the time-period of the blinking connections was small, i.e. the links switched on-off rapidly. Now we will investigate the influence of the time-period T_{blink} of the blinking oscillator-environment connections on the dynamics. Fig. 4.16 displays the effect of increasing blinking time-period on the state of the oscillators.

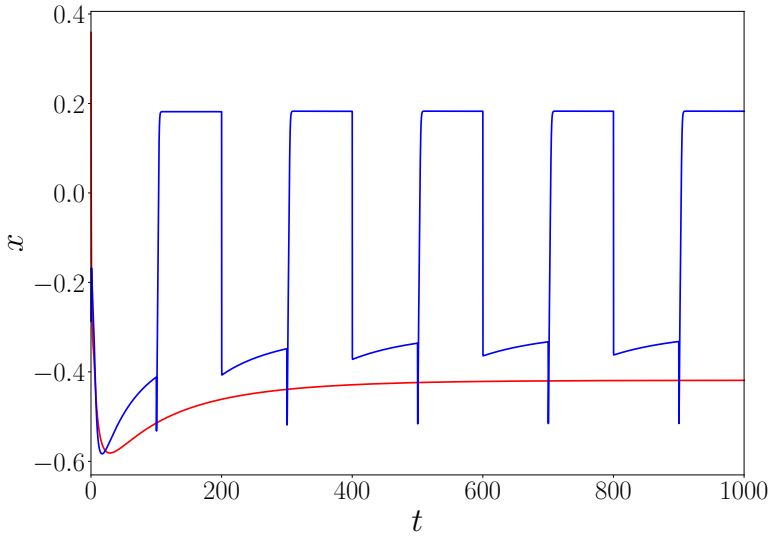

Figure 4.16: Time series of one of the oscillators in group for $T_{\text{blink}} = 0.02$ (red), 200.0 (blue). Here $N = 20$, $f_{\text{blink}} = 0.1$, $\varepsilon_{\text{ext}} = 0.6$ and $k = 0.01$.

It is evident from the time-series of the oscillators (cf. Fig. 4.16) that after a critical blinking time-period the system starts to oscillate and the OD steady state is destroyed. That is, *slow blinking of links leads to oscillation revival.* This is also quantitatively demonstrated in Fig. 4.17, which shows the amplitude of the oscillators. Clearly up to $T_{\text{blink}} \sim 0.1$ the amplitude is zero and one obtains a Oscillator Death state. However, when T_{blink} increases further, the amplitude grows from zero to a finite value, indicating the emergence of oscillations whose amplitude increases with T_{blink}. After a large value T_{blink} (~ 10) the amplitude of the oscillations saturate to a maximum value (cf. Fig. 4.17).

We find that this maximum amplitude is the difference between the steady state solution of the oscillator for the case of $\varepsilon_{\text{ext}} = 0$ (i.e. when uncoupled from the external system) and the steady state arising for $\varepsilon_{\text{ext}} > 0$ (i.e. when the oscillator group is coupled to a common environment). So the oscillator moves periodically between the two steady state solutions when the blinking is slow enough to allow the system to reach the two distinct steady states during the on and off period respectively.

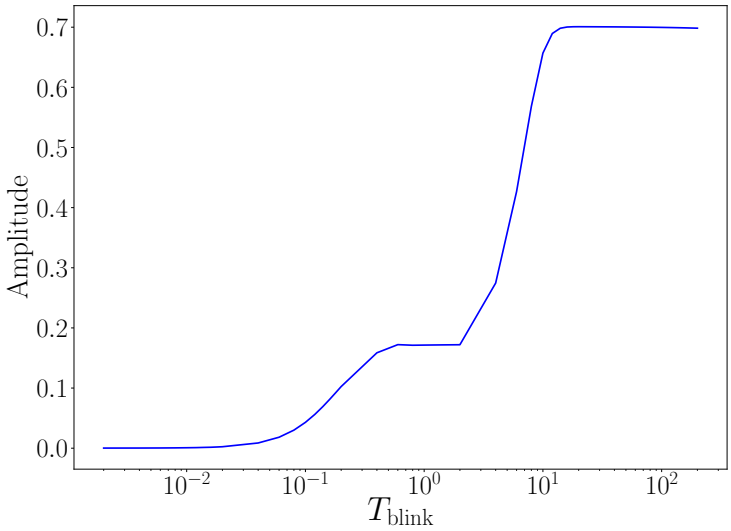

Figure 4.17: Amplitude of the x-variable for different T_{blink}. Here $N = 20$, $f_{\text{blink}} = 0.1$, $\varepsilon_{\text{ext}} = 0.6$ and $k = 0.01$.

Further, notice that there are two distinct transitions to oscillation revival. The first occurs around $T_{\text{blink}} \sim 0.1$, with fixed states transitioning to non-zero amplitude oscillations, saturating around amplitude ~ 0.2. The second transition commences around $T_{\text{blink}} \sim 2\pi/\omega$, where the amplitude starts to grow rapidly again, from amplitudes around 0.2, to the maximum amplitude.

4.5 Fractionally Disconnected Links

Previously, in Fig.4.2 we saw that coupling to an external damped environment lead all the oscillators to one particular OD state, thereby breaking the symmetry of the distribution of the OD states. Now, we will disconnect the oscillator-environment links one at a time till all of the oscillators in the group are uncoupled to the external medium and look for the changes in distribution of oscillators in the Oscillation Death states. In

our case, we have two OD states on either side of the origin i.e positive x which we will call x^+ and another on the negative side which we name x^- from now on. Without any external environment the oscillators occur almost equally (statistically speaking) in the positive and negative OD states. To quantify this observation we have shown in Fig.4.3 the probability distribution of the oscillators in the positive x^+ steady state, obtained by sampling over 50000 initial conditions, uniformly distributed over phase space volume $[-1,1]$, of globally coupled SL oscillators without external environment.

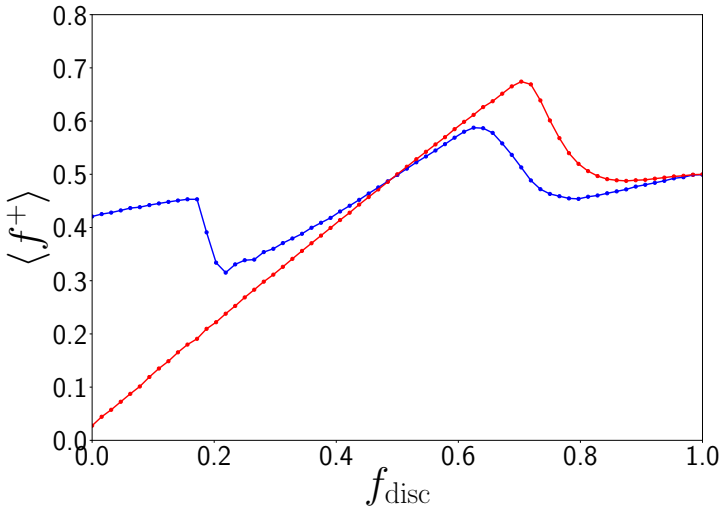

Figure 4.18: Average fraction of oscillators in positive OD-state ($\langle f^+ \rangle$), obtained by sampling over 10000 initial conditions, with respect to the fraction of oscillators-environment links for $\varepsilon_{ext} = 0.2$ (blue) and 0.5 (red). Here $N = 64$ and $k = 0.1$.

In Fig.4.18 we plot the fraction of oscillators that go to the positive OD state (x^+) with respect to varying number of oscillator-environment links. In particular, we disconnect one environment-oscillator link at a time, and we denote the fraction of disconnected links by f_{disc}. So $f_{disc} = 0$ corresponds to the case where all oscillators in the group are connected to the external environment, while $f_{disc} = 1$ corresponds to the limit of a group of SL oscillators having no interactions with the common environment. We observe changes in the fraction of oscillators in the positive OD-state, averaged over different initial conditions, denoted by $\langle f^+ \rangle$, as a function of f_{disc}. That is, we investigate how the distribution of the oscillators between the two available OD states changes as the number of environment-oscillator links changes. The results of the dependence of $\langle f^+ \rangle$ on f_{disc} for different values of external environment coupling ($\varepsilon_{ext} = 0.2$ and 0.5) are displayed. It is clear that this dependence is *non-monotonic* and has several non-trivial features. For instance, if we consider the case of $\varepsilon = 0.5$ in Fig. 4.18, we find that at $f_{disc} \simeq 0.2$ the oscillators are predominately in the negative OD state and $\langle f^+ \rangle$ is $\simeq 0.2$,

i.e. around 20% of the oscillators in the group go to the positive OD state, while the rest are attracted to the negative OD state. As we change f_{disc} the probability of being in the positive OD state increases to a maximum of $\langle f^+ \rangle \simeq 0.7$ at $f_{disc} \simeq 0.7$. After that, $\langle f^+ \rangle$ decreases again and reaches 0.5, namely the completely symmetric situation, in the limit of $f_{disc} = 1$ where we have completely disconnected the oscillator group from the environment. One remarkable observation is that at $f_{disc} \simeq 0.5$ the value of $\langle f^+ \rangle$ is 0.5. This implies that when half of the oscillators are connected with the external common medium the statistical symmetry of the OD states returns i.e both the positive and negative OD states are equally occupied by the oscillators. So when half of the oscillators in the group are connected to the environment ($f_{disc} = 0.5$) we obtain a dynamical outcome that is equivalent to the case of the oscillator group being completely unconnected to the external environment ($f_{disc} = 1$).

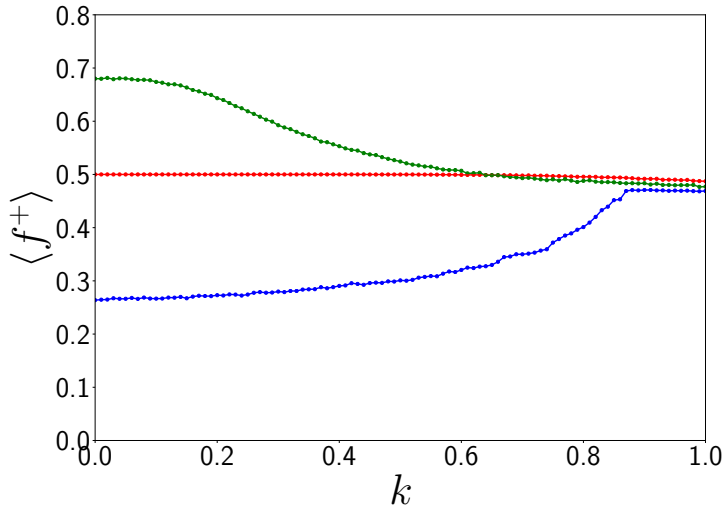

Figure 4.19: Average fraction of oscillators in positive OD-state ($\langle f^+ \rangle$), obtained by sampling over 10000 initial conditions, with respect the damping constant of the common external environment k, for f_{disc}=0.25 (blue), 0.5 (red) and 0.7 (green). Here $\varepsilon_{ext} = 0.5$ and $N = 64$.

Further, we examine the effect of the damping constant k of the external environment on the distribution of the oscillators between the positive and negative OD-states, i.e. the dependence of $\langle f^+ \rangle$ (and $\langle f^- \rangle$) on k for different values of f_{disc}. To illustrate this, we show results for three values of external coupling ($\varepsilon_{ext} = 0.25, 0.5$ and 0.7) in Fig.4.19. For $f_{disc} = 0.25$ (blue), the fraction of positive OD-state ($\langle f^+ \rangle$) always remain less than 50% for the entire range of k sampled, and it slowly increases to $\sim 50\%$ for $k \geq 0.85$. The oscillator distribution tends to maintain its symmetry (i.e $\langle f^+ \rangle \sim 0.5$) for all values of k when only half of the oscillators are connected/disconnected with the external environment (i.e. $f_{disc} = 0.5$). For $f_{disc} = 0.7$ (green) the oscillator distribution

reaches its most skewed position when $\langle f^+ \rangle$ becomes maximum at ~ 0.7 (cf. Fig. 4.18). On increasing k, this again approaches $\langle f^+ \rangle \sim 0.5$ as k approaches 1. This suggests that the environmental damping constant can be utilized as a parameter to *control the distribution of oscillators in the positive and negative OD-states.*

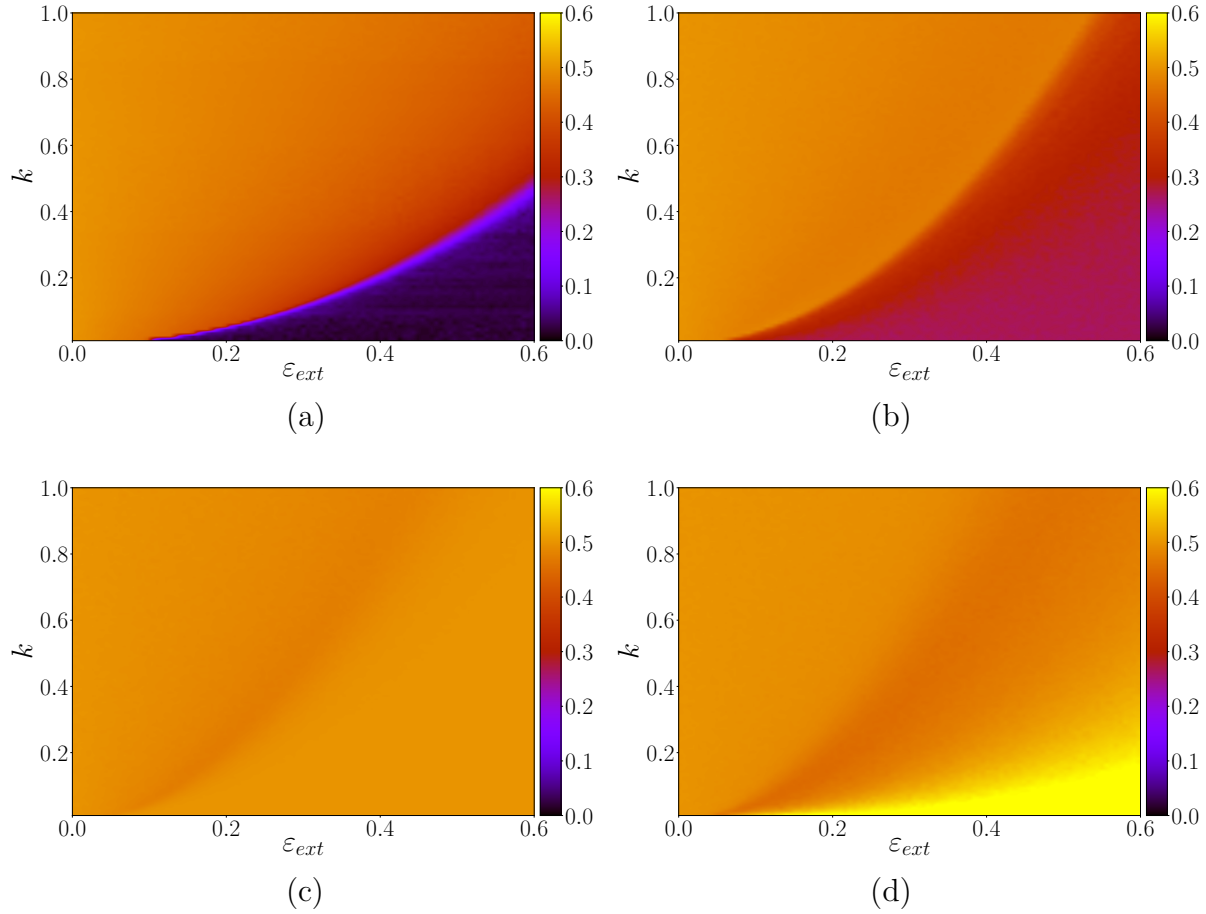

Figure 4.20: Average fraction of oscillators in positive OD-state ($\langle f^+ \rangle$), estimated by sampling over 10000 initial conditions, in the parameter space of $\varepsilon_{ext} - k$ for f_{disc} (a) 0.0, (b) 0.25, (c) 0.5 and (d) 0.75, with $N = 64$.

The coupling strength between the external medium and the oscillators in the group (ε_{ext}) is vital in controlling the flow of information between the group of oscillators. So we look for changes in $\langle f^+ \rangle$ in the parameter space of $\varepsilon_{ext} - k$. Fig. 4.20 (a) shows $\langle f^+ \rangle$ when all oscillators are connected to the environment (i.e. $f_{disc} = 0.0$). This will act as a reference for comparison with the case where some fraction of environment-oscillator links are disconnected. For higher ε_{ext} values and lower damping constant (k) the fraction $\langle f^+ \rangle$ is almost 0 (or $\langle f^- \rangle \simeq 1$). Interestingly, at this particular region of the $\varepsilon_{ext} - k$ parameter space, $\langle f^+ \rangle$ increases for increasing f_{disc}. This demonstrates that as increasing number of disconnections of the environment-oscillator links, the number of oscillators going to

the positive OD state increases, leading to a more symmetric distribution of oscillators among the two OD states. Further we consider the variation of $\langle f^+ \rangle$ with respect to ε_{ext} at fixed k in Fig. 4.21, for $k = 0.1$. Three scenarios become clearly evident from the figure, corresponding to three different fractions of disconnected links. So we can conclude that along with environmental damping constant (k), oscillator-environment coupling strength (ε_{ext}) is also an important parameter controlling the distribution of oscillators between the positive and negative OD-states.

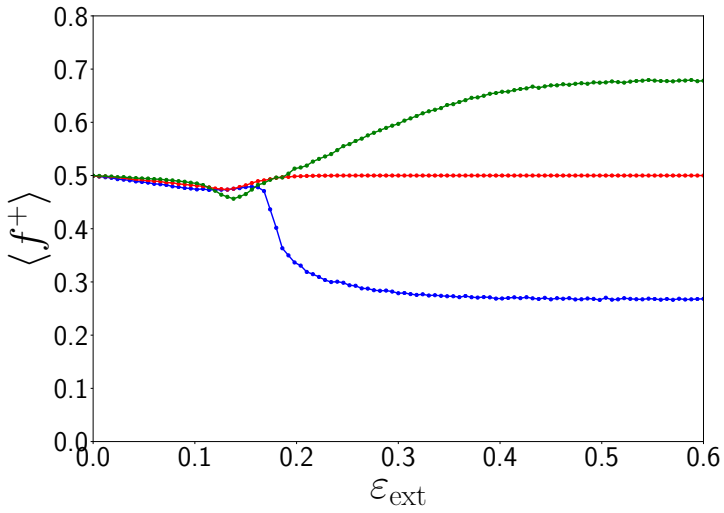

Figure 4.21: Average fraction of oscillators in positive OD-state ($\langle f^+ \rangle$), estimated by sampling over 10000 initial conditions, with respect to ε_{ext}, for f_{disc}=0.25 (blue), 0.5 (red) and 0.7 (green), with $k = 0.1$ and $N = 64$.

We had shown the histogram of the probability of obtaining fraction f^+ in the positive OD state, in Fig.4.3, for globally coupled SL oscillators in OD-state without environmental coupling, and seen a symmetric distribution of the oscillators around 0.5. Similarly, we now estimate the distribution of oscillators in the positive OD-state in the presence of a common environment. We explore cases with different fractions of disconnected environment-oscillator links. In Fig. 4.22(a) we show the distribution for $f_{disc} = 0.25$, with $\varepsilon_{ext} = 0.5$ and $k = 0.1$. Interestingly, there is no spread in the distribution of oscillators, as is clearly seen from the single pronounced peak in the distribution at 0.5 for Fig. 4.22(b) and around 0.7 in Fig. 4.22(c). This sharp localization of oscillators in one of the two available stable states is in contradistinction to the usual statistical spread observed in Fig. 4.3. This is especially remarkable for the case of the symmetric distribution that arises in Fig. 4.22(b), vis-a-vis the statistically symmetric case seen in Fig. 4.3. So we can infer that one can tailor the distribution of oscillators in positive and negative OD-states by disconnecting a suitable number of environment-oscillator links (f_{disc}) and

adjusting the control parameters ε_{ext} and k.

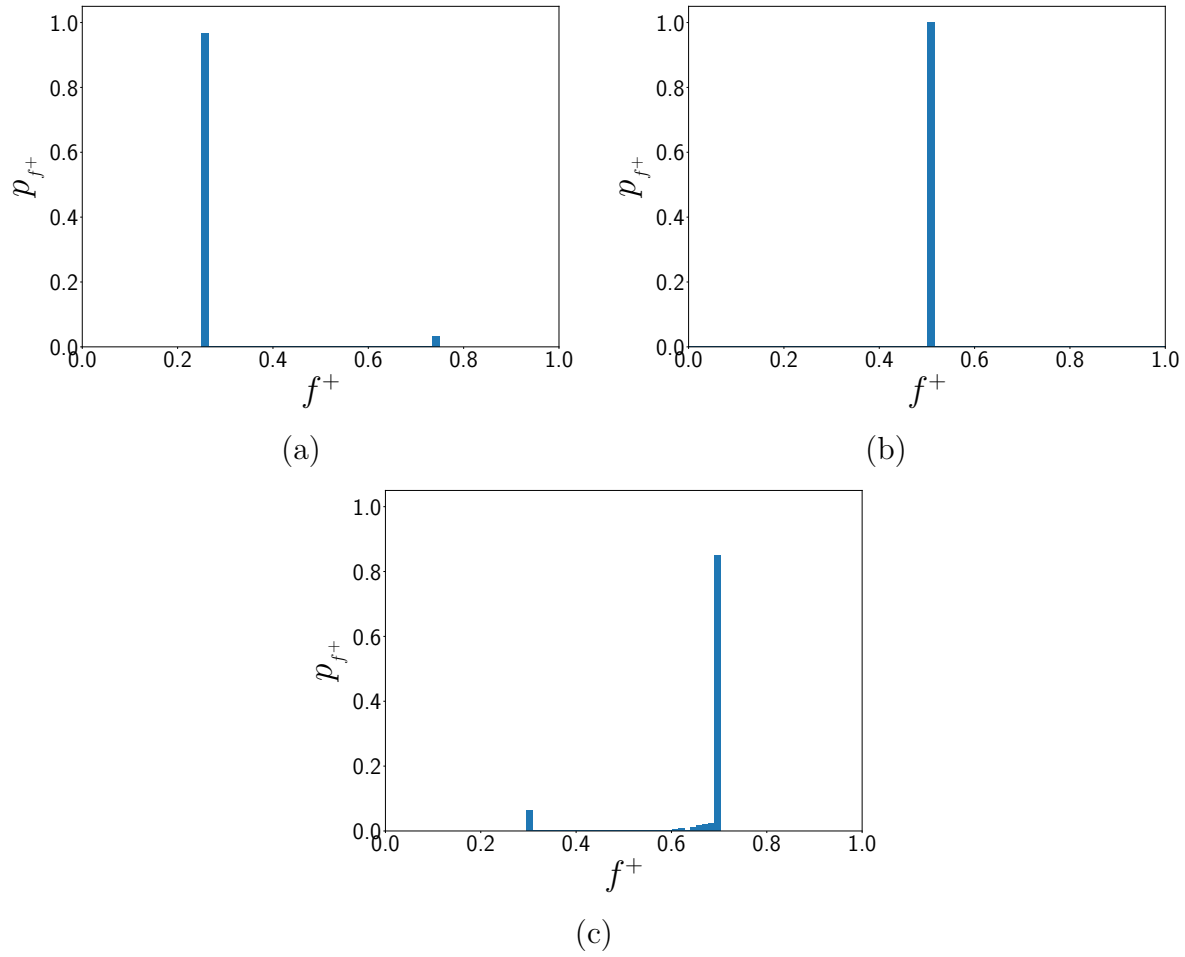

Figure 4.22: Histogram showing the probability of the fraction of oscillators in positive state when the coupling of the oscillator group to the environment $\varepsilon_{ext} = 0.5$ and damping constant of the environment $k = 0.1$, with fraction of disconnected links (a) $f_{disc} = 0.25$, (b) $f_{disc} = 0.5$, (c) $f_{disc} = 0.7$.

4.6 Constant Common environment

We have shown the effect of exponentially decaying external environment on the OD state and the effect of blinking connections. This mimics a situation where the external environment is a small bath, and so the dynamics of the oscillator group affects the dynamics of the common environment.

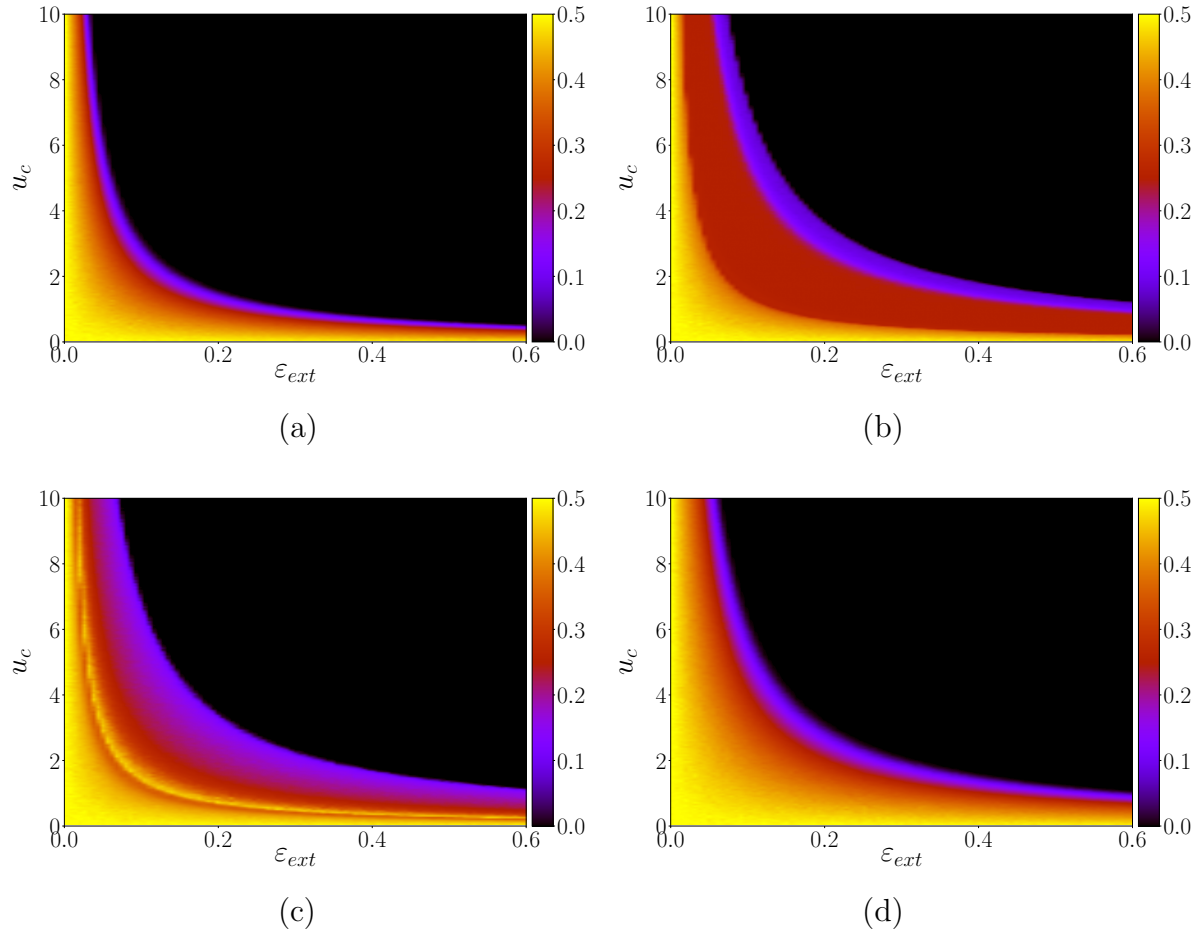

Figure 4.23: Basin Stability of the positive Oscillator Death state in the parameter space of coupling strength ε_{ext} and constant environment (u_c), with fraction of blinking oscillators (a) $f_{\text{blink}} = 0.0$, (b) $f_{\text{blink}} = 0.25$, (c) $f_{\text{blink}} = 0.50$, (d) $f_{\text{blink}} = 1.0$. Here the time period of blinking T=0.02 and the number of oscillators in the group $N = 64$.

In this section, we will consider a common external environmental system mimicking a large bath, where the external environment does not get affected by the oscillator group. Rather it acts as a *constant drive*, which we denote by u_c. The strength of this oscillator-external drive connection is given by the coupling strength ε_{ext}. So the complete dynamics of the group of oscillators is now given by the following evolution equations:

$$\begin{aligned} \dot{x}_i &= (1 - x_i^2 - y_i^2)x_i - \omega y_i + \varepsilon_{\text{intra}}(q\bar{x} - x_i) \\ \dot{y}_i &= (1 - x_i^2 - y_i^2)y_i + \omega x_i + \varepsilon_{\text{ext}} u_c \end{aligned} \tag{4.5}$$

where $\bar{x} = \frac{1}{N}\sum_{i=1}^{N} x_i$.

Fig. 4.23 shows the fraction of oscillators in positive Oscillator Death state, in the parameter space of u_c and ε_{ext}. Different panels correspond to different fraction of blinking connections, and the black regions in the figures represent the asymmetric state. It is evident that even for the case of constant drive, the symmetry of the Oscillator Death state is broken, and the system moves preferentially to the negative state. Interestingly, for constant negative drive, i.e. $u_c < 0$, the positive Oscillator Death state is preferentially selected. This further indicates the generality of our observations, and emergence of symmetry-breaking in a group of oscillators due to coupling to a common external system.

4.7 Conclusion

We investigated the impact of a common external system, which we call a *common environment*, on the Oscillator Death states of a group of Stuart-Landau oscillators. First we consider external systems that exponentially decay to zero when uncoupled from the oscillator group. Note that a group of oscillators yield a completely symmetric Oscillator Death state when uncoupled to the external system, i.e. the positive and negative OD states occur with equal probability, and so in a large ensemble of oscillators the fraction of oscillators attracted to the positive/negative state is very close to half. However, remarkably, when coupled to a common external system this symmetry is significantly broken. This symmetry breaking is very pronounced for low environmental damping and strong oscillator-environment coupling, as evident from the sharp transition from the symmetric to asymmetric state occurring at a critical oscillator-environment coupling strength and environmental damping rate.

Further, we consider a group of oscillators with time-varying connections to the common external environment. In particular, we study the system with a fraction of oscillator-environment links that switch on-off. Interestingly, we noticed that the asymmetry induced by environmental coupling decreases as a power law with increase in fraction of such on-off connections. This suggests that blinking oscillator-environment links can restore the symmetry of the Oscillator Death state.

In the next section we demonstrated the effect of permanently disconnection of the oscillation-environment links. The symmetry breaking in the basin stability of OD states depends on damping constant of the external system k, environment-oscillator coupling strength ε_{ext} and the fraction of oscillators connected to the external system. When very

few oscillators are connected to the environment, the OD states are almost symmetrically distributed. On the other hand when a large fraction of oscillators are coupled to the environment, the symmetry is broken to a very high extent, for high environment-oscillator coupling strengths and low environmental damping constants. Interestingly, when half the environment-oscillator links are disconnected, the symmetry is restored, independent of the damping constant of the environment and the environment-oscillator coupling strength. In fact in this case, exactly half of the oscillators attain positive OD states and the other half attain negative OD states.

Lastly, we demonstrated the generality of our results for a constant external drive, i.e. a constant environment, and found marked breaking of symmetry Oscillator Death states there as well. When the constant drive is large, the asymmetry in OD-state is very large, and the transition between the symmetric and asymmetric state, with increasing oscillator-environment coupling, is sharp.

In summary, we have shown the existence of a pronounced breaking of symmetry in the Oscillator Death states of a group of oscillators induced by a common external environment. So our results demonstrate an environment-mediated mechanism for the prevalence of certain states in a system of oscillators, and suggests an underlying process for obtaining certain states preferentially in ensembles of oscillators. So our work here suggests a potent method to control the basin stability of the oscillation death states.

Chapter 5

Suppression and revival of oscillations through time-varying interaction

Adapted from the work published in :

Chaurasia, S. S., Choudhary, A., Shrimali, M. D., Sinha, S., "Suppression and revival of oscillations through time-varying interaction", ***Chaos, Solitons and Fractals*** 118., (2019) 249-254

5.1 Introduction

Coupled dynamical systems have been extensively studied over the last few decades as they provide us a framework for modelling many complex systems [83, 84]. The focus of investigations have mostly been on phenomena emerging under variation of the local dynamics of the units and the interactions among them. Most studies have assumed the interactions among the nodes to be invariant over time. However in recent times there have been efforts to incorporate a time-varying links, namely changing connections between the units in a dynamical network [85, 86, 87, 88, 89, 90, 91, 92, 93, 94]. Such time varying interactions model the evolution of connections over time, and are commonly found in physical, biological, social and engineered systems [95, 96, 97, 98, 99, 100, 101]. Studies so far have considered the variation in links as a function of time, while the form of coupling remains the same. Here we will explore a new direction in time-varying interactions: we will study the *effect of switched coupling forms* on the emergent behaviour.

We consider two coupling functions, one diffusive and the other conjugate coupling between the two oscillators. Coupling via conjugate variables is natural in a variety of experimental situations where sub-systems are coupled by feeding the output of one into the other. An example from the recent literature is provided by the experiments of Kim and Roy on coupled semiconductor laser systems [18], where the photon intensity fluctuation from one laser is used to modulate the injection current of the other, and vice versa. Hybrid coupling [102, 103] also has relevance in ecological models, where migration and cross-predation (analogous to conjugate coupling) [104] occurs between two population patches, namely over some time migration or diffusive coupling may be dominant, while at other times cross-predation between the two patches is prevalent.

The primary goal of this study is to demonstrate the non-trivial dynamical states arising out of the temporal interplay between two coupling forms, through extensive bifurcation analysis. The test-bed of our inquiry will be a generic system of coupled oscillators, which we describe in detail below.

5.2 Coupled oscillators

A general form of coupled dynamical oscillators is given by:

$$\dot{X}_i = F(X_i) + KG_i(X_j, X'_j, X_i) \tag{5.1}$$

where X_i denotes the set of m dynamical variables of the ith oscillator. The matrix K of dimension $m \times m$ contains information on the coupling topology. G_i is the coupling function that represents the nature of the interaction and the variables involved in the interaction term, with the superscript primes ($'$) on X denoting conjugate or "dissimilar" variables [105].

Now, complex systems often undergo Hopf bifurcations and sufficiently close to such a bifurcation point, the variables which have slower time-scales can be eliminated. This leaves us with a couple of simple first order ordinary differential equations, popularly known as the Stuart-Landau system [1]. In this work we will consider two diffusively coupled oscillators of this form, namely two coupled Stuart-Landau systems.

When the coupling between the oscillators is through *similar* variables, the dynamical equations are given by:

$$\begin{aligned} \dot{x_1} &= f^x(x_1, y_1) + \varepsilon(x_2 - x_1) \\ \dot{y_1} &= f^y(x_1, y_1) \\ \dot{x_2} &= f^x(x_2, y_2) + \varepsilon(x_1 - x_2) \\ \dot{y_2} &= f^y(x_2, y_2) \end{aligned} \tag{5.2}$$

and when the oscillators are coupled to each other through *dissimilar* variables, the dynamical equations are given by:

$$\begin{aligned} \dot{x_1} &= f^x(x_1, y_1) + \varepsilon(y_2 - x_1) \\ \dot{y_1} &= f^y(x_1, y_1) \\ \dot{x_2} &= f^x(x_2, y_2) + \varepsilon(y_1 - x_2) \\ \dot{y_2} &= f^y(x_2, y_2) \end{aligned} \tag{5.3}$$

with

$$\begin{aligned} f^x(x, y) &= x(1 - (x^2 + y^2)) - \omega y \\ f^y(x, y) &= y(1 - (x^2 + y^2)) + \omega x \end{aligned} \tag{5.4}$$

Specifically, in this work we consider the angular frequency ω of the Stuart-Landau

oscillator to be 5, and the coupling strength ε to be in the range $[0, 10]$.

Now coupled Stuart-Landau oscillators have been a good model for the study of oscillation death [55, 106] and amplitude death [107, 108, 32, 109]. When the coupling is through similar variables (cf. Eqn. 5.2), the oscillators get synchronized at a very low coupling strengths, and remain oscillatory and synchronized up to very high coupling strength. However when coupling is through dissimilar variables (cf. Eqn. 5.3), the system shows oscillatory behaviour for small coupling strengths, and increasing coupling strengths give rise to amplitude death and subsequently oscillation death [110].

5.3 Time-varying Coupling Form

Now we consider a scenario where the form of the coupling between the oscillators is time dependent, namely, the form of coupling *switches between the similar and dissimilar variables*. The switching of the coupling form may be periodic or probabilistic.

5.3.1 Periodic Switching of Coupling Forms

Here the oscillators change their coupling form periodically. If the time period of the switch is T, we consider the system to be coupled via similar variables for fraction f_{sim} of the cycle, followed by coupling to dissimilar variables for the remaining part. So when $f_{sim} = 0$, the oscillators are always coupled to dissimilar variables and when $f_{sim} = 1$ the oscillators are coupled through similar variable for all time. For $0 < f_{sim} < 1$, the oscillators experience coupling through similar variables for time $f_{sim}T$, followed by coupling through dissimilar variables for time $T(1 - f_{sim})$, in each cycle of period T.

$$\begin{aligned} \dot{x_1} &= f^x(x_1, y_1) + \varepsilon\delta(x_2 - x_1) + \varepsilon(1-\delta)(y_2 - x_1) \\ \dot{y_1} &= f^y(x_1, y_1) \\ \dot{x_2} &= f^x(x_2, y_2) + \varepsilon\delta(x_1 - x_2) + \varepsilon(1-\delta)(y_1 - x_2) \\ \dot{y_2} &= f^y(x_2, y_2) \end{aligned} \tag{5.5}$$

where

$$\delta = \begin{cases} 1, & \text{if } t \in [NT, (f_{sim} + N)T) \\ 0, & \text{if } t \in [(f_{sim} + N)T, (N+1)T) \end{cases} \tag{5.6}$$

where T is the switching period, $N = 0, 1, 2, ...$ is the number of periods.

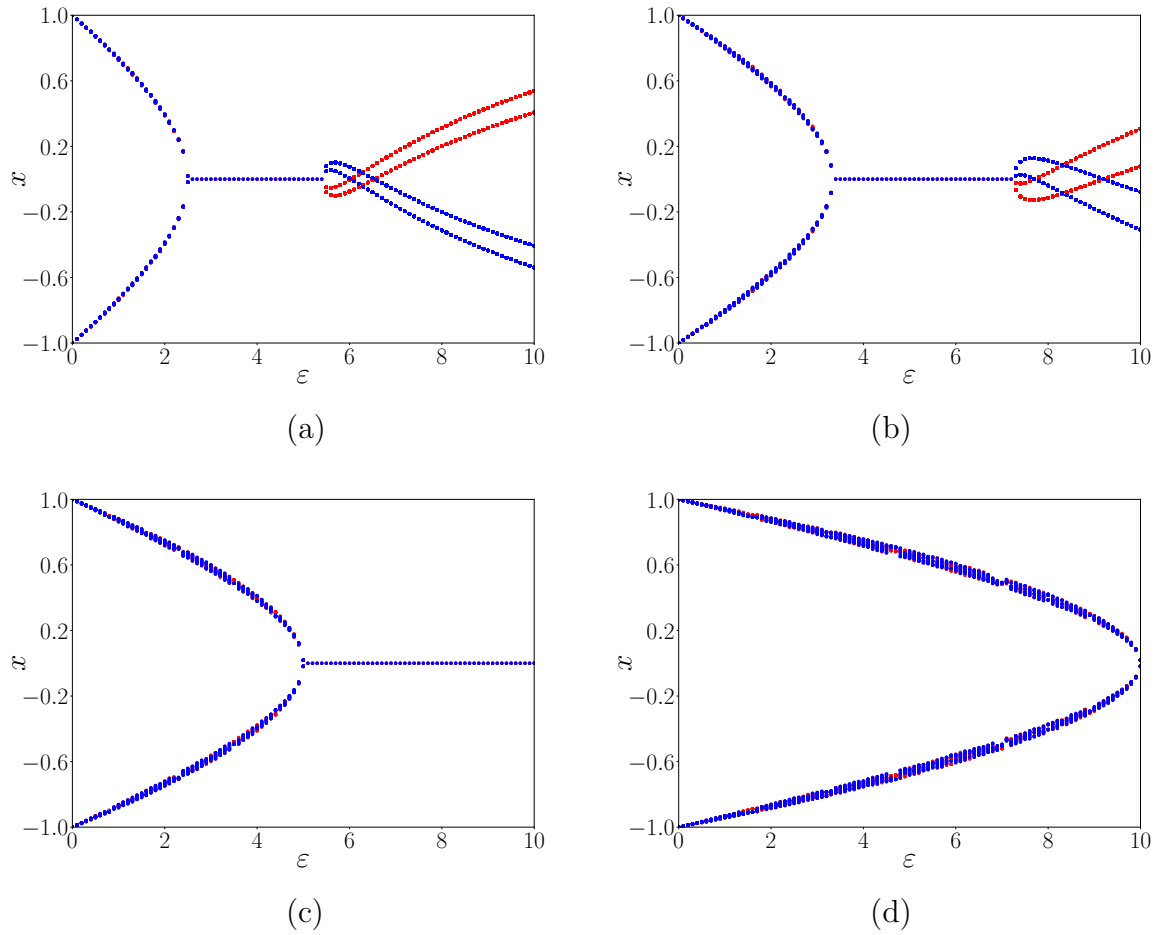

Figure 5.1: Bifurcation diagram displaying variable x of one of the oscillators, with respect to coupling strength ε. Here the coupling switches between similar and dissimilar variables periodically, with similar-variable coupling (for time $f_{sim}T$) followed by dissimilar-variable coupling (for time $(1 - f_{sim})T$), for (a) f_{sim}=0.2, (b) f_{sim}=0.4, (c) f_{sim}=0.6 and (d) f_{sim}=0.8, and time period of switching $T = 0.10$. The two colours represent symmetric solutions around the unstable fixed point, arising from different initial conditions. In all these diagrams, we display the x variable on the Poincaré section of the phase curves of the oscillators at $y = y_{\text{mid}}$, where y_{mid} is the mid-point of the span of phase space along the y-axis.

In this work we will consider coupling forms switching at frequencies ranging from very high to very low, as compared to the frequency of oscillation of the Stuart-Landau oscillators (cf. Eqn. 5.4). So when we refer to fast changes in coupling forms, we imply

that these changes occur at timescales significantly shorter than the oscillatory time period, namely, the switching time period T is much smaller than $2\pi/\omega$ (which is ~ 1.26 here).

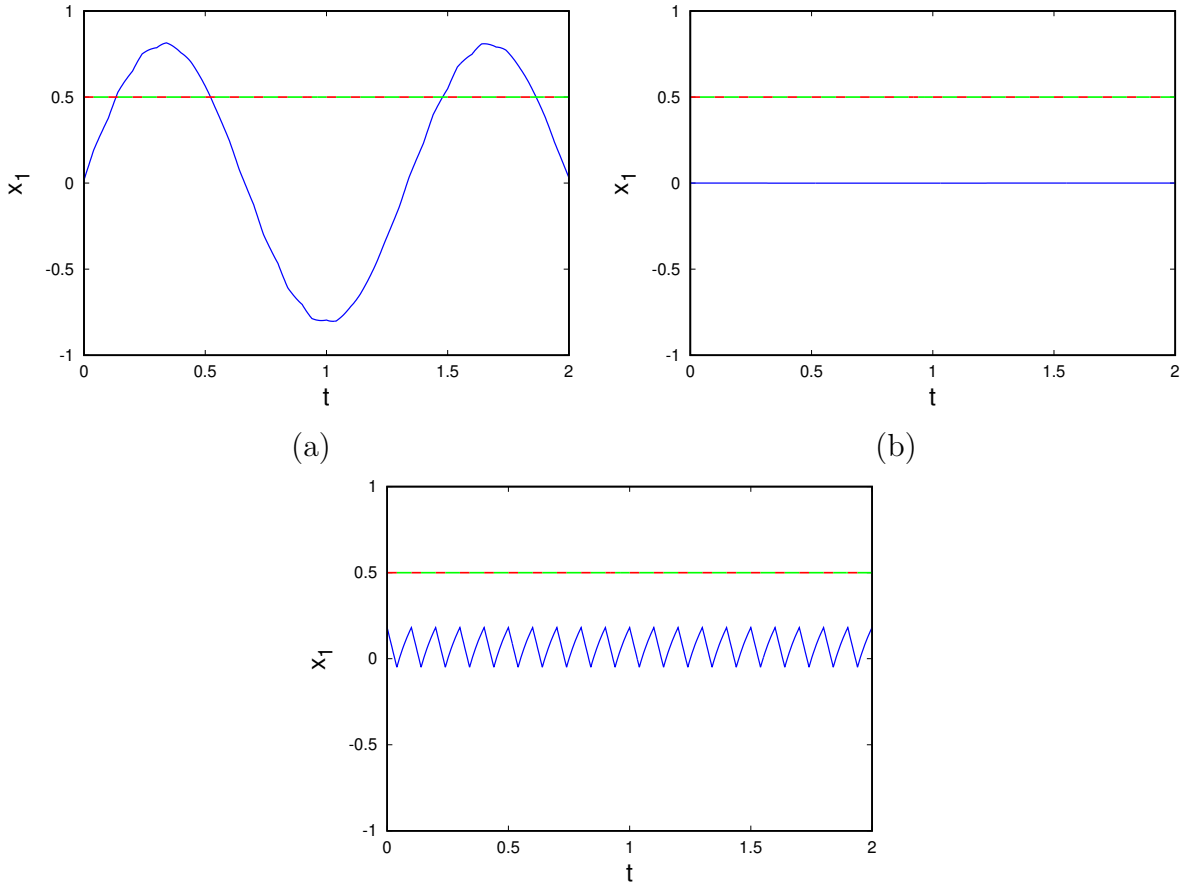

Figure 5.2: Time series of the variable x of one of the oscillators, shown in blue. The periodically switched coupling form is shown schematically, with red representing similar-variable coupling and green representing dissimilar-variable coupling. Here $f_{sim} = 0.4$, $T = 0.10$ and the coupling strengths are: (a) $\varepsilon = 1.0$, (b) $\varepsilon = 4.0$ and (c) $\varepsilon = 9.0$. Note that both the oscillators are synchronized, i.e. $x_1(t) = x_2(t)$

Fig. 5.1 shows the bifurcation diagram for a system of two coupled oscillators with periodically changing coupling form, with respect to coupling strength, for different f_{sim}. At $\varepsilon = 0$, i.e. for uncoupled Stuart-Landau oscillators, one naturally obtains period 1 oscillations. Increasing the coupling strength results in suppression of oscillations. Interestingly though, the window of coupling strength over which oscillations are suppressed depends non-monotonically on f_{sim}. At first, as f_{sim} increases the fixed point window increases (cf. Fig. 5.1a for $f_{sim} = 0.2$ vis-a-vis Fig. 5.1c at $f_{sim} = 0.6$). However, when f_{sim} gets even larger this window vanishes entirely (cf. Fig. 5.1d), namely the oscillations are

no longer suppressed anywhere. So importantly, it is evident from Fig. 5.1a-b that low-amplitude oscillations are restored at higher coupling strengths again, for intermediate f_{sim}.

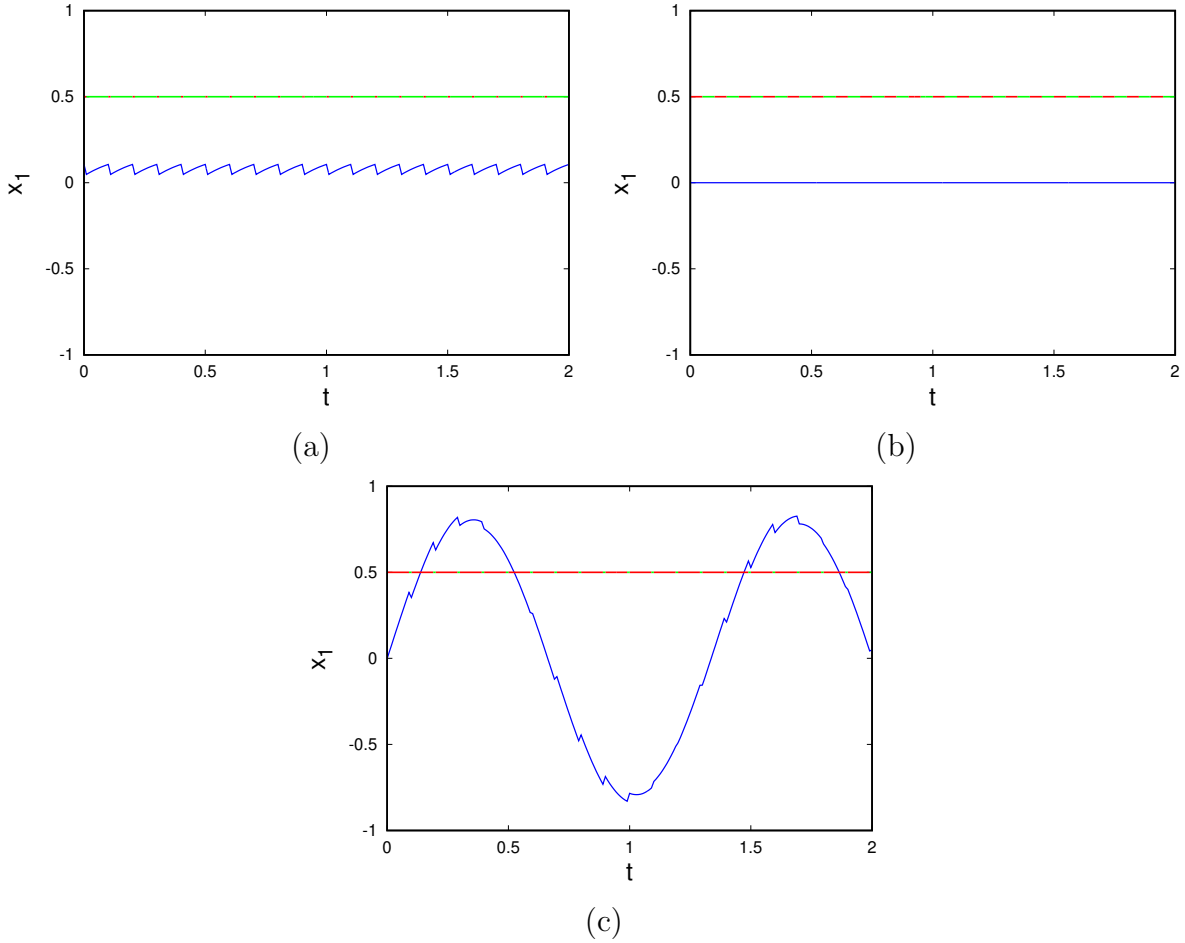

Figure 5.3: Time series of the variable x of one of the oscillators, shown in blue. The periodically switched coupling form is shown schematically, with red representing similar-variable coupling and green representing dissimilar-variable coupling. Here coupling strength $\varepsilon = 6$, $T = 0.10$ and f_{sim} is: (a) 0.1 (namely, dissimilar-variable coupling operates over much larger intervals than similar-variable coupling), (b) 0.5 (namely, successive equal time intervals of similar and dissimilar-variable coupling occurs) and (c) 0.9 (namely, similar-variable coupling operates over much larger intervals than dissimilar-variable coupling).

In order to gain an intuitive understanding of the suppression and revival of oscillations, we now examine the time series of the system with relation to the periodic switching of coupling forms. Fig. 5.2 shows the illustrative case of $f_{sim} = 0.4$, namely the case where the system experiences similar-variable coupling for a duration that is shorter than the duration of dissimilar-variable coupling. It is evident from Fig. 5.2a that when coupling

strength is relatively small, the dissimilar-variable coupling does not manage to influence the dynamics enough to suppress the oscillations induced by similar-variable coupling. This holds true, even though the dissimilar-variable coupling is operative for a much longer period than the similar-variable coupling.

Increasing the coupling strength decreases the amplitude of the oscillations, and beyond a critical value of coupling the oscillations are entirely suppressed (cf. Fig. 5.2b). However, beyond a window of coupling strengths, the oscillations are restored again (cf. Fig 5.2c). That is, for very high coupling strengths, the system evolves towards the attractor of the coupling form it experiences, and after the coupling switches, the system evolves towards the attractor characteristic of the other coupling form. Namely, for the duration the coupling is via similar variables, the system tends towards the limit cycle, and when the coupling is via dissimilar variables, the system tends towards the attractive fixed point. So, unlike the case of intermediate coupling strengths, the system switches its behaviour and never settles down to the fixed point attractor. This results in a cyclic behaviour following the periodic switching pattern. So remarkably different dynamical behaviour arises under identical switching of coupling forms, for different coupling strengths.

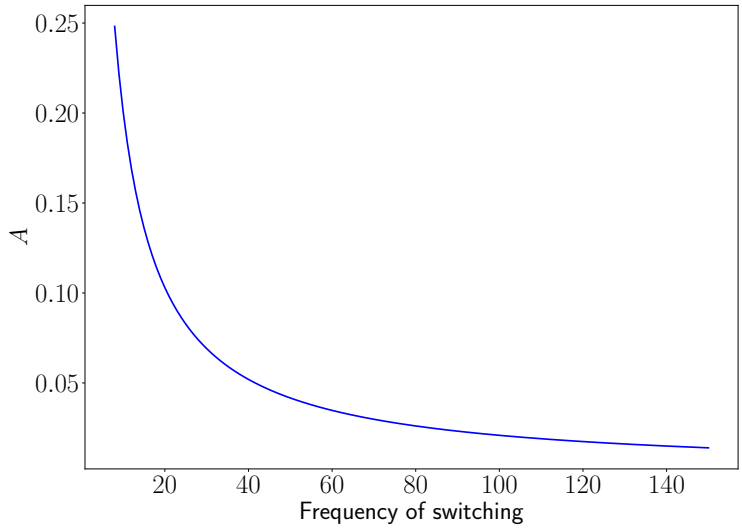

Figure 5.4: Dependence of $A = x_{max} - x_{min}$ on the frequency of switching (where x_{max}/x_{min} are the maximum/minimum values of variable x of an oscillator). Here $f_{sim} = 0.4$, $\varepsilon = 9.0$, and the coupling switches between similar and dissimilar variables periodically, with similar-variable coupling for time $f_{sim}T$, followed by dissimilar-variable coupling for time $(1 - f_{sim})T$, where $1/T$ is the frequency of switching.

Further, it is very illustrative to examine the time series of the system with relation to the switching of coupling forms, ranging from the case where dissimilar-variable coupling occurs over much longer time intervals than similar-variable coupling (i.e. f_{sim} close to zero) to the case where similar-variable coupling dominates (i.e. f_{sim} close to one), via the balanced case where equal periods of similar-variable and dissimilar-variable coupling occurs. It is evident from Fig. 5.3 that oscillation suppression occurs when there is balance in the two types of coupling. So very distinct dynamical behaviour arises under identical coupling strengths, but different switching patterns of the coupling forms.

Further, Fig. 5.4 shows the effect of the frequency of switching coupling forms upon the amplitude of the revived oscillations. Increase in frequency of switching leads to the reduction of oscillation amplitude, and the results approach those arising from effective mean-field like dynamical equations (cf. Eqn. 5.9) which will be presented in Section 5.5 (namely, Fig. 5.1(b) approaches Fig. 5.13(b) obtained from an approximate effective description of the system).

5.3.2 Probabilistic Switching of Coupling Forms

Here the oscillators change their coupling form at intervals of time T, with the coupling form chosen probabilistically. We consider the probability for the oscillators to be coupled via similar variables to be p_{sim}, and the probability of coupling mediated via dissimilar variables to be $(1-p_{sim})$. For $0 < p_{sim} < 1$, at the time of switching, the similar-variable coupling form is chosen with probability p_{sim} and the dissimilar-variable form is chosen with probability $(1-p_{sim})$. So larger p_{sim} favours coupling through similar variables and smaller p_{sim} favours dissimilar-variable coupling, with the oscillators always experiencing dissimilar-variable coupling for the limiting case of $p_{sim} = 0$ and similar-variable coupling for $p_{sim} = 1$. Here the probability p_{sim} plays a role equivalent to f_{sim} in the case of periodic switching of coupling forms.

This is explicitly given as follows:

$$\begin{aligned} \dot{x_1} &= f^x(x_1, y_1) + \varepsilon\delta(x_2 - x_1) + \varepsilon(1-\delta)(y_2 - x_1) \\ \dot{y_1} &= f^y(x_1, y_1) \\ \dot{x_2} &= f^x(x_2, y_2) + \varepsilon\delta(x_1 - x_2) + \varepsilon(1-\delta)(y_1 - x_2) \\ \dot{y_2} &= f^y(x_2, y_2) \end{aligned} \tag{5.7}$$

where

$$\delta = \begin{cases} 1, & \text{if } p \leq p_{sim} \text{ at } t = NT \\ 0, & \text{if } p > p_{sim} \text{ at } t = NT \end{cases} \tag{5.8}$$

where T is the switching period, $N = 0, 1, 2, ...$ is the number of periods.

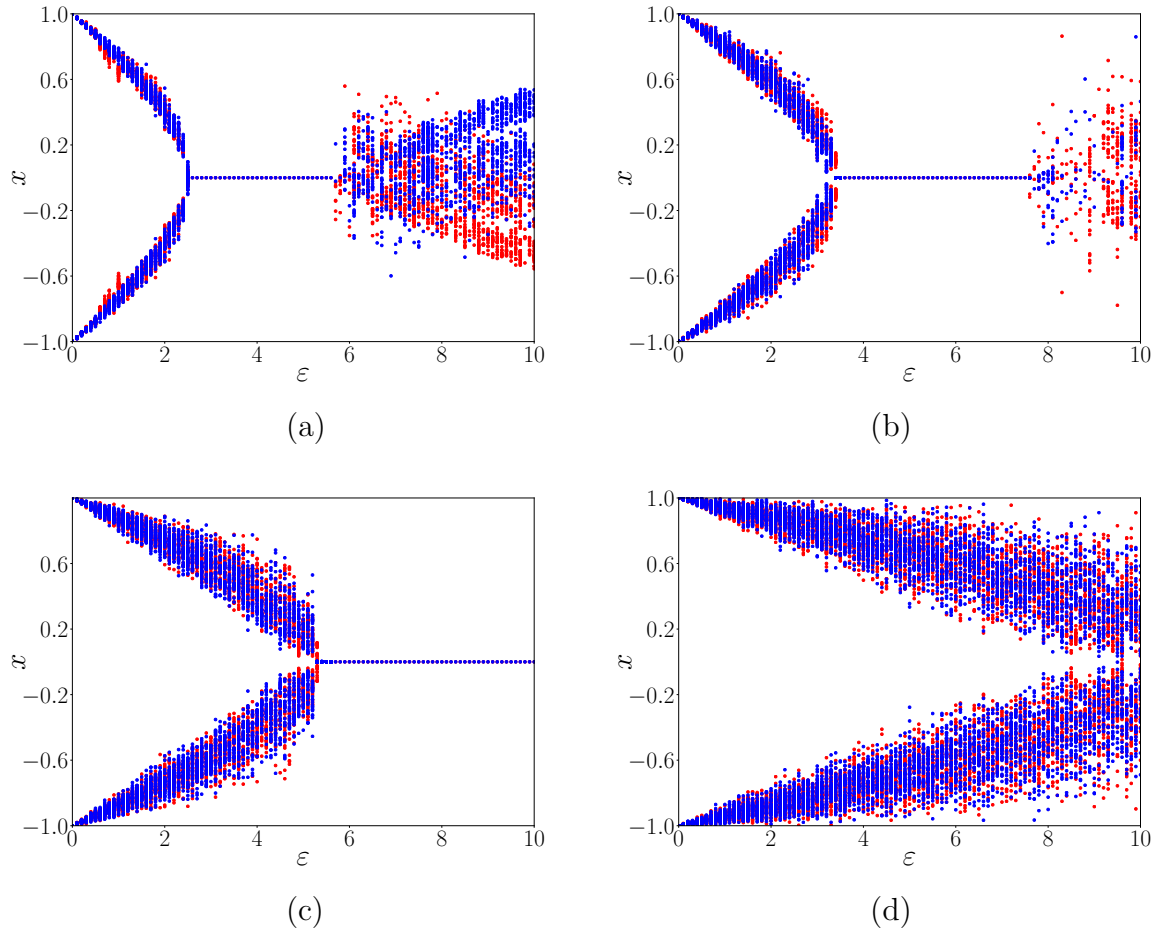

Figure 5.5: Bifurcation diagram displaying variable x of one of the oscillators, with respect to coupling strength ε. Here the coupling form probabilistically switches at time intervals of T between similar and dissimilar variables, with the probability of similar-variable coupling being p_{sim}, and the probability of dissimilar-variable coupling being $(1 - p_{sim})$, for (a) $p_{sim} = 0.2$, (b) $p_{sim} = 0.4$, (c) $p_{sim} = 0.6$ and (d) $p_{sim} = 0.8$ (with $T = 0.02$). The two colours represent emergent dynamics from different initial conditions

Fig. 5.5 shows the bifurcation diagram, with respect to coupling strength, for different p_{sim}. Again it is evident that the window of coupling strength over which oscillations are suppressed, depends non-monotonically on p_{sim}, as it did under variation of f_{sim} for the case of periodically switched coupling forms (cf. Fig. 5.8). First, as p_{sim} increases from zero, the fixed point window increases, as seen from Fig. 5.5a for $p_{sim} = 0.2$ vis-a-vis

Fig. 5.5c for $p_{sim} = 0.6$. However, when p_{sim} gets even larger this window vanishes entirely, as evident from Fig. 5.5d, and the oscillations are no longer suppressed anywhere. This suggests that when the probability of coupling through similar variables and dissimilar variables is similar (i.e. $p_{sim} \sim 0.5$) oscillations are suppressed to the greatest degree.

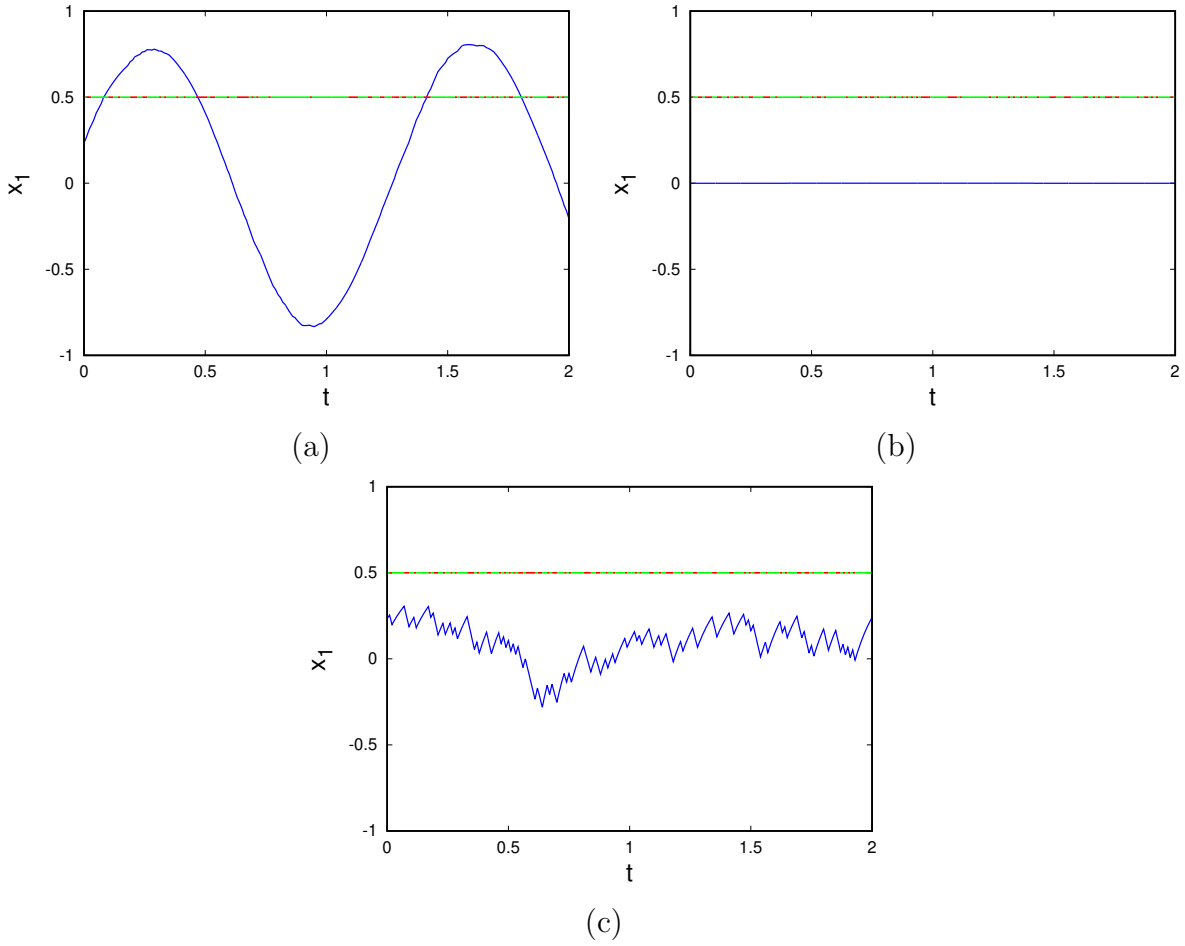

Figure 5.6: Time series of the variable x of one of the oscillators, shown in blue. The probabilistically switched coupling form is shown schematically, with red representing similar-variable and green representing dissimilar-variable coupling. Here $p_{sim} = 0.4$, $T = 0.01$ and the coupling strengths are: (a) $\varepsilon = 1.0$, (b) $\varepsilon = 4.0$ and (c) $\varepsilon = 9.0$

In order to gain an intuitive understanding of the revival of oscillations, we now examine the time series of the system with relation to the random switching of coupling forms. Fig. 5.6 shows the illustrative case of $p_{sim} = 0.4$. It is evident that when coupling strength is relatively small (cf. Fig. 5.6a), the dissimilar-variable coupling does not manage to influence the dynamics enough to suppress the oscillations arising from the similar-variable coupling. So one obtains noisy cycles. The amplitude of the oscillations again decreases with increasing coupling strength, and after a critical value the oscilla-

tions are fully suppressed (cf. Fig. 5.6b). However when the coupling strength is too high, oscillatory behaviour is revived once more. Underlying this revival of noisy oscillations is the following dynamics: the system evolves towards the attractor characterizing a coupling form for the duration that it experiences that particular coupling form. Namely, for the duration of similar-variable coupling, the system tends towards a limit cycle, and when the coupling is via dissimilar variables, the system tends towards the attractive fixed point (cf. Fig 5.6c). So the system switches its behaviour and never settles down to the fixed point attractor. This results in a fuzzy cyclic behaviour and so for coupling strengths higher than a critical value, noisy oscillations emerge again.

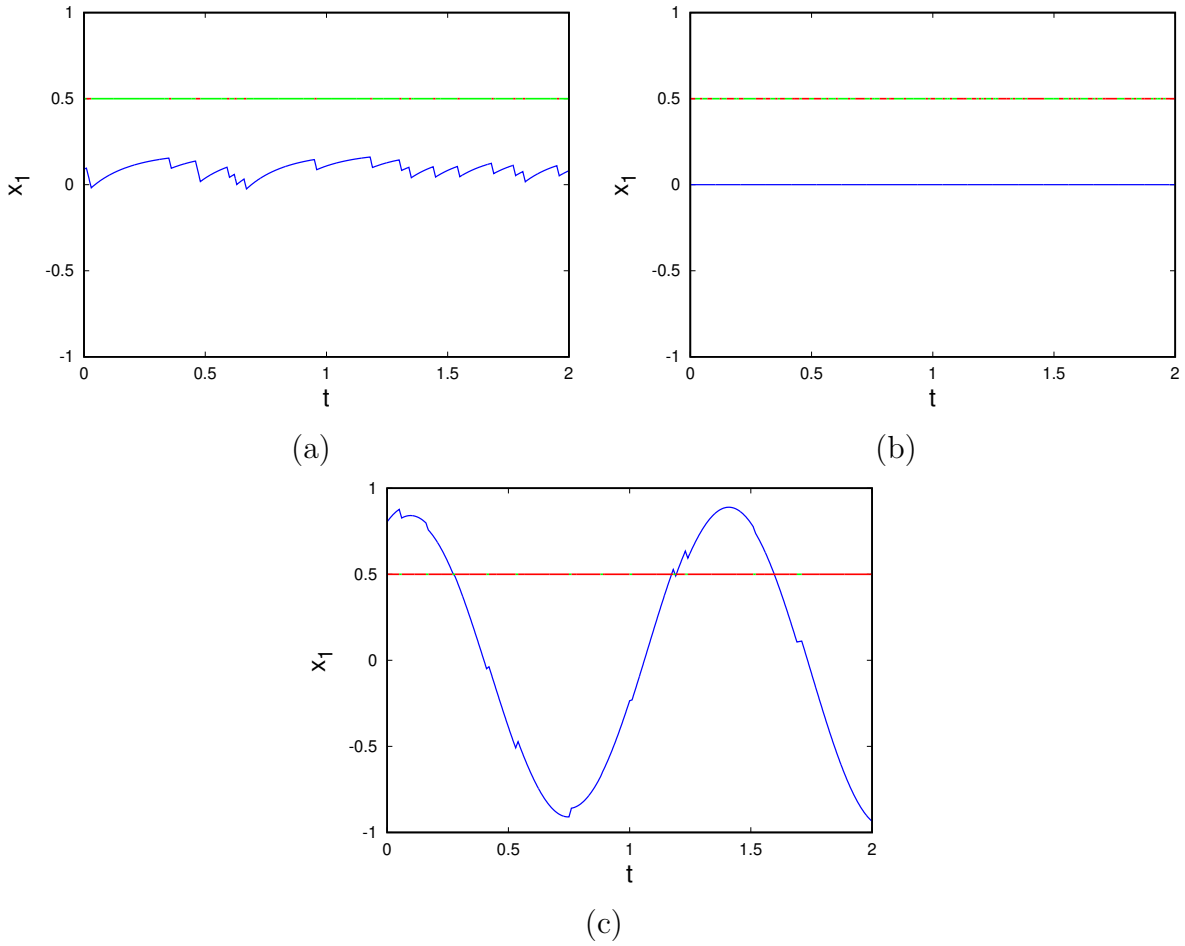

Figure 5.7: Time series of the variable x of one of the oscillators, shown in blue. The probabilistically switched coupling form is shown schematically, with red representing similar-variable coupling and green representing dissimilar-variable coupling. Here coupling strength $\varepsilon = 6$, $T = 0.01$ and p_{sim} is: (a) 0.1 (namely, dissimilar-variable coupling occurs much more frequently than similar-variable coupling), (b) 0.5 (namely, similar and dissimilar-variable coupling occurs equally often on an average) and (c) 0.9 (namely, similar-variable coupling occurs much more frequently than dissimilar-variable coupling).

Further, it is very illustrative to examine the time series of the system with relation to the switching of coupling forms, ranging from the case where dissimilar-variable coupling occurs more frequently than similar-variable coupling (i.e. p_{sim} close to zero) to the case where similar-variable coupling dominates (i.e. p_{sim} close to one), via the balanced case where similar-variable and dissimilar-variable coupling occurs equally often on an average. It is evident from Fig. 5.7 that very distinct dynamical behaviour arises under identical coupling strengths, but different switching patterns of the coupling forms, with oscillation suppression occurring when there is balance in the two types of coupling.

5.3.3 Dependence of the fixed point window on switching parameters

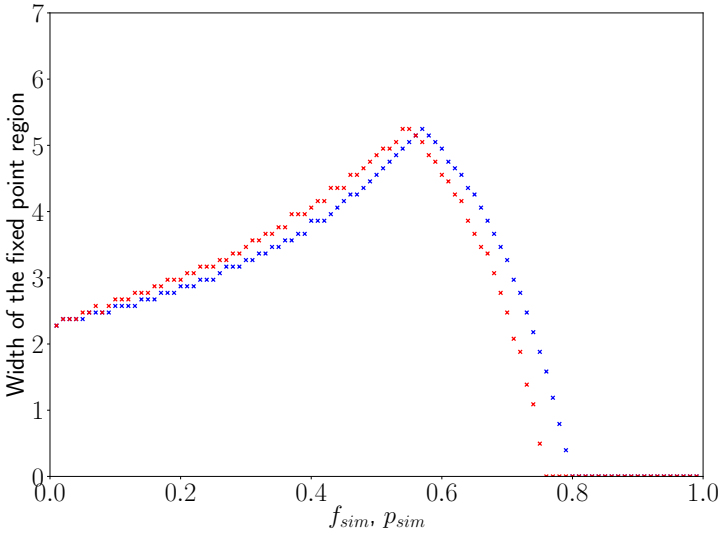

Figure 5.8: Relative width of the fixed point window (namely, the fraction of the coupling range under consideration that is occupied by the fixed point regime), as a function of f_{sim} (blue) for the case of periodic switching of coupling forms, and p_{sim} (red) for the case of probabilistic switching of coupling forms, with switching period $T = 0.02$. Here we consider coupling strengths ε in the range $[0 : 10]$.

Fig. 5.8 shows the width of fixed point window, with respect to f_{sim} for the case of periodic switching of coupling forms, and p_{sim} for the case of probabilistic switching of coupling forms. Now it is evident that if one has only similar-variable coupling, one obtains *no* fixed point states. On the other hand completely dissimilar-variable coupling yields a large amplitude death region. As one intuitively expects, one needs the system to experience dissimilar-variable coupling for sufficient time to yield fixed points. However,

one may also have expected simplistically that the amplitude-death window would reduce monotonically to zero as the probability of similar-variable coupling increased to one. But counter-intuitively, the size of the amplitude-death window in coupling parameter space is *non-monotonic*, and the largest window is obtained when dissimilar-variable coupling is switched approximately equally with similar-variable coupling. Namely, the width of the fixed point window has a maximum at $f_{sim}(p_{sim}) \sim 0.58$, an so the largest window of fixed point dynamics arises where there is balance in the probability of occurrence of the coupling forms.

5.4 Global stability measure

The commonly employed linear stability analysis, based on the linearization in the neighbourhood of fixed points, provides only local information about the stability at the fixed point. It cannot accurately indicate the stability for large perturbations, nor the basin of attraction of the dynamics, especially in the presence of other attractors in phase space.

Here we calculate the Basin Stability of the dynamical states [3]. This is a more robust and global estimate of stability, and effectively incorporates non-local and non-linear effects on the stability of fixed points. Specifically, Basin Stability is calculated as follows: we choose a large number of random initial conditions, spread uniformly over a volume of phase space, and find what fraction of these are attracted to stable fixed points.

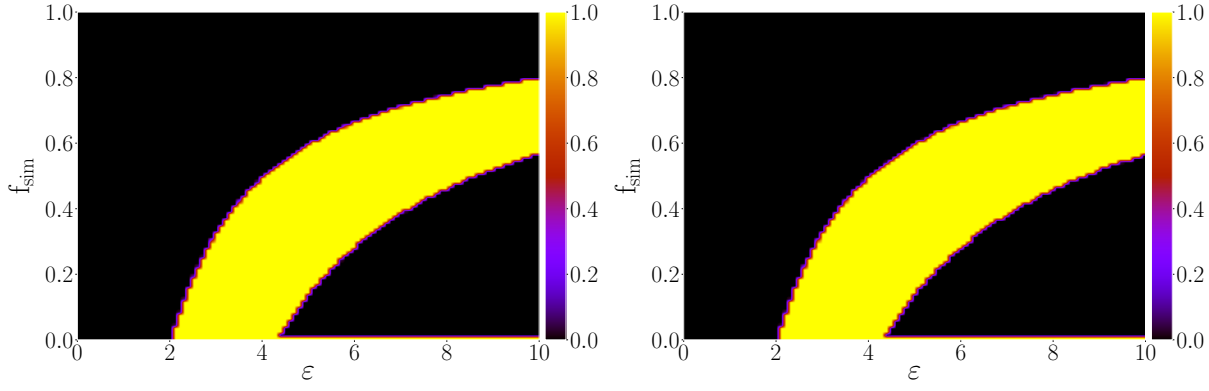

(a) (b)

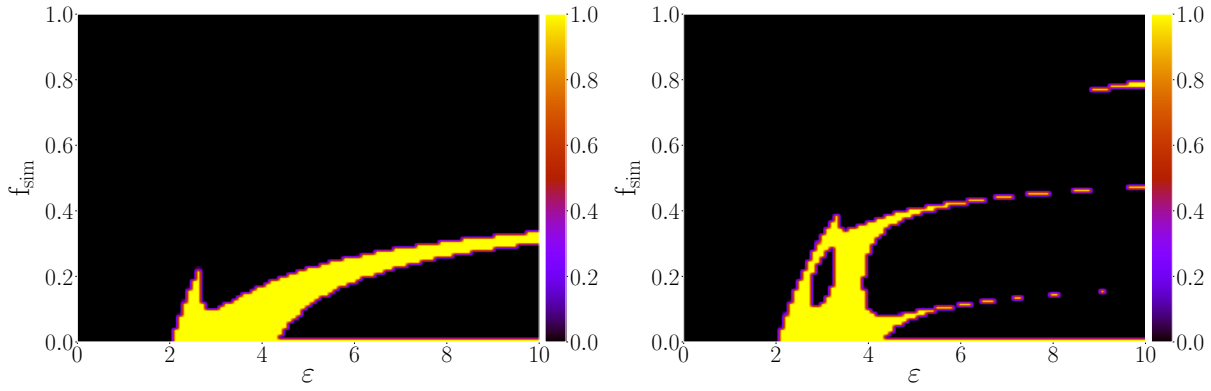

Figure 5.9: Basin Stability of the fixed point state of coupled oscillators, in the parameter space of coupling strength ε and f_{sim}. Here the coupling periodically switches between similar and dissimilar variables, with similar-variable coupling (for time $f_{sim}T$), followed by dissimilar-variable coupling (for time $(1 - f_{sim})T$), for (a) $T = 0.01$, (b) $T = 0.10$, (c) $T = 1.00$ and (d) $T = 2.00$. The region in yellow represents fixed point dynamics (i.e. oscillation suppression), and the region in black represents oscillatory dynamics.

Figs 5.9 shows the Basin Stability of the fixed point state, in the parameter space of f_{sim} and coupling strengths, for different time periods of switching T. Clearly one obtains oscillation suppression in windows of coupling strength and f_{sim}, and oscillation revival again beyond the window. The window of coupling strengths that gives rise to fixed points is very sensitive to the frequency of switching, at low frequencies, namely at frequencies that are considerably smaller than the oscillator frequency. After a high enough switching frequency (i.e. low enough T), the fixed point region remains unchanged, as evident through the fact that Fig. 5.9a and Fig. 5.9b are identical.

Now, the dependence of the fixed point window on f_{sim} is actually quite counter-intuitive, as already indicated in the bifurcation diagrams. For rapidly switched coupling forms, at large coupling strengths, the oscillation suppression occurs at an *intermediate* value of f_{sim}. Namely, as the dominance of similar-variable coupling f_{sim} increases the oscillations are first suppressed and then after a point the oscillations are revived again, with the window of fixed points shifting towards higher f_{sim}, as coupling strength increases. This is counter-intuitive, as similar-variable coupling is known to only allow oscillations, while dissimilar-variable coupling can yield some windows of oscillation suppression. Also interestingly for low f_{sim}, as we increase the coupling strength, first we encounter oscillation suppression and then on further increase of coupling strength the oscillations are restored. So there exists an intermediate window of coupling strength

that yields fixed point dynamics.

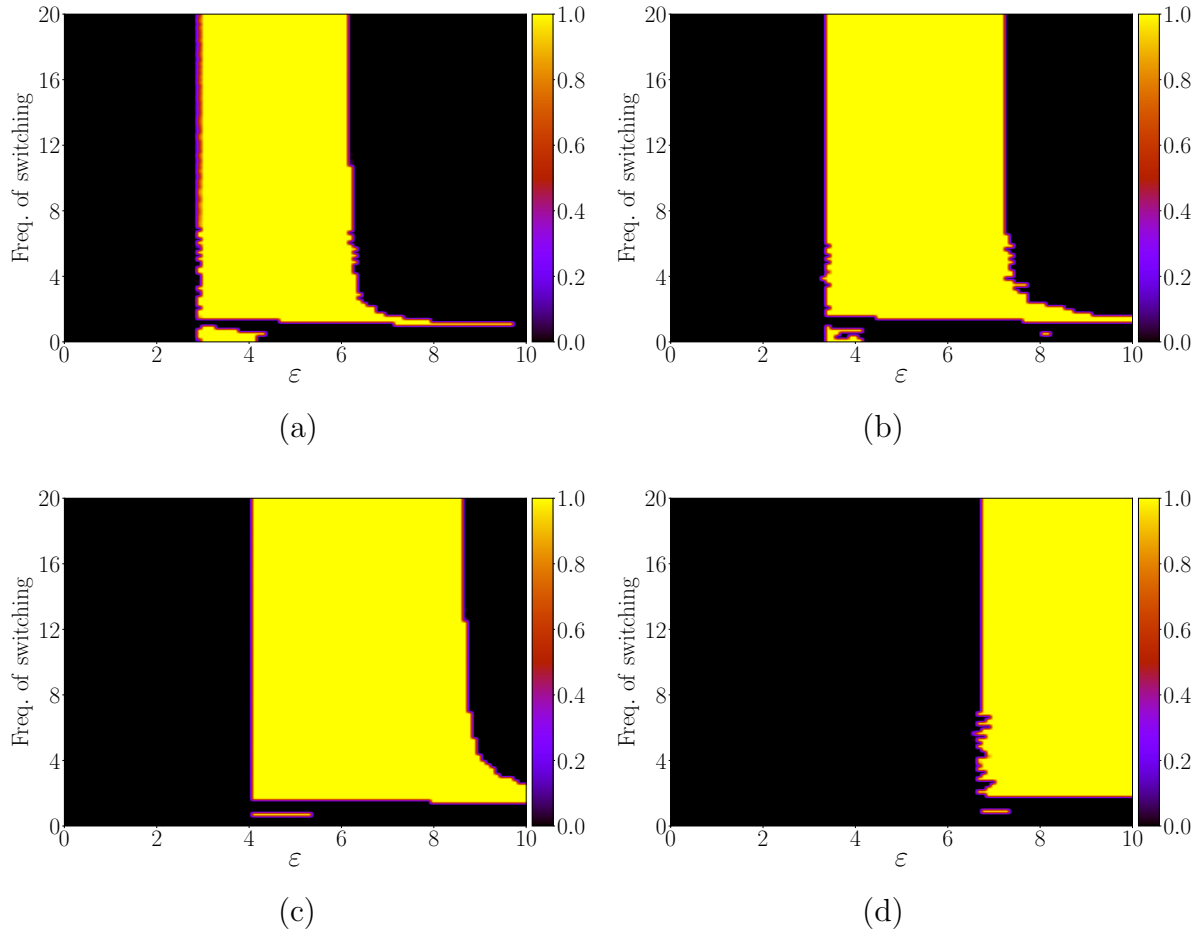

Figure 5.10: Basin Stability of the fixed point state of coupled oscillators, in the parameter space of coupling strength ε and frequency of switching. Here the coupling periodically switches between similar and dissimilar variables, with similar-variable coupling (for time $f_{sim}T$), followed by dissimilar-variable coupling (for time $(1-f_{sim})T$), for (a) $f_{sim} = 0.3$, (b) $f_{sim} = 0.4$, (c) $f_{sim} = 0.5$ and (d) $f_{sim} = 0.7$. The region in yellow represents fixed point dynamics (i.e. oscillation suppression), and the region in black represents oscillatory dynamics.

Fig 5.10 shows the Basin Stability of the fixed point state, in the parameter space of the frequency of switching and coupling strengths, for different f_{sim}. It is clear again that after a critical switching frequency the dynamics does not depend on the rate at which the coupling form is changed. Significantly, it is also evident that *fast changes in coupling form, namely lower time period for change, yields large fixed point regions in parameter space.* However, at low switching frequencies the emergent dynamics is sensitive to how rapidly the coupling form varies.

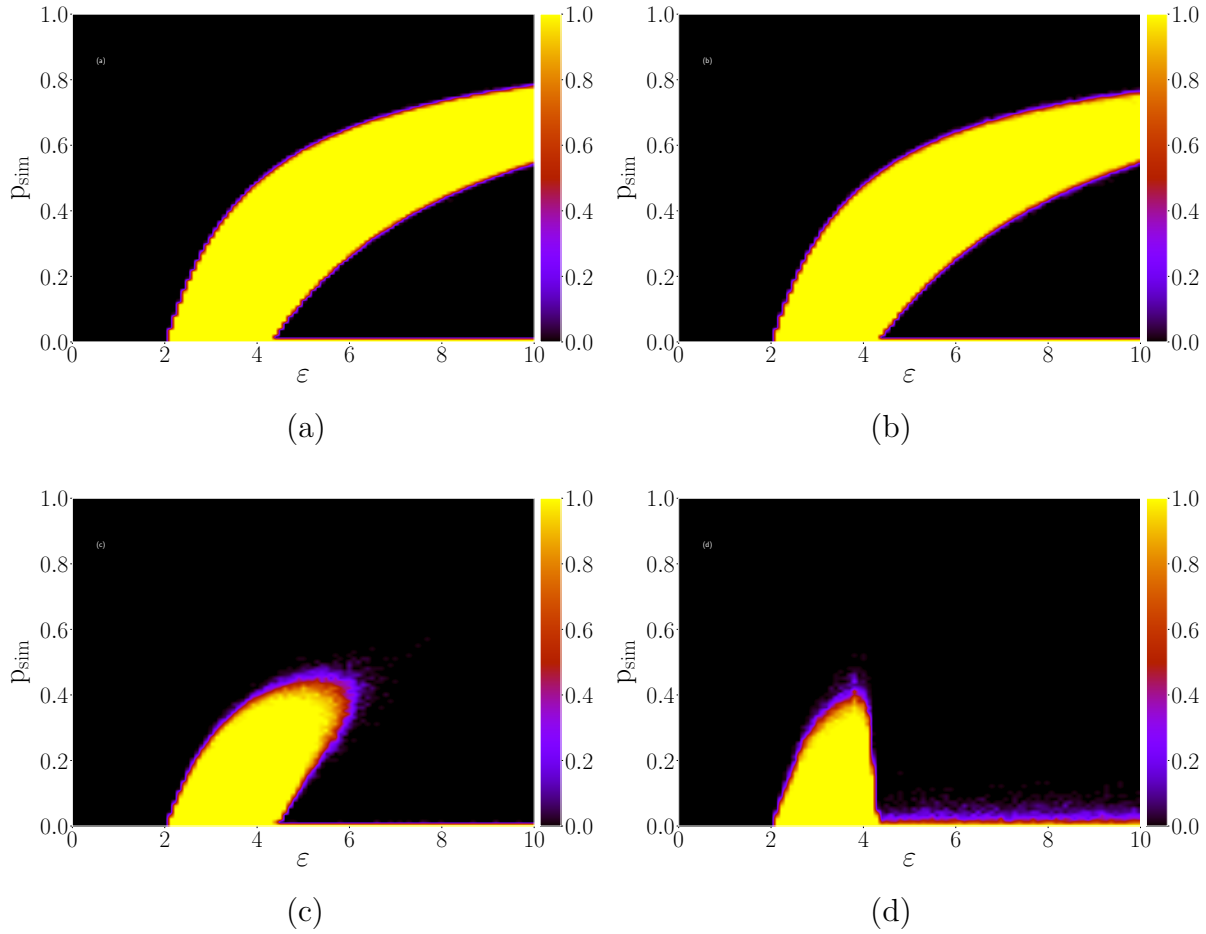

Figure 5.11: Basin Stability of the fixed point state of coupled oscillators, in the parameter space of coupling strength ε and p_{sim}. Here the coupling probabilistically switches between similar and dissimilar variables, with the probability of similar-variable coupling being p_{sim}, and the probability of dissimilar-variable coupling being $(1 - p_{sim})$ with the period of switching (a) $T = 0.01$, (b) $T = 0.02$, (c) $T = 0.10$ and (d) $T = 1.00$. The region in yellow represents fixed point dynamics (i.e. oscillation suppression), and the region in black represents oscillatory dynamics. Notice the marked similarity of panel (a) with Fig. 5.9a.

Fig 5.11 shows the Basin Stability of the fixed point state for the case of probabilistically varying coupling form, in the parameter space of p_{sim} and coupling strengths. *Interestingly again, as we increase the coupling strength, oscillations first get suppressed and then restored.* Also notice the marked similarity of Fig. 5.11a and Fig. 5.9a. Namely frequent periodic switching of coupling forms yields the same result as the frequent probabilistic switching of coupling forms.

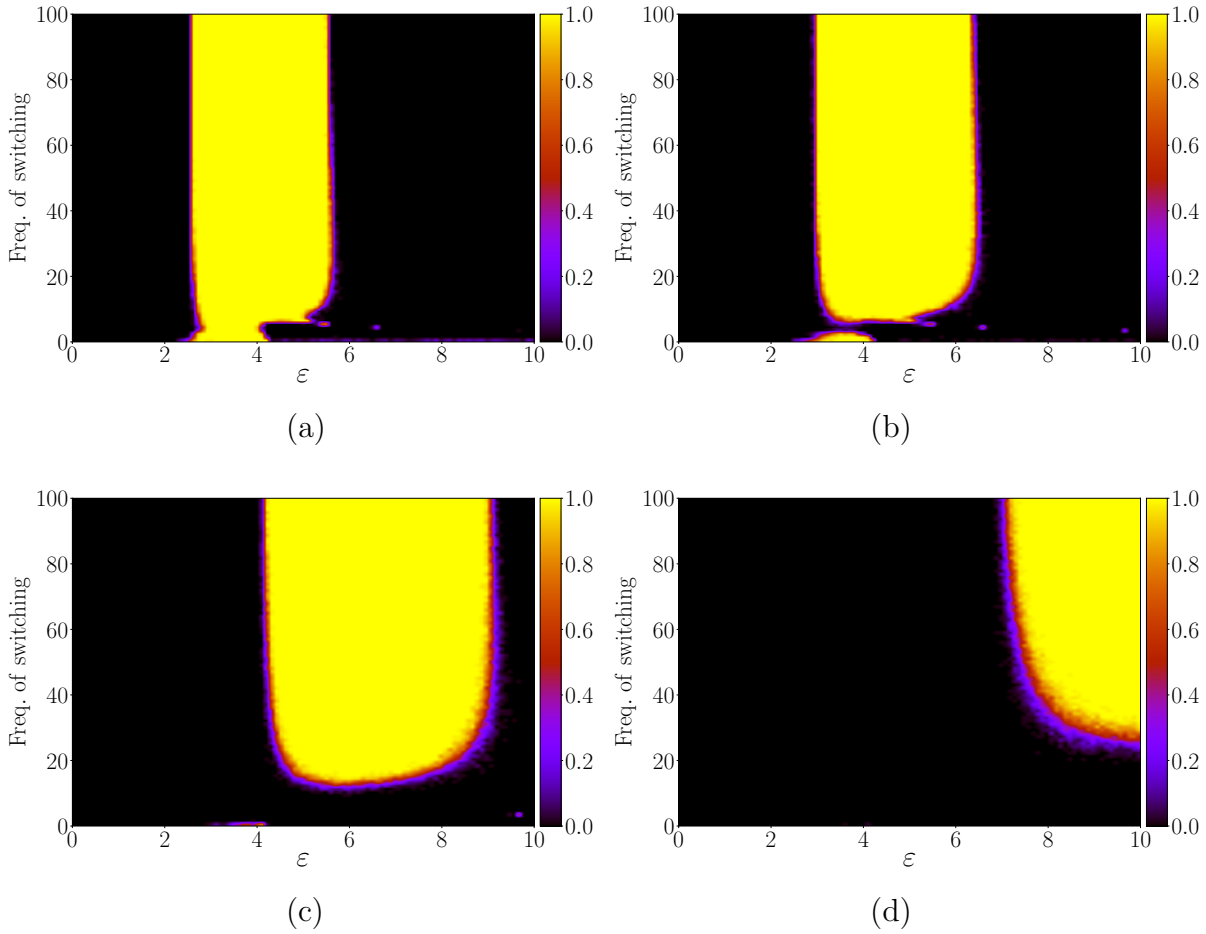

Figure 5.12: Basin Stability results for coupled oscillators, in the parameter space of coupling strength ε and frequency of switching, when coupling switches between similar and dissimilar variables probabilistically, with a probability of similar coupling p_{sim}, and probability of dissimilar coupling $(1 - p_{sim})$, for (a) $p_{sim} = 0.2$, (b) $p_{sim} = 0.3$, (c) $p_{sim} = 0.5$ and (d) $p_{sim} = 0.7$. The region in yellow represents fixed point dynamics (i.e. oscillation suppression), and the region in black represents oscillatory dynamics.

Fig. 5.12 shows the Basin Stability of the fixed point state, in the parameter space of frequency of switching and coupling strengths. Clearly the effects of the frequency of switching are pronounced over a larger range of switching frequency for probabilistic switching, as compared to periodic switching. But significantly again, it is evident that *fast changes in coupling form, namely lower time period for change, yields large fixed point regions in parameter space.* Lastly, it is also clear that as the frequency of switching increases, the fixed point region moves towards higher values of p_{sim} where similar-variable coupling dominates. This is again surprising, as similar-variable coupling is known to support only oscillations, while dissimilar-variable coupling has more propensity towards oscillation suppression.

5.5 Effective model for time dependent coupling

Now we attempt to rationalize our results through an effective phenomenological model for the dynamics. The idea is to mimic the time-dependent coupling by a coupling form where the similar and dissimilar coupling forms are appropriately weighted by f_{sim}. This is given by:

$$\begin{aligned} \dot{x_1} &= f^x(x_1, y_1) + \varepsilon[f_{sim}(x_2 - x_1) + (1 - f_{sim})(y_2 - x_1)] \\ \dot{y_1} &= f^y(x_1, y_1) \\ \dot{x_2} &= f^x(x_2, y_2) + \varepsilon[f_{sim}(x_1 - x_2) + (1 - f_{sim})(y_1 - x_2)] \\ \dot{y_2} &= f^y(x_2, y_2) \end{aligned} \tag{5.9}$$

This effective picture is then akin to *hybrid coupling*, and this is expected to hold true when the frequency of switching is very high (namely T is very small). Completely equivalent results can be obtained with p_{sim} in place of f_{sim} in the equations above.

The Jacobian of the effective system is given by:

$$\begin{pmatrix} 1 - 3x_1^2 - y_1^2 - \varepsilon & -2x_1y_1 - \omega & \varepsilon f_{sim} & \varepsilon(1 - f_{sim}) \\ -2x_1y_1 + \omega & 1 - x_1^2 - 3y_1^2 & 0 & 0 \\ \varepsilon f_{sim} & \varepsilon(1 - f_{sim}) & 1 - 3x_2^2 - y_2^2 - \varepsilon & -2x_2y_2 - \omega \\ 0 & 0 & -2x_2y_2 + \omega & 1 - x_2^2 - 3y_2^2 \end{pmatrix} \tag{5.10}$$

The eigenvalues of the matrix above, evaluated at the fixed points, determine the stability of the fixed points, and the change in the eigenvalues under variation of parameters indicates the nature of bifurcations. Thus the mechanism for the suppression of oscillations following the stabilization of fixed points, and the revival of oscillations following the destabilization of fixed points, can be obtained by inspection of the eigenspectrum.

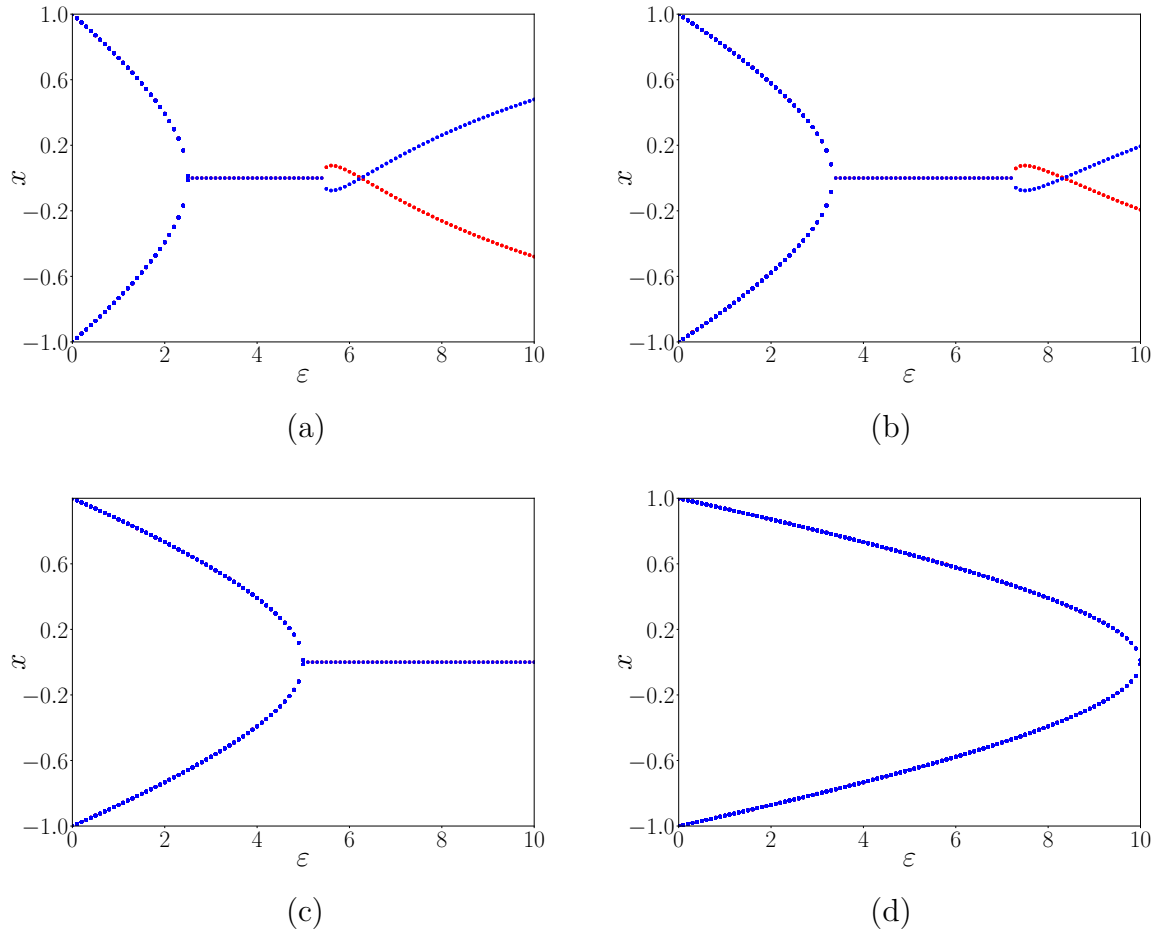

Figure 5.13: Bifurcation diagram displaying variable x of one of the oscillators of the effective coupled system given by Eqn. 5.9, with respect to coupling strength ε, at different f_{sim} values: (a) f_{sim}=0.2, (b) f_{sim}=0.4, (c) f_{sim}=0.6 and (d) f_{sim}=0.8. The two colours represent symmetric solutions around the unstable fixed point, arising from different initial conditions.

Fig. 5.13 displays the bifurcation diagram of the effective coupled system given by Eqn. 5.9. The nature of the bifurcations is determined by the change in the eigenspectrum under varying coupling strength. For instance, for $f_{sim} < 0.58$, there are two bifurcation points. At the first bifurcation point occuring at low coupling strength, the real parts of complex eigenvalues cross zero and become positive as coupling strength is decreased, leading to a transition from a stable fixed point to a limit cycle, namely we have a supercritical Hopf bifurcation. At the second bifurcation point occuring at high coupling strength, the real eigenvalues cross zero and become positive as coupling strength increases, leading the fixed point to become unstable and this is accompanied by the creation of two new fixed points, namely we have a supercritical pitchfork bifurcation. In particular, notice the marked similarity of the fixed point region in Fig. 5.13 with the

fixed point regions evident in Figs. 5.1 and 5.5.

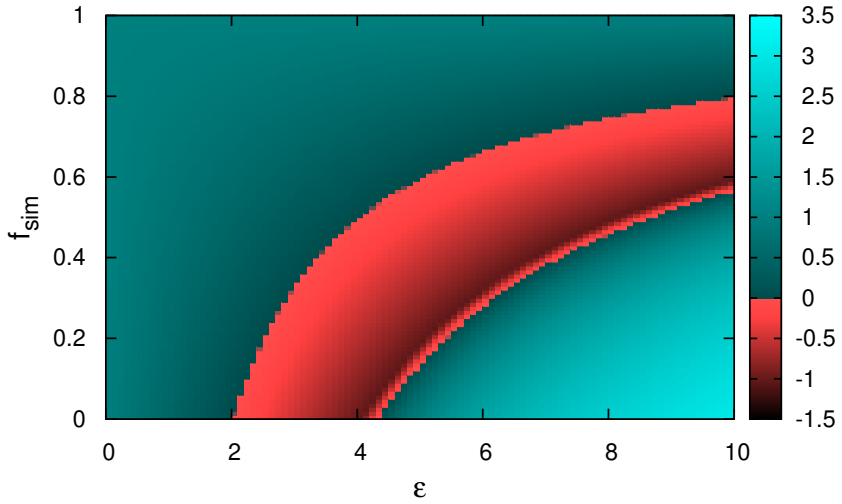

Figure 5.14: Results from Linear Stability analysis of the effective model of the coupled oscillators given by Eqn. 5.9, in the parameter space of coupling strength ε and f_{sim}. The colour code represents the value of the maximum eigen value of the Jacobian given by Eqn. 5.10, λ_{max}. The region in pink, where $\lambda_{max} < 0$, represents stable fixed points. The region in green, where $\lambda_{max} > 0$, represents unstable fixed points. Notice the marked similarity with Figs. 5.9a and 5.11a.

Further, Fig. 5.14 shows results from the linear stability analysis of Eqn. 5.9, in the neighbourhood of the fixed point at zero. The region in pink represents the stable fixed point, where the maximum eigen value of the Jacobian (cf. Eqn. 5.10) corresponding to Eqn. 5.9, λ_{max}, is negative. The region in green represents unstable fixed points, and this corresponds to the parameter region where $\lambda_{max} > 0$. Notice the marked similarity of these results with Fig. 5.9a (or equivalently Fig. 5.11a), namely the fixed point region is completely well-described by the analysis of Eqn. 5.9 when the frequency of switching is high ($\sim$ 100 Hz). Significantly then, the results from the global estimates of the basin of stability of the fixed point, for rapid periodic and probabilistic switching of coupling form, are *recovered accurately through the linear stability analysis of a set of effective dynamical equations.* So our effective picture provides insight into the suppression and revival of oscillations in the coupled oscillator system with time-varying coupling forms.

5.6 Conclusions

While the variation in links, namely the connectivity matrix, as a function of time has been investigated in recent times, the dynamical consequences of time-varying coupling forms is still not understood. In this work we have explored this new direction in time-varying interactions, namely we have studied the effect of switched coupling forms on the emergent behaviour. The test-bed of our enquiry is a generic system of coupled Stuart-Landau oscillators, where the form of the coupling between the oscillators switches between the similar and dissimilar (or conjugate) variables. We consider two types of switching, one where the coupling function changes periodically and one where it changes probabilistically. When the oscillators change their coupling form periodically, they are coupled via similar variables for fraction f_{sim} of the cycle, followed by coupling to dissimilar variables for the remaining part. In the case of probabilistic switching, the probability for the oscillators to be coupled via similar variables is p_{sim}, and the probability of coupling mediated via dissimilar variables is $(1 - p_{sim})$.

We find that time-varying coupling forms suppress oscillations in a window of coupling strengths, with the window increasing with the frequency of switching. That is, *more rapid changes in coupling form leads to large windows of oscillation suppression*, with the window of amplitude death saturating after a high enough switching frequency. Interestingly, for low f_{sim} (p_{sim}), the *oscillations are revived* again beyond this window. That is, too low or too high coupling strengths yield oscillations, while coupling strengths in-between suppress oscillations.

Also interestingly, the width of the coupling strength window supporting oscillation suppression is non-monotonic with respect to $f_{sim}(p_{sim})$, and has a maximum at $f_{sim}(p_{sim}) \sim 0.58$. Namely, the largest window of fixed point dynamics arises where there is balance in the probability of occurrence of the coupling forms.

Focusing on the dependence of the window of oscillation suppression, at fixed coupling strengths and varying predominance of coupling forms, we observe the following: for rapidly switched coupling forms, at large coupling strengths, the oscillation suppression occurs at an *intermediate* value of f_{sim} (p_{sim}). Namely, as the dominance of similar-variable coupling increases the oscillations are first suppressed, and then after a point the oscillations are revived again. The fixed point window shifts towards a higher probability of similar-variable coupling, as coupling strength increases. This is counter-intuitive, as purely similar-variable coupling yields oscillatory behaviour, while dissimilar-variable coupling supports oscillation suppression.

Lastly, we have suggested an effective dynamics that successfully yields the observed behaviour for rapidly switched coupling forms, including an accurate estimate of the fixed point window through stability analysis. Thus our results will enhance the broad understanding of coupled systems with time-varying connections, and may have potential applications in certain natural and human engineered systems.

Chapter 6

Summary and future directions

In this thesis, we have focussed on the effect of external systems on a group of chaotic oscillators, symmetry breaking of oscillation death states in the presence of an external environment and revival of oscillations via time-varying interactions in oscillators that are in the oscillation death state. So the main focus of my thesis is on mechanisms that suppress oscillations or control chaotic oscillations, as well as revive oscillations in the oscillation death region.

In the first problem of the thesis, we have explored the dynamics of an ensemble of uncoupled chaotic oscillators where the group is coupled bi-directionally to an external system. So the oscillators in the ensemble are not directly connected to each other, but information transfer of their states is mediated by the external oscillator. The model is reminiscent of a pacemaker controlling the dynamics of a group of oscillators. We consider the case where the external system is similar to those in the group, as well as the case where it is dissimilar to the group. The question we focus is the following: can a single external system control a large number of chaotic oscillators onto regular dynamical states? In our work, we have considered Rössler oscillators in the group and varied the external system. First we considered the external system to be similar to the group, namely the external system was also a Rössler oscillator. We found that at low coupling strength, all the oscillators were desynchronized. As coupling strength was increased, after a critical coupling strength, all the oscillators in the group and the external oscillator, were in complete synchronization. (Note that we considered coupling strength in the range $[0, 1]$). So except for the transition to synchronization, no other significant phenomena emerged for the case of similar external systems.

We then changed the external system to a Lorenz oscillator, i.e. the external system

was now dissimilar to the oscillator group, and now the results were significantly different. At low coupling strength, all systems were desynchronized. On increasing the coupling strength, at some critical value, all the oscillators in the group synchronized, except the external system. This is not surprising, as the intrinsic dynamics of the external system is completely different. However the surprising part is that, even though there is no direct connection between the oscillators in the group, they synchronize while sustaining their chaotic dynamics. As coupling strength was further increased an interesting phenomenon emerged: there exists a second critical coupling strength beyond which all chaotic oscillators in the system went to a suppressed state, i.e. they were all controlled to fixed points. In this oscillation-suppression regime, the oscillators in the ensemble evolved to one fixed point, while the external dissimilar system evolved to a different fixed point. The value of the second critical coupling strength is dependent upon the initial state of the oscillators and the external system. If the initial conditions are very close to the fixed points, very low coupling strength is required to suppress the oscillations. As the initial state moves away from the fixed points, higher coupling strength is required for suppression. But the important point is that the chaos was suppressed to fixed point dynamics in all cases at sufficiently high coupling strengths. Since the Lorenz system supports two stable fixed points, there is bi-stability in the coupled system as well, with two sets of fixed points arising in the oscillation-suppressed external system depending upon the initial conditions. We have also analysed the system, by calculating the maximum eigenvalue of the Jacobian of a system consisting of a Lorenz oscillator as the external system, and two Rössler oscillators in the group. We have shown that the fixed points become stable at higher coupling strengths, as the maximum eigenvalue becomes negative after a certain critical coupling strength. This analysis is consistent with the numerical simulations.

For the generality of the work, we have also considered the external system to be a hyper-chaotic oscillator, namely a system with more than one positive Lyapunov exponent. Now the external system is not only different in dynamical equations, but different in dimensionality as well. We again found that the chaotic oscillations were suppressed at sufficiently high coupling strengths. The results shown are independent of system size, i.e. any number of oscillators can be controlled by this method. So this suggests that our work is quite general and can be applied to different fields where obtaining a steady state is important, like in laser systems. Also vice-versa, in some cases suppression of oscillation is not desired, like in Alzheimer and Parkinson disease, and here too it is important to find underlying mechanisms that may give rise to oscillation suppression in order to maintain the oscillatory dynamics.

The second problem is an extension of the idea of controlling chaotic oscillation via

a single external system. After finding that just one dissimilar external system manages to suppress the oscillations of all oscillators in the group, we then wanted to focus on the more general problem: What if, instead of the star-like network above, we consider hierarchical networks – would chaos suppression still emerge? Hierarchical networks combine properties of scale-free topology and high clustering of the nodes and describe connections characteristic of many real-life networks ranging from metabolic networks to webpage and social networks. There are different levels in such networks and an element at a level is connected to those in the level above and in the level below it in the network. We consider the external system to be at the zeroth level (i.e. "top") of the hierarchy. We first considered an external system similar to the rest of the oscillators in the network, i.e. an external Rössler oscillator. We found that in the coupling range $[0, 1]$, an external system that is dynamically similar to those in the rest of the hierarchical network does not suppress the oscillations of any oscillators in the network. It takes coupling strengths higher than 1.0 to suppress the chaotic oscillations in such a network. We then consider a dissimilar chaotic system as the external system, specifically the Lorenz oscillator. Remarkably, we now find that the chaotic oscillations are suppressed beyond a critical coupling strength ($< 1.$). Interestingly, all the oscillators at all levels get suppressed at the same critical coupling strength, and oscillators in a level attain the same fixed point, with the emergent fixed points being different at different levels in the hierarchy. Linear stability analysis of the system reveals that the oscillations are suppressed and the fixed point stabilized when the maximum eigenvalue of the relevant Jacobian becomes negative. To ascertain the generality of our results, we have also considered the external system to be hyper-chaotic systems, limit cycle oscillators and linear oscillators. We observe that suppression of chaos occurs for all these external systems. The critical coupling strength beyond which chaos is controlled depends upon the initial conditions and the nature of the external oscillator. So in summary, in this chapter we have investigated the behaviour of hierarchical networks of chaotic oscillators, where at the zeroth level of the hierarchy we have a single external system that is dissimilar to the rest of the oscillators in the network. Remarkably, this external system managed to successfully steer the chaotic oscillators at all levels of the hierarchy onto steady states, at sufficiently high coupling strengths. So this suggests a potent method to efficiently control chaotic dynamics in a hierarchical network to stable steady states, by simply coupling to an external chaotic system. Hierarchical networks are more general than star networks, but the same question can be investigated in even more general classes of networks, like random scale-free networks which are widely applicable models of human-engineered and naturally occurring networks. So a natural extension of the ideas in the first two chapters of this thesis is to explore the possibility of chaos suppression through a single dissimilar system in

other broad network classes.

An extension of this work can be made to networks of other topologies, such as a random scale-free network or a random network. It would be very interesting to ascertain the nature of the nodes where a dissimilar system can be placed for most effect on the dynamics of the full system. In the context of control, it would be valuable to find out what property of the dissimilar node is most influential for suppression of chaos in different network classes.

In the next problem of the thesis, we have explored another aspect of oscillation suppression: Oscillation Death (OD) states. Oscillation death is quite interesting in itself because a system can attain different fixed points. So if we have an ensemble of oscillators, statistically half of them go to one fixed point and half to the other fixed point, i.e. the sizes of the basins of attraction for the fixed points of the OD state are equal. Here we have considered Stuart-Landau oscillators coupled via mean field interaction, with parameters chosen such that the oscillators are in the Oscillation Death state. We denote the fixed point of the OD state with positive x-value as the "positive state" and the other fixed point with negative x-value to be the "negative state".

The question we wanted to focus on was the following: *can the symmetry of the basin stability of the oscillation death states be broken in the presence of an environment?* As a test-bed of our investigation we have considered a simple exponentially decaying environment, i.e. if the environment receives no feedback from the oscillators, it will decay to zero. We have coupled this environment to the group of oscillators in OD states, and varied the coupling strength and environmental damping constant. For a fixed value of damping constant, when we increase the coupling strength, the oscillators evolve preferentially to the negative state from generic random initial conditions. Increasing the coupling strength further, we find that the basin stability of the negative state jumps to almost 1 (and the basin stability of the positive state shows a sudden transition to nearly zero). So the symmetry of the basin stability of the oscillation death states is significantly broken. The same phenomenon is observed for fixed coupling strength and varying damping constant. For low damping constant, the symmetry is significantly broken, and there is a sharp transition from the asymmetric to the symmetric state as the value of damping constant increases. We have also empirically found an analytic expression to describe the asymmetry-symmetry transition curve in the parameter space of environment-oscillator coupling strength and environmental damping constant.

Next, we have focussed on the links between the oscillators and the environment.

Specifically, we investigate the effect of blinking links or completely disconnected links. For the scenario of blinking links, we have one more significant parameter to consider: the fraction of blinking connections. We fix the coupling strength and damping constant near the transition curve, in the asymmetric region, and increase the fraction of blinking connections. We find that there is a sharp transition from the asymmetric state to the symmetric state on increasing the fraction of blinking links, i.e. the fraction of oscillators in the positive state boosts up to nearly half when the number of blinking connections is sufficiently high. We have calculated the fraction of oscillators in the positive state in the parameter space of environment-oscillator coupling strength and environmental damping constant for a different fractions of blinking connections. It is evident that the transition curve shifts monotonically in such a way that the symmetric region increases and the asymmetric region decreases. But this monotonicity is lost, if the links are permanently broken or disconnected, rather than blinking. When very few oscillators are connected to the environment, the OD states are almost symmetrically distributed. On the other hand, when a large fraction of oscillators are coupled to the environment, the symmetry is broken to a very great extent, for high environment-oscillator coupling strengths and low environmental damping constants. Interestingly, when half the environment-oscillator links are disconnected, the symmetry is restored, independent of the damping constant of the environment and the environment-oscillator coupling strength. In fact, in this case, exactly half of the oscillators attain positive OD states and the other half attain negative OD states.

In the last section of this chapter, we have changed the environment. The exponentially decaying environment mimics a situation where the external environment is a small bath, and so the dynamics of the oscillator group affects the dynamics of the common environment. Now we have considered a common external environmental system mimicking a large bath, where the external environment does not get affected by the oscillator group, rather it acts as a constant drive. Here we also found marked breaking of symmetry in the basin stability of oscillator death states. When the constant drive is large, the asymmetry in the OD-states is very large as well, and the transition between the symmetric and asymmetric state, with increasing oscillator-environment coupling, is sharp. So this work suggests easy controllability of the basin stability of oscillation death states and a mechanism to obtain certain states preferentially.

In the last problem of the thesis, we have focussed on the dynamics of two Stuart-Landau oscillators, interacting with time-varying coupling forms. We have considered two types of coupling forms: diffusive coupling (coupling in similar variable) and conjugate coupling (coupling in dissimilar variable). The diffusive coupling form leads to synchro-

nized oscillations, while conjugate coupling form leads to oscillation suppression. While time-varying links have been investigated in recent times, time-varying coupling forms have not been in focus. We considered two different mechanisms of switching coupling forms, namely, periodic switching and probabilistic switching. We find that time-varying coupling forms suppress oscillations in a window of coupling strengths, with the window increasing with the frequency of switching. That is, more rapid changes in coupling form leads to large windows of oscillation suppression, with the window of amplitude death saturating after a high enough switching frequency. Interestingly, the oscillations are revived again beyond this window. That is, too low or too high coupling strengths yield oscillations while coupling strengths in-between suppress oscillations. Also interestingly, the width of the coupling strength window supporting oscillation suppression is non-monotonic, and the largest window of fixed point dynamics arises where there is a balance in the probability of occurrence of the coupling forms. Further, we have analyzed an effective dynamics of the oscillators under time-varying coupling forms that successfully yields the observed behaviour for rapidly switched coupling forms. Our analysis also provides an accurate estimate of the fixed point window through linear stability analysis. Thus our results will enhance the broad understanding of coupled systems with time-varying connections and may have potential applications in certain natural and human engineered systems.

For future work, one can explore the revival of oscillations in other dynamical systems, such as a group of neurons, which may be inactive or active. For instance, one can investigate if a group of inactive neurons that are not bursting, can be revived through coupling to a small set of active neurons. The significant parameters in such a scenario would be connection density and the balance of intra-group and inter-group coupling strengths. We anticipate that our results above will provide the base and intuition for addressing this class of problems.

In summary, we have explored a broad range of problems concerning the control of networks of chaotic oscillators including hierarchical networks. Further we have explored the suppression and revival of oscillations, as well as the phenomena of symmetry breaking in the basin stability of oscillation death states in coupled nonlinear oscillators. So our results shed light on the emergent collective dynamics of interactive nonlinear systems, thus serving to enhance the general understanding of such complex systems.

Bibliography

[1] Yoshiki Kuramoto. *Chemical oscillations, waves, and turbulence*, volume 19. Springer Science & Business Media, 2012.

[2] OE Rossler. An equation for hyperchaos. *Physics Letters A*, 71(2-3):155–157, 1979.

[3] Peter J Menck, Jobst Heitzig, Norbert Marwan, and Jürgen Kurths. How basin stability complements the linear-stability paradigm. *Nature physics*, 9(2):89, 2013.

[4] Marco Storace, Daniele Linaro, and Enno de Lange. The hindmarsh–rose neuron model: bifurcation analysis and piecewise-linear approximations. *Chaos: An Interdisciplinary Journal of Nonlinear Science*, 18(3):033128, 2008.

[5] Andrey Shilnikov. Complete dynamical analysis of a neuron model. *Nonlinear Dynamics*, 68(3):305–328, 2012.

[6] Jun Ma, Chun-Ni Wang, Wu-Yin Jin, and Ying Wu. Transition from spiral wave to target wave and other coherent structures in the networks of hodgkin–huxley neurons. *Applied Mathematics and Computation*, 217(8):3844–3852, 2010.

[7] Maruthi Pradeep Kanth Jampa, Abhijeet R Sonawane, Prashant M Gade, and Sudeshna Sinha. Synchronization in a network of model neurons. *Physical Review E*, 75(2):026215, 2007.

[8] Grigory V Osipov, Jürgen Kurths, and Changsong Zhou. *Synchronization in oscillatory networks*. Springer Science & Business Media, 2007.

[9] György Buzsáki and Andreas Draguhn. Neuronal oscillations in cortical networks. *science*, 304(5679):1926–1929, 2004.

[10] Kedma Bar-Eli. On the stability of coupled chemical oscillators. *Physica D: Nonlinear Phenomena*, 14(2):242–252, 1985.

[11] Milos Dolnik and Irving R Epstein. Coupled chaotic chemical oscillators. *Physical Review E*, 54(4):3361, 1996.

[12] Krasimira Tsaneva-Atanasova, Charles L Zimliki, Richard Bertram, and Arthur Sherman. Diffusion of calcium and metabolites in pancreatic islets: killing oscillations with a pitchfork. *Biophysical journal*, 90(10):3434–3446, 2006.

[13] A Koseska, E Volkov, and J Kurths. Parameter mismatches and oscillation death in coupled oscillators. *Chaos: An Interdisciplinary Journal of Nonlinear Science*, 20(2):023132, 2010.

[14] I Ozden, S Venkataramani, MA Long, BW Connors, and AV Nurmikko. Strong coupling of nonlinear electronic and biological oscillators: reaching the "amplitude death" regime. *Physical review letters*, 93(15):158102, 2004.

[15] Neeraj Kumar Kamal and Sudeshna Sinha. Emergent patterns in interacting neuronal sub-populations. *Communications in Nonlinear Science and Numerical Simulation*, 22(1-3):314–320, 2015.

[16] Jun Ma, Xinlin Song, Wuyin Jin, and Chuni Wang. Autapse-induced synchronization in a coupled neuronal network. *Chaos, Solitons & Fractals*, 80:31–38, 2015.

[17] Ming-Dar Wei and Jau-Ching Lun. Amplitude death in coupled chaotic solid-state lasers with cavity-configuration-dependent instabilities. *Applied Physics Letters*, 91(6):061121, 2007.

[18] Min-Young Kim, Rajarshi Roy, Joan L Aron, Thomas W Carr, and Ira B Schwartz. Scaling behavior of laser population dynamics with time-delayed coupling: theory and experiment. *Physical review letters*, 94(8):088101, 2005.

[19] Pramod Kumar, Awadhesh Prasad, and R Ghosh. Stable phase-locking of an external-cavity diode laser subjected to external optical injection. *Journal of Physics B: Atomic, Molecular and Optical Physics*, 41(13):135402, 2008.

[20] David C Johns, Ruth Marx, Richard E Mains, Brian O'Rourke, and Eduardo Marbán. Inducible genetic suppression of neuronal excitability. *Journal of Neuroscience*, 19(5):1691–1697, 1999.

[21] Dennis J Selkoe. Toward a comprehensive theory for alzheimer's disease. hypothesis: Alzheimer's disease is caused by the cerebral accumulation and cytotoxicity of amyloid β-protein. *Annals of the New York Academy of Sciences*, 924(1):17–25, 2000.

[22] Rudolph E Tanzi. The synaptic aβ hypothesis of alzheimer disease. *Nature neuroscience*, 8(8):977, 2005.

[23] Byron Caughey and Peter T Lansbury Jr. Protofibrils, pores, fibrils, and neurodegeneration: separating the responsible protein aggregates from the innocent bystanders. *Annual review of neuroscience*, 26(1):267–298, 2003.

[24] Sudeshna Sinha and William L Ditto. Exploiting the controlled responses of chaotic elements to design configurable hardware. *Philosophical Transactions of the Royal Society A: Mathematical, Physical and Engineering Sciences*, 364(1846):2483–2494, 2006.

[25] J Pun and SE Semercigil. Joint stiffness control of a two-link flexible arm. *Nonlinear Dynamics*, 21(2):173–192, 2000.

[26] PA Meehan and SF Asokanthan. Control of chaotic motion in a spinning spacecraft with a circumferential nutational damper. *Nonlinear Dynamics*, 17(3):269–284, 1998.

[27] Nilesh Bhoir and Sahjendra N Singh. Output feedback modular adaptive control of a nonlinear prototypical wing section. *Nonlinear Dynamics*, 37(4):357–373, 2004.

[28] JR Pratt and AH Nayfeh. Design and modeling for chatter control. *Nonlinear Dynamics*, 19(1):49–69, 1999.

[29] Yuanqing Wu, Hongye Su, Peng Shi, Zhan Shu, and Zheng-Guang Wu. Consensus of multiagent systems using aperiodic sampled-data control. *IEEE transactions on cybernetics*, 46(9):2132–2143, 2016.

[30] Yuan-Qing Wu, Hongye Su, Renquan Lu, Zheng-Guang Wu, and Zhan Shu. Passivity-based non-fragile control for markovian jump systems with aperiodic sampling. *Systems & Control Letters*, 84:35–43, 2015.

[31] Yuanqing Wu, Hongye Su, Peng Shi, Renquan Lu, and Zheng-Guang Wu. Output synchronization of nonidentical linear multiagent systems. *IEEE transactions on cybernetics*, 47(1):130–141, 2017.

[32] V Resmi, G Ambika, and RE Amritkar. General mechanism for amplitude death in coupled systems. *Physical Review E*, 84(4):046212, 2011.

[33] P Hadley, MR Beasley, and K Wiesenfeld. Phase locking of josephson-junction series arrays. *Physical Review B*, 38(13):8712, 1988.

[34] Michael F Crowley and Irving R Epstein. Experimental and theoretical studies of a coupled chemical oscillator: phase death, multistability and in-phase and out-of-phase entrainment. *The Journal of Physical Chemistry*, 93(6):2496–2502, 1989.

[35] PM Varangis, A Gavrielides, Thomas Erneux, Vassilios Kovanis, and LF Lester. Frequency entrainment in optically injected semiconductor lasers. *Physical review letters*, 78(12):2353, 1997.

[36] Peter J Menck and Jürgen Kurths. Topological identification of weak points in power grids. In *NDES 2012; Nonlinear Dynamics of Electronic Systems*, pages 1–4. VDE, 2012.

[37] Giuliano Andrea Pagani and Marco Aiello. Power grid complex network evolutions for the smart grid. *Physica A: Statistical Mechanics and its Applications*, 396:248–266, 2014.

[38] Chunguang Li, Luonan Chen, and Kazuyuki Aihara. Transient resetting: A novel mechanism for synchrony and its biological examples. *PLoS computational biology*, 2(8):e103, 2006.

[39] Serge Daan and Charles Berde. Two coupled oscillators: simulations of the circadian pacemaker in mammalian activity rhythms. *Journal of Theoretical Biology*, 70(3):297–313, 1978.

[40] Stefano Boccaletti, Jürgen Kurths, Grigory Osipov, DL Valladares, and CS Zhou. The synchronization of chaotic systems. *Physics reports*, 366(1-2):1–101, 2002.

[41] Alex Arenas, Albert Díaz-Guilera, Jurgen Kurths, Yamir Moreno, and Changsong Zhou. Synchronization in complex networks. *Physics reports*, 469(3):93–153, 2008.

[42] Sudeshna Sinha, Ramakrishna Ramaswamy, and J Subba Rao. Adaptive control in nonlinear dynamics. *Physica D: Nonlinear Phenomena*, 43(1):118–128, 1990.

[43] Adilson E Motter. Cascade control and defense in complex networks. *Physical Review Letters*, 93(9):098701, 2004.

[44] Sudeshna Sinha and Neelima Gupte. Adaptive control of spatially extended systems: targeting spatiotemporal patterns and chaos. *Physical Review E*, 58(5):R5221, 1998.

[45] P Parmananda, P Sherard, RW Rollins, and HD Dewald. Control of chaos in an electrochemical cell. *Physical Review E*, 47(5):R3003, 1993.

[46] K Murali and Sudeshna Sinha. Experimental realization of chaos control by thresholding. *Physical Review E*, 68(1):016210, 2003.

[47] Alan Garfinkel, Mark L Spano, William L Ditto, and James N Weiss. Controlling cardiac chaos. *Science*, 257(5074):1230–1235, 1992.

[48] Sudhanshu Shekhar Chaurasia and Sudeshna Sinha. Suppression of chaos through coupling to an external chaotic system. *Nonlinear Dynamics*, 87(1):159–167, 2017.

[49] Sudeshna Sinha, Gabriel Pérez, and Hilda A Cerdeira. Hierarchical globally coupled systems. *Physical Review E*, 57(5):5217, 1998.

[50] Isao Nishikawa, Naofumi Tsukamoto, and Kazuyuki Aihara. Switching phenomenon induced by breakdown of chaotic phase synchronization. *Physica D: Nonlinear Phenomena*, 238(14):1197–1202, 2009.

[51] Chiranjit Mitra, Anshul Choudhary, Sudeshna Sinha, Jürgen Kurths, and Reik V Donner. Multiple-node basin stability in complex dynamical networks. *Physical Review E*, 95(3):032317, 2017.

[52] Aneta Koseska, Evgeny Volkov, and Jürgen Kurths. Oscillation quenching mechanisms: Amplitude vs. oscillation death. *Physics Reports*, 531(4):173–199, 2013.

[53] DV Ramana Reddy, Abhijit Sen, and George L Johnston. Time delay induced death in coupled limit cycle oscillators. *Physical Review Letters*, 80(23):5109, 1998.

[54] Wei Zou and Meng Zhan. Partial time-delay coupling enlarges death island of coupled oscillators. *Physical Review E*, 80(6):065204, 2009.

[55] Rajat Karnatak, Ram Ramaswamy, and Awadhesh Prasad. Amplitude death in the absence of time delays in identical coupled oscillators. *Physical Review E*, 76(3):035201, 2007.

[56] Donald G Aronson, G Bard Ermentrout, and Nancy Kopell. Amplitude response of coupled oscillators. *Physica D: Nonlinear Phenomena*, 41(3):403–449, 1990.

[57] Aneta Koseska, Ekkehard Ullner, Evgenii Volkov, Juergen Kurths, and Jordi García-Ojalvo. Cooperative differentiation through clustering in multicellular populations. *Journal of theoretical biology*, 263(2):189–202, 2010.

[58] Narito Suzuki, Chikara Furusawa, and Kunihiko Kaneko. Oscillatory protein expression dynamics endows stem cells with robust differentiation potential. *PloS one*, 6(11):e27232, 2011.

[59] Wei Zou, DV Senthilkumar, Aneta Koseska, and Jürgen Kurths. Generalizing the transition from amplitude to oscillation death in coupled oscillators. *Physical Review E*, 88(5):050901, 2013.

[60] Aneta Koseska, Evgenii Volkov, and Jürgen Kurths. Transition from amplitude to oscillation death via turing bifurcation. *Physical review letters*, 111(2):024103, 2013.

[61] AN Pisarchik. Oscillation death in coupled nonautonomous systems with parametrical modulation. *Physics Letters A*, 318(1-2):65–70, 2003.

[62] Aneta Koseska, Evgenij Volkov, and Juergen Kurths. Detuning-dependent dominance of oscillation death in globally coupled synthetic genetic oscillators. *EPL (Europhysics Letters)*, 85(2):28002, 2009.

[63] CR Hens, Olasunkanmi I Olusola, Pinaki Pal, and Syamal K Dana. Oscillation death in diffusively coupled oscillators by local repulsive link. *Physical Review E*, 88(3):034902, 2013.

[64] Wei Zou, Chenggui Yao, and Meng Zhan. Eliminating delay-induced oscillation death by gradient coupling. *Physical Review E*, 82(5):056203, 2010.

[65] Jana Wolf and Reinhart Heinrich. Dynamics of two-component biochemical systems in interacting cells; synchronization and desynchronization of oscillations and multiple steady states. *Biosystems*, 43(1):1–24, 1997.

[66] WOLF Jana and Reinhart Heinrich. Effect of cellular interaction on glycolytic oscillations in yeast: a theoretical investigation. *Biochemical Journal*, 345(2):321–334, 2000.

[67] VP Zhdanov and B Kasemo. Synchronization of metabolic oscillations: Two cells and ensembles of adsorbed cells. *Journal of biological physics*, 27(4):295–311, 2001.

[68] Ruiqi Wang and Luonan Chen. Synchronizing genetic oscillators by signaling molecules. *Journal of biological Rhythms*, 20(3):257–269, 2005.

[69] Alexey Kuznetsov, Mads Kærn, and Nancy Kopell. Synchrony in a population of hysteresis-based genetic oscillators. *SIAM Journal on Applied Mathematics*, 65(2):392–425, 2004.

[70] Florian Geier, Sabine Becker-Weimann, Achim Kramer, and Hanspeter Herzel. Entrainment in a model of the mammalian circadian oscillator. *Journal of biological rhythms*, 20(1):83–93, 2005.

[71] Didier Gonze, Samuel Bernard, Christian Waltermann, Achim Kramer, and Hanspeter Herzel. Spontaneous synchronization of coupled circadian oscillators. *Biophysical journal*, 89(1):120–129, 2005.

[72] Guy Katriel. Synchronization of oscillators coupled through an environment. *Physica D: Nonlinear Phenomena*, 237(22):2933–2944, 2008.

[73] Erika Camacho, Richard Rand, and Howard Howland. Dynamics of two van der pol oscillators coupled via a bath. *International Journal of Solids and Structures*, 41(8):2133–2143, 2004.

[74] Chikara Furusawa and Kunihiko Kaneko. Emergence of rules in cell society: differentiation, hierarchy, and stability. *Bulletin of Mathematical Biology*, 60(4):659–687, 1998.

[75] Jordi Garcia-Ojalvo, Michael B Elowitz, and Steven H Strogatz. Modeling a synthetic multicellular clock: repressilators coupled by quorum sensing. *Proceedings of the National Academy of Sciences*, 101(30):10955–10960, 2004.

[76] Michael A Henson. Modeling the synchronization of yeast respiratory oscillations. *Journal of theoretical biology*, 231(3):443–458, 2004.

[77] Peter Richard, Barbara M Bakker, Bas Teusink, Karel Van Dam, and Hans V Westerhoff. Acetaldehyde mediates the synchronization of sustained glycolytic oscillations in populations of yeast cells. *European journal of biochemistry*, 235(1-2):238–241, 1996.

[78] Mads F Madsen, Sune Danø, and Preben G Sørensen. On the mechanisms of glycolytic oscillations in yeast. *The FEBS journal*, 272(11):2648–2660, 2005.

[79] Kevin Shockley, Matthew Butwill, Joseph P Zbilut, and Charles L Webber Jr. Cross recurrence quantification of coupled oscillators. *Physics Letters A*, 305(1-2):59–69, 2002.

[80] Manish Yadav, Amit Sharma, Manish Dev Shrimali, and Sudeshna Sinha. Revival of oscillations via common environment. *Nonlinear Dynamics*, 91(4):2219–2225, 2018.

[81] Amit Sharma, Umesh Kumar Verma, and Manish Dev Shrimali. Phase-flip and oscillation-quenching-state transitions through environmental diffusive coupling. *Physical Review E*, 94(6):062218, 2016.

[82] Umesh Kumar Verma, Neeraj Kumar Kamal, and Manish Dev Shrimali. Coexistence of in-phase oscillations and oscillation death in environmentally coupled limit cycle oscillators. *Chaos, Solitons & Fractals*, 110:55–63, 2018.

[83] Arthur T Winfree. Biological rhythms and the behavior of populations of coupled oscillators. *Journal of theoretical biology*, 16(1):15–42, 1967.

[84] Anshul Choudhary and Sudeshna Sinha. Balance of interactions determines optimal survival in multi-species communities. *PloS one*, 10(12):e0145278, 2015.

[85] Arghya Mondal, Sudeshna Sinha, and Juergen Kurths. Rapidly switched random links enhance spatiotemporal regularity. *Physical Review E*, 78(6):066209, 2008.

[86] Paul So, Bernard C Cotton, and Ernest Barreto. Synchronization in interacting populations of heterogeneous oscillators with time-varying coupling. *Chaos: An Interdisciplinary Journal of Nonlinear Science*, 18(3):037114, 2008.

[87] John Tang, Salvatore Scellato, Mirco Musolesi, Cecilia Mascolo, and Vito Latora. Small-world behavior in time-varying graphs. *Physical Review E*, 81(5):055101, 2010.

[88] Vivek Kohar and Sudeshna Sinha. Emergence of epidemics in rapidly varying networks. *Chaos, Solitons & Fractals*, 54:127–134, 2013.

[89] Naoki Masuda, Konstantin Klemm, and Víctor M Eguíluz. Temporal networks: slowing down diffusion by long lasting interactions. *Physical Review Letters*, 111(18):188701, 2013.

[90] Anshul Choudhary, Vivek Kohar, and Sudeshna Sinha. Taming explosive growth through dynamic random links. *Scientific reports*, 4:4308, 2014.

[91] Vivek Kohar, Peng Ji, Anshul Choudhary, Sudeshna Sinha, and Jüergen Kurths. Synchronization in time-varying networks. *Physical Review E*, 90(2):022812, 2014.

[92] Soma De and Sudeshna Sinha. Effect of switching links in networks of piecewise linear maps. *Nonlinear Dynamics*, 81(4):1741–1749, 2015.

[93] Neeraj Kumar Kamal and Sudeshna Sinha. Dynamic random links enhance diversity-induced coherence in strongly coupled neuronal systems. *Pramana*, 84(2):249–256, 2015.

[94] Pranay Deep Rungta and Sudeshna Sinha. Random links enhance the sensitivity of networks to heterogeneity. *EPL (Europhysics Letters)*, 112(6):60004, 2016.

[95] K Hoppe and GJ Rodgers. Mutual selection in time-varying networks. *Physical Review E*, 88(4):042804, 2013.

[96] Juliette Stehlé, Alain Barrat, and Ginestra Bianconi. Dynamical and bursty interactions in social networks. *Physical review E*, 81(3):035101, 2010.

[97] F De Vico Fallani, Vito Latora, Laura Astolfi, Febo Cincotti, Donatella Mattia, Maria Grazia Marciani, Serenella Salinari, Alfredo Colosimo, and Fabrizio Babiloni. Persistent patterns of interconnection in time-varying cortical networks estimated from high-resolution eeg recordings in humans during a simple motor act. *Journal of Physics A: Mathematical and Theoretical*, 41(22):224014, 2008.

[98] Miguel Valencia, J Martinerie, S Dupont, and M Chavez. Dynamic small-world behavior in functional brain networks unveiled by an event-related networks approach. *Physical Review E*, 77(5):050905, 2008.

[99] Amr Ahmed and Eric P Xing. Recovering time-varying networks of dependencies in social and biological studies. *Proceedings of the National Academy of Sciences*, 106(29):11878–11883, 2009.

[100] Arturo Buscarino, Mattia Frasca, Marco Branciforte, Luigi Fortuna, and Julien Clinton Sprott. Synchronization of two rössler systems with switching coupling. *Nonlinear Dynamics*, 88(1):673–683, 2017.

[101] Sarbendu Rakshit, Soumen Majhi, Bidesh K Bera, Sudeshna Sinha, and Dibakar Ghosh. Time-varying multiplex network: Intralayer and interlayer synchronization. *Physical Review E*, 96(6):062308, 2017.

[102] Jinde Cao, Guanrong Chen, and Ping Li. Global synchronization in an array of delayed neural networks with hybrid coupling. *IEEE Transactions on Systems, Man, and Cybernetics, Part B (Cybernetics)*, 38(2):488–498, 2008.

[103] Baocheng Li. Finite-time synchronization for complex dynamical networks with hybrid coupling and time-varying delay. *Nonlinear Dynamics*, 76(2):1603–1610, 2014.

[104] Rajat Karnatak, Ram Ramaswamy, and Ulrike Feudel. Conjugate coupling in ecosystems: Cross-predation stabilizes food webs. *Chaos, Solitons & Fractals*, 68:48–57, 2014.

[105] Amit Sharma, Manish Dev Shrimali, and K Aihara. Effect of mixed coupling on relay-coupled rössler and lorenz oscillators. *Physical Review E*, 90(6):062907, 2014.

[106] Amit Sharma and Manish Dev Shrimali. Amplitude death with mean-field diffusion. *Physical Review E*, 85(5):057204, 2012.

[107] V Resmi, G Ambika, RE Amritkar, and G Rangarajan. Amplitude death in complex networks induced by environment. *Physical Review E*, 85(4):046211, 2012.

[108] Garima Saxena, Awadhesh Prasad, and Ram Ramaswamy. Amplitude death: The emergence of stationarity in coupled nonlinear systems. *Physics Reports*, 521(5):205–228, 2012.

[109] Awadhesh Prasad. Time-varying interaction leads to amplitude death in coupled nonlinear oscillators. *Pramana*, 81(3):407–415, 2013.

[110] Tanmoy Banerjee and Debarati Ghosh. Transition from amplitude to oscillation death under mean-field diffusive coupling. *Physical Review E*, 89(5):052912, 2014.